Quantification of macromolecular crowding and ionic strength in living cells

Liu, Boqun

Quantification of macromolecular crowding and ionic strength in Living cells

BOQUN LIU

Quantification of macromolecular crowding and ionic strength in Living cells

Academic Thesis, University of Groningen, the Netherlands

The work published in this thesis was carried out in the Membrane Enzymology group of the Biochemistry Department of the University of Groningen, the Netherland. This work was financially supported by the China Scholarship Council grant, ERC Advanced Grant, and Netherlands Organization for Scientific Research Vidi grant.

ISBN:	978-94-034-0718-0 (printed book)
	978-94-034-0717-3 (ebook)
Printing:	Eikon +
Cover & layout:	Lovebird design. www.lovebird-design.com

rijksuniversiteit
groningen

Quantification of macromolecular crowding and ionic strength in Living cells

PhD thesis

to obtain the degree of PhD at the
University of Groningen
on the authority of the
Rector Magnificus Prof. E. Sterken
and in accordance with
the decision by the College of Deans.

This thesis will be defended in public on

Friday 1 June 2018 at 12.45 hours

by

Boqun Liu

born on 2 September 1987
in Jilin, China

Supervisor
Prof. B. Poolman

Co-supervisor
Dr. A.J. Boersma

Assessment Committee
Prof. G. Maglia
Prof. M. Heinemann
Prof. P. Swain

Table of contents

CHAPTER 1

Quantification of macromolecular crowding in the intracellular environment

Abstract

Macromolecular crowding alters the biochemical processes in living cells. Here, we present an overview on the complex composition of the cytoplasm, the effects the crowded interior exert on the macromolecular diffusion and conformational changes of proteins, and the quantification of crowding in cells. The recent developments in crowding sensing will be discussed in detail, including the sensing mechanisms, applications, and (dis)advantages of the available probes.

Introduction

The cell is the fundamental unit of all living matter[1,2]. In the cytoplasm of a cell, there are many proteins, mRNAs, sugars, ions, and other molecules (Fig. 1). The high density of molecules makes the cytoplasm very crowded and under certain conditions, e.g., osmotic upshift and starvation, the cytosol can change into a glass-like solution[3]. Hence, the intracellular environment is markedly different from aqueous solutions of proteins and nucleic acids. The terms that are employed to describe the crowded situation *in vivo* are listed in table 1[4]. In this chapter, we summarize the (macro)molecules that contribute to macromolecular crowding of the cytoplasm, the influence of crowding on certain biochemical processes, and the recent developments on macromolecular crowding determination in living cells.

The composition of the cytoplasm

To have a general perception of the macromolecular crowding of the cytoplasm, it is helpful to know the volume of the cell as well as the type and amount of (macro)molecules in the cytoplasm. Cell volume is not a static value and depends on the cell type, the growth and environmental conditions, and the growth rate of the cell[10,11]. A typical cell volume varies from 0.3–3 µm³ for a bacterial *E. coli* cell, to 1000–10,000 µm³ for mammalian Hela cells[12,13] (Fig. 2). An alternative way to illustrate the crowdedness of the cytoplasm is to take *E. coli* as an example; there are ~1.4 proteins in every 1000 nm³ cubic

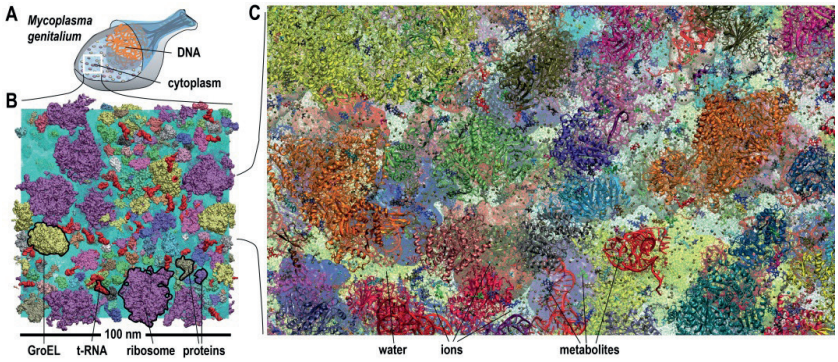

Fig. 1. The crowded situation in the cytoplasm of Mycoplasma genitalium. A: *Schematic illustration of M. genitalium.* ***B:*** *Cartoon illustration of an enlarged section of the cytoplasm showing proteins, tRNA, GroEL, and ribosomes.* ***C:*** *A further enlarged section of the cytoplasm which is from an all-atomistic molecular dynamics simulation showing water, ions, metabolites, and proteins. Figure adapted from Yu et al.*[5].

Table 1. *Crowding-related terms and methods (taken from ref. [4])*

Macromolecular volume fraction Φ:
The volume fraction (Φ) is the volume that is occupied by macromolecules relative to the volume of the compartment (for example, the cytoplasm) and is expressed as volume per volume (v/v)
Excluded volume
The volume that is accessible to a tracer molecule is decreased in the presence of crowder molecules. The volume excluded is the apparent volume of the crowder molecules, which is given by the distance between the centre of a tracer particle and the centre of the crowding molecule.
A selection of theories that are relevant to macromolecular crowding
The Asakura–Oosawa depletion theory[6] describes the effect of the attraction of two particles due to the depletion of solutes in between those particles. This local solute depletion induces an osmotic pressure difference within the bulk solution that pushes the particles together. The depletion force occurs in crowded solutions and might be applicable to protein crowding, albeit only on a qualitative level. The depletion force explains, for example, the compression of tracer molecules and the size-dependent sorting of crowder molecules in dense solutions. The Flory Huggins theory[7] describes the thermodynamics of polymer solutions but has been adapted to explain the effects of crowding on intrinsically disordered proteins. Besides excluded volume, this theory contains an interaction parameter to account for the miscibility between disordered proteins and crowders. The scaled-particle theory[8] has been adapted to quantify the effects of macromolecular crowding. The theory treats proteins and crowders as hard convex particles that cannot overlap, inducing an entropic cost when placing the tracer molecule in a crowded solution compared with a dilute solution. The entropic cost increases (that is, entropy decreases) with larger overlap volume between the crowder and tracer molecule, and the concentration of the crowder.
Soft interactions, weak chemical interactions
Soft interactions affect both entropy and enthalpy, and include non-covalent interactions, such as electrostatic, hydrogen bonding, van der Waals and hydrophobic interactions. Unlike steric interactions, they are caused by the chemical nature of the molecules. Soft interactions can either counteract or enhance the effects of the excluded volume.
Macromolecular confinement
Confinement refers to the phenomenon of volume exclusion due to a fixed (that is, confining) boundary to a macromolecule[9] — for example, the membranes that confine the narrow space of the periplasm. Contrary to macromolecular crowding, the free energy cost of confinement is not necessarily minimal when a molecule is in its most compact conformation, and whether the molecule has a complementary shape to the confining boundary becomes a factor in the free energy term.
Phase separation
Attractions between macromolecules can lead to macromolecule-enriched and macromolecular-depleted phases, or phases that are enriched in a certain type of macromolecule, such as in the eukaryotic nucleolus and in germ cell granules (P-granules) of *Caenorhabditis elegans*. Attraction can be induced by the depletion force (Asakura-Oosawa depletion theory) or chemical interaction (similar to the Flory Huggins theory). The phases need to be in osmotic equilibrium, and thus the presence of osmolytes enhances the possibility of forming phases, as high local concentrations of macromolecules need to be osmotically balanced. In the bacterial cell, this may lead to spatial heterogeneity and vectorial chemistry.
Homeocrowding
We use homeocrowding as an acronym of 'macromolecular crowding homeostasis'; it refers to the ability of the cell to maintain relatively constant levels of macromolecules, similarly to the ability of a system to regulate its internal pH and ion concentration (that is, pH and ion homeostasis or ionic strength homeostasis)
Donnan effect
The Donnan effect (also known as the Gibbs-Donnan effect or Donnan equilibrium) occurs when large particles (for example, anionic proteins) are present on one side of a membrane and create an uneven electrical charge. This will attract small cations, such as K^+, the accumulation of which will increase internal osmotic pressure

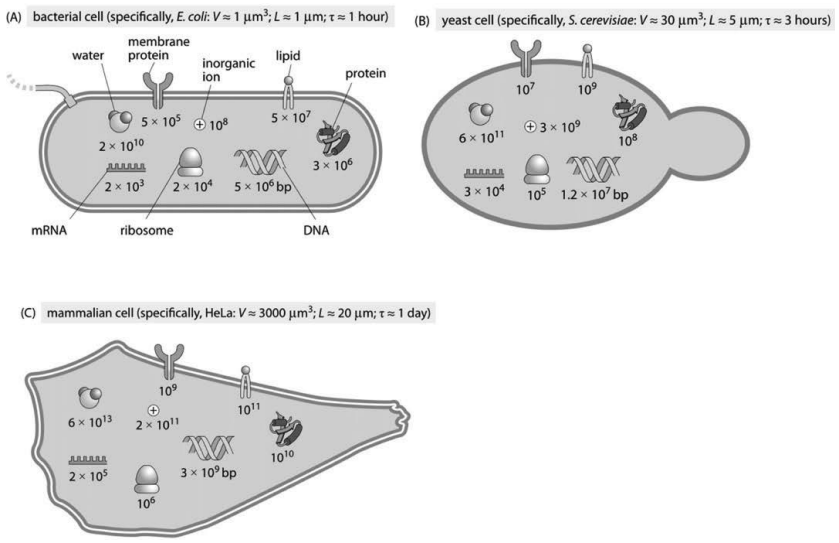

Fig. 2. Schematic illustration of the major components of three typical model cells. *A bacterial cell (E. coli), a unicellular eukaryote (the budding yeast S. cerevisiae), and a mammalian cell line (HeLa). Figure adapted from Milo & Phillips*[18].

box (10x10x10 nm) in the cytoplasm. The diameter of a protein with 300 residues is about 4.5 nm and that of a protein of 1000 amino acids is about 7 nm[14], which corresponds to a volume fraction of ~8% and ~25%, respectively. This means that on average, proteins are separated from each by distances less than their own dimensions.

Proteins

Here, we first discuss the molecules that crowd the cytoplasm. Proteins are the most abundant type of macromolecules in the cytoplasm with an estimated concentration ranging from 0.2×10^6 fL^{-1} for U2OS cell to 5×10^6 fL^{-1} for *Leptospira interrogans15*, and for a single type protein, it can be over its solubility limit[16,17]. Proteins occupy a relatively large volume in comparison with other molecules such as metabolites and ions. The large amount and volume makes proteins one of the main crowders in the cell.

Proteins are influenced by macromolecular crowding as a result of the excluded volume effect[19] (see below). Most of proteins need to fold and assemble into unique three-dimensional structures to fulfill their biological functions[20,21]. Proteins also oligomerize[22–24] and aggregate[25,26] *in vivo*. The conformational changes and associations depend on the properties of the protein and are affected by excluded volume effects and soft interactions (Table 1). Additionally, proteins themselves and other molecules, including mRNA, DNA and small molecules may associate in larger organizations[27–29], which are also

influenced by excluded volume effects and soft interactions. Thus, proteins are a major crowder in the cytoplasm and they are influenced by macromolecular crowding themselves

Genome (DNA)

In prokaryotic cells, genomic DNA is exposed to the cytoplasm, whereas in eukaryotic cells, the DNA is present in the nuclear matrix. Genomic DNA occupies about 1% of the dry weight of *E. coli*, which is not expected to contribute significantly to macromolecular crowding. Nevertheless, it encodes the proteins[27] that crowd the cytoplasm. Additionally, DNA influences viscosity and heterogeneity in the cell due to various factors[30]. Ribosome complexes (polysomes) are excluded from the nucleus due to the depletion force (Table 1) of DNA, which is a macromolecular crowding effect[31]. Macromolecular crowding influences the structure and function of DNA by influencing for example the conformation of DNA hairpins[32]. Additionally, increasing crowding *in vitro* by the addition of PEG leads to enhancement of DNA replication[33] and transcription/translation[34].

Ribosome

The ribosome is a complex macromolecule consisting of ribosomal RNA molecules and proteins. Ribosomes occupy 21–37% of the dry weight of *E. coli*[35]. The high volume of ribosomes suggests that they would play an important role in macromolecular crowding. Additionally, the ribosome functions as a factory for protein synthesis[36–38], and the cell regulates ribosome concentration as a function of growth rate and the nutritional contents of the medium[39]. Hence, the ribosome machinery may directly or indirectly control the macromolecular crowding *in vivo*[40]. Macromolecular crowding affects the assembly of ribosomes. For example, the presence of a synthetic polymer can increase the formation of 70 S ribosomes from 30 S and 50 S ribosomal subunits as a result of excluded volume effects[41]. Hence, ribosomes influence macromolecular crowing by their abundance and activity, and are affected by the macromolecular crowding themselves.

Small molecules

The cell contains a large amount of small molecules. Researchers have quantified more than 100 types of small molecules in exponentially growing *E. coli*[42]. Small molecules themselves do not contribute much to the crowding effect. However, they are able to influence macromolecular crowding by affecting molecular interactions. For example, small ions screen electrostatic interaction and specific molecules, such as ATP which can function as a biological hydrotrope, may influence the macromolecular crowding by keeping proteins soluble and preventing protein aggregate formation[43].

In brief, the composition of the cytoplasm, which include proteins, rRNA and other macromolecules, results in macromolecular crowding effects. The molecules in the cell influence macromolecular crowding by changing the abundance, assembly and aggregation of macromolecules[44–49], which influences many biochemical functions.

The effect of macromolecular crowding

Due to the crowded nature of the cytoplasm, most biochemical processes in *vivo*, such as lateral diffusion, conformational changes, and aggregation or association of the biomacromolecules, are different from those in dilute aqueous solutions[9,50]. Here we provide further detail on the influence of macromolecular crowding on protein diffusion and conformation, because these phenomena are used for benchmarking of the quantification of macromolecular crowding with sensors.

The effect of macromolecular crowding on lateral diffusion

Diffusion is the main process for transporting and mixing of components in prokaryotic cells. The quantitative description of the diffusion coefficient (*D*) is shown by the Stoke-Einstein equation (Eq. 1) in which *kB* is Boltzmann's constant. According to the equation, we can see that the diffusion coefficient of macromolecules depends on temperature (*T*), hydrodynamic radius of the particle (*Rs*), and viscosity (μ) of the medium, which is determined by factors like macromolecular crowding[51].

$$D = \frac{K_B T}{6\pi R_s \mu} \qquad \text{Eq. 1}$$

The macromolecular crowding decreases the mobility of molecules, which then may become rate-limiting for a given biochemical process. In a crowded solution, the diffusion of both small and large molecules decreases but the impact of crowding is more pronounced for large than for small molecules[52]. *In vitro*, both the diffusion of small (rhodamine green) and large molecules (DNA, RNA, proteins, and nanosphare) decrease as a function of increasing concentration of Ficoll 70 (Fig. 3)[53]. The highly branched polymeric nature of Ficoll 70 may prevent size selective diffusion that would be expected from hard-sphere crowders. *In vivo*, the decrease of diffusion is more complex, where it is influenced by spatial heterogeneity and weak interactions. It has been hypothesized that the cytoplasm is spatially organized, which allows the free passage of small molecules while restricting the diffusion of macromolecules[52,54].

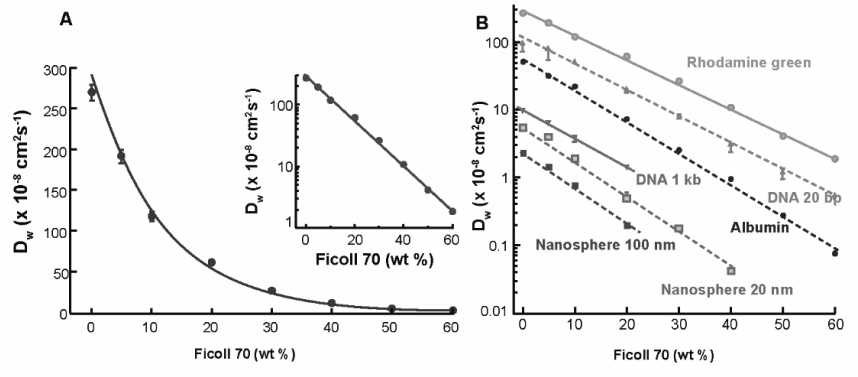

Fig. 3. Diffusion coefficients of different (macro)molecules as a function of Ficoll 70 concentration. ***A:*** *Diffusion coefficients of rhodamine green as a function of Ficoll 70 concentration shown on linear and log (inset) scales (mean ± SE, 10–20 measurements).* ***B:*** *Diffusion of indicated small solutes, macromolecules, and nanospheres in saline solutions crowded with Ficoll 70. Figures adapt from Dauty et al.* [55].

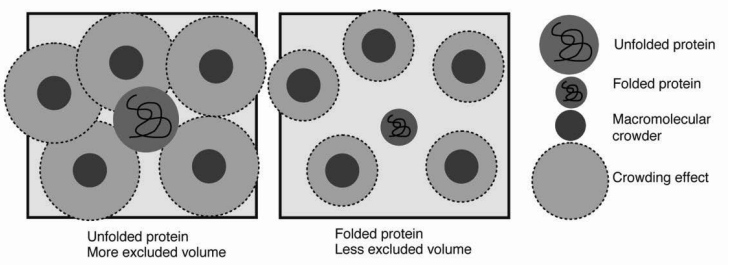

Fig. 4. Effects of macromolecular crowding on protein folding. *The folded native state of a biomolecule (red) is favored compared to the unfolded state (green), because it is more compact and occupies less volume, leaving more volume for the crowders. Figure adapted from Gnutt et al.*[61].

The effect of macromolecular crowding on protein conformational changes

Most proteins need to fold to be functional. There are several environmental factors that influence protein folding and conformational changes[19,56,57]. Macromolecular crowding influences protein folding by the excluded volume effect and soft interactions. The excluded volume effect is dependent on the radius of crowder and the radius of the tracer molecule, i.e. smaller tracers experience less excluded volume effects than bigger ones (Fig. 4). Macromolecular crowding decreases the available volume for the tracer, decreasing the entropy, which raises the free energy of the system. To minimize the decrease in entropy, the available volume is increased by e.g. folding or compression of proteins[4,8,58]. In general, molecular crowding favors more

compact forms over extended ones and can thereby shift the equilibrium towards the folded state[59]. However, some intrinsically disordered proteins do not show significant compaction in the presence of macromolecular crowding agents[60], which has been ascribed to compensation by weak attractive interactions with the crowders.

Techniques for quantification of macromolecular crowding in living cells

We discuss the techniques for quantification of macromolecular crowding, which either probe the lateral diffusion of fluorescent molecules or sense the conformation fluorescent reporters as a function of crowding strength. Various techniques allow estimation of macromolecular crowding by determining the cellular dry weight fraction and volume determination[4], but they are not considered here because of the limited temporal and spatial resolution as well as the requirement to disrupt the cells. Here, we focus on NMR, FRAP and FCS to measure crowding in the physiological environment. Moreover, we will also discuss the newly developed crowding sensors, which are based on FRET or fluorescence anisotropy.

NMR (Nuclear magnetic resonance spectroscopy)

NMR spectroscopy is a powerful tool for the characterization of protein conformations *in vivo*[62,63]. NMR can provide the conformations at the atomic level and has a distinct time window which ranges from picoseconds to seconds[64]. Labeling protein with ^{19}F allows characterizing large proteins up to 100 kDa in living cells[65,66]. For example, by labeling globular and disordered proteins with ^{19}F, Li *et al.* observed the site-specific structural and dynamic information of a set of different proteins in cells, which are influenced by macromolecular crowding, among other effects. The high temporal resolution of NMR enables investigation of the protein conformation changes *in vivo*; thus, probing the macromolecular crowding effect.

Even though there are several advantages, NMR is still limited by several factors; NMR demands a high concentration of protein, which can be achieved by over-expression and microinjection, but both of these two strategies may influence the *in vivo* macromolecular crowding. The high concentration of protein also may lead to inclusion body formation *in vivo*, which influences the protein conformations[67,68]. The need for long acquisition times in a NMR tube can result in a different physiology of the cell compared to regular growth conditions. In short, NMR can be employed for quantification of macromolecular crowding in the living cell, but requires high protein expression of the proteins and relatively long acquisition times.

FRAP (Fluorescence recovery after photobleaching)

FRAP is a method for quantifying molecular mobility, which is influenced by macromolecular crowding[69–71]. By measuring the rate of fluorescence recovery at a previously bleached site, one can estimate the diffusion coefficient of any fluorescently labeled molecule. For example, Konopka *et al.*[54] determined the diffusion coefficient of green fluorescent protein (GFP) within the cytoplasm of *E. coli* by FRAP and they found that the diffusion of GFP decreases with the osmotic upshift. Van den Bogaart *et al.*[72] determined the diffusion coefficients of (macro)molecules of different sizes (from ~0.5 to 600 kDa) in *E. coli* under normal osmotic conditions and osmotic upshift; they showed the cytoplasm of *E. coli* appears as a meshwork allowing the free passage of small molecules while restricting the diffusion of bigger ones. Drawbacks of FRAP are that the spatial resolution is limited to one dimension, the size of the bleached spot, and the fluorescent proteins need to be expressed at relatively high levels. Furthermore, the methodes do not have single molecule resolution, reporting the ensemble average of the diffusion coefficient.

FCS (Fluorescence correlation spectroscopy)

FCS detects the diffusion by tracking the temporal correlations in fluorescence intensity fluctuations, which is caused by one or more fluorescent molecules diffusing in and out of an illuminated excitation volume. It allows measuring protein diffusion at low concentrations without the need of overexpression and provides quantitative data on diffusion coefficients[73]. By tagging one domain of the C/EBPα with either RFP, mCherry, or Ruby2, Tsekouras *et al.*[74] characterized the diffusion of the proteins in solution and in mouse cells. Within the cell, they looked at diffusion of the labeled proteins in the cytosol and in the nucleus, that is, away from areas of heterochromatin. They found that the complex heterogeneous environment of the cell often shows strong deviations from normal diffusion, which may relate to crowding or confinement.

However, FCS works only within a very limited concentration range. If the concentration is too high (typically > 10^{-8} M), the amount of signal may be too high for the detector which results in inefficient photon counting. If the concentration is too small (typically < 10^{-13} M), the probability to find a molecule within the detection region becomes extremely small. Moreover, FCS is dependent on the geometry of the detection volume for which the appropriate corrections need to be made. The geometry can be influenced by factors including refractive index of the sample, thickness of the coverslips, and optical saturation[75], which can alter the measurement of the correlation function. In brief, FCS can be employed to quantify crowding differences through changes in lateral diffusion of a reporter, but the analysis of fluctuation data obtained from fluorescent proteins is not trivial.

Fluorescence anisotropy

Fluorescence anisotropy or polarization measures the difference in fluorescence intensities emitted parallel and perpendicular to the polarization of the excitation light, which reports on the rotational motion of the entire dye molecule within the excited-state lifetime[76,77]. Based on fluorescence anisotropy, researchers reported a new strategy that allows spatiotemporal visualization of the macromolecular crowding effect in cells[78]. Briefly, an amine-reactive aggregation-induced emission fluorogen is used to label proteins in the cytoplasm, and the change in protein mobility and local viscosity can be monitored by fluorescence anisotropy and fluorescence lifetime imaging, respectively (Fig. 5).

The crowding measurement depends on the quantification of intracellular viscosity, which can be quantified by monitoring the rotation of the phenyl ring. The crowding measurement is also influenced by the labeling process, which includes the concentrations of dye used, and the labeling selectivity. For instance, the dye TPE-Py-NCS can also light up the membrane-bound organelles. Hence, because of the dependence on viscosity and staining, this approach has limited usefulness.

FRET (Förster resonance energy transfer)

FRET (Förster resonance energy transfer) is an electrodynamic phenomenon that is widely used in biology[79–81]. Our probes, and later

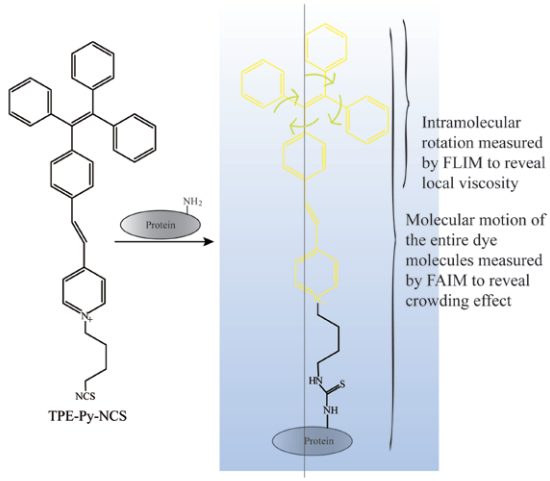

Fig. 5 Design principle of a crowding sensor based on fluorescence anisotropy. *An amine-reactive dye TPE-Py-NCS labels proteins and probes the macromolecular crowding. The viscosity of the micro-environment can be monitored by determining the rotation of the phenyl ring, which is not affected by crowding, through fluorescence lifetime imaging microscopy (FLIM). The crowding will slow the rotation of the entire protein, which can be quantified with fluorescence anisotropy imaging microscopy (FAIM). Figure adapted from Soleimaninejad et al.*[78].

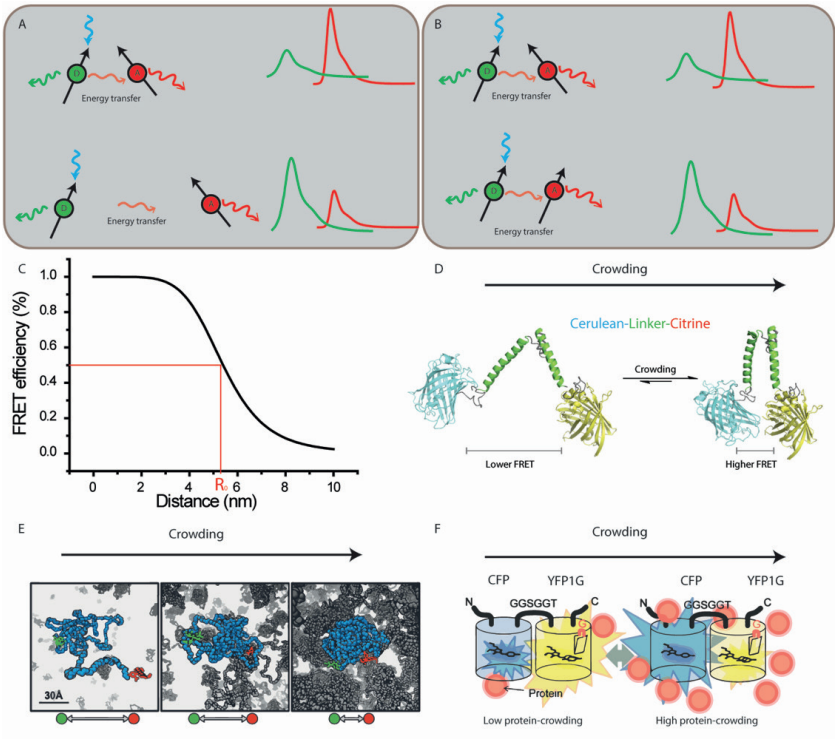

***Fig. 6. The mechanism of FRET and the crowding sensors. A**: The FRET efficiency increases with the distance decrease between donor and acceptor. When the distance between donor and acceptor is short, the FRET efficiency is high, yielding a high intensity of acceptor. **B**: The dipole orientation (indicated by arrow) influences the FRET efficiency. When the dipoles are in head-to-tail parallel orientation, there is more energy transfer from donor to acceptor yielding a high intensity of acceptor. **C**: An example of the FRET efficiency (Eq. 1) varying with distance (R0 = 5.4 nm) **D**: Schematic drawing of crowding sensor from Boersma et al. A conformationally flexible linker connects a mCerulean3 (cyan fluorescent protein) and a mCitrine (yellow fluorescent protein). Sensor compaction results in a change in FRET efficiency. Figure adapted from Boersma et al.[86]. **E**: Schematic drawing of a sensor based PEG (shown in blue)[87], labeled at the N- and C-termini, using Atto488 and Atto565. Figure adapted from Gnutt et al.87. **F**: Schematic drawing of the sensor from Morikawa et al. CFP and YFP1G (A destabilized YFP) were fused with a GGSGGT linker. The fluorescence of YFP1G decreases with high protein concentration, while the fluorescence of cyan fluorescent protein (CFP) is insensitive to protein concentration. Figure adapted from Morikawa et al.[88].*

developed sensors for the quantification of macromolecular crowding *in vivo*, are based on FRET readout.

BASIC PRINCIPLE OF FRET

The basic mechanism of FRET can be explained with classical physics. FRET occurs between a donor (D) in the excited state and an acceptor

(A) molecule in the ground state. The donor molecules emit at shorter wavelengths that overlap with the absorption spectrum of the acceptor. Energy transfer occurs without the appearance of a photon and is the result of long-range dipole-dipole interactions between the donor and acceptor[82].

The energy transfer efficiency, which is termed FRET efficiency, depends on the donor-acceptor distance and the orientation of the dipoles relative to each other (Fig. 6A and B). When the donor-acceptor distance decreases, more energy is transferred from donor to acceptor yielding a decrease in intensity of the donor and an increase in intensity of the acceptor. (Fig. 6A). When the dipoles are in head-to-tail parallel orientation, there is more energy transfer from donor to acceptor; there is no energy transfer when the dipoles are oriented perpendicular to each other.

The quantitative relationship of FRET efficiency is shown in Eq. 2 and Fig 6C, in which *E* is the FRET efficiency; *r* is the radius between donor and acceptor; and *R0* the Förster distance of this pair of donor and acceptor, *i.e.* the distance at which the energy transfer efficiency is 50%. R_0 depends on the fluorescence quantum yield of the donor in the absence of the acceptor (*QD*), Avogadro's number (N_A), the dipole orientation factor (κ), the refractive index of the medium (*n*), and the spectral overlap integral (*J*). For a chosen FRET pair, the dipole orientation factor (κ) is the main factor that influences the *R0* and is in the range from 0 to 4; 0 referring to perpendicular orientation and 4 corresponding to head-to-tail parallel orientation. Generally, for a flexible and freely rotating FRET pair, the orientation factor (κ) equals 2/3[83].

$$E = \frac{R_0^6}{R_0^6 + r^6} \qquad \text{Eq. 2}$$

$$R_0 = \frac{9 \ln 10}{128 \pi^5 N_A} \frac{K^2 Q_D}{n^4} J \qquad \text{Eq. 3}$$

As shown in Fig. 6A, B and C, FRET causes an intensity change in both donor and acceptor emission. Hence, by detecting the change, we can quantify FRET either in fluorescence microscopy or fluorescence spectroscopy. An alternative way to quantify FRET is to determine the fluorescence lifetime of donor[84,85].

MACROMOLECULAR CROWDING SENSORS BASED ON FRET.

Due to the advantageous properties of FRET, researchers have been able to develop several sensors for quantification of macromolecular crowding (See Table 2 and Fig 6D, E, and F). We designed a genetically-encoded FRET sensor by linking mCerulean3 and mCitrine with a conformational flexible linker[86], and applied the sensor in bacterial and mammalian cells (Fig 6F). The crowding conditions *in vivo*

Table 2. *A summary of crowding sensors*

Donor[1]	Acceptor	Genetically Encoded	Donor λ_{Ex} (nm)	Donor λ_{Em} (nm)	Acceptor λ_{Em} (nm)	Cell type	Result	Ref
Fluorescent protein destabilization								
CFP	YFP1G	Yes	880	460–500	520–560	HeLa	Not clear	[88]
Compression								
Atto488	Atto565	No	490	497-527	581-679	HeLa	No crowding	[87]
mCerulean3	mCitrine	Yes	405	450–505	505–797	E. coli HEK293	~19% Ficoll	[86,96]
AcGFP[1]	mCherry	Yes	470	500-600	600-800	Gel U-2 OS cells		[90,91]
Clover	mRuby2	Yes	490	497-527	581-679	HeLa	-	[92]

were equivalent to ~ 19% Ficoll, which corresponds reasonably well with the overall dry weight measurements[89]. Gruebele *et al.*[90,91] also employed this crowding sensor as a template and varied the FRET pair to AcGFP-mCherry for investigating the folding stability and dynamics of proteins in gel as well as cellular crowding in U2OS cells. They found that the crowding change responded linearly to cell-volume.

Simultaneously and independent of us, Gnutt *et al.*[87] demonstrated that a synthetic polymer based FRET sensor also allows probing of macromolecular crowding. They determined macromolecular crowding in HeLa cells (Fig. 6E), and observed a very low crowding in HeLa cells. This could be due to compensating forces, e.g. van der Waals and hydrophobic forces between the PEG and crowders. These forces can counteract depletion forces and promote stabilization of expanded chain conformations. Later they observed the macromolecular crowding effect with a modified version of our sensor[92].

Morikawa et al.[88] used a variant of YFP, whose fluorescence intensity depends on the surrounding protein concentration, as an intracellular protein-crowding sensor (Fig. 6D). However, the crowding sensing mechanism of the sensor from Morikawa *et al.* is not yet clear (see below), and they can only describe qualitative changes in crowding rather than determine absolute crowding values.

Although these sensors have been specifically designed for crowding sensing, other sensors and macromolecules respond to macromolecular crowding as well. For example, NKCC1 (functioning as a Na-K-Cl cotransporter)[93], ATeam (ATP sensor) and DTeam (control for ATeam)[94], PGK (phosphoglycerate kinase)[95] are all labeled with FRET pairs and show macromolecular crowding sensitivity, which are due to the excluded volume effect and the relatively large volume of these sensors. Nevertheless, these labeled proteins are also strongly influenced by other interactions or the analyte that they bind. As a result, they are less suitable for the quantification of macromolecular crowding and very useful to determine the concentration of specific ligands.

When applying crowding sensors, it is beneficial to understand their mechanism of operation. The mechanism of sensing by the probes of Boersma *et al.* (Fig. 6F) and the sensor from Gnutt *et al.* (Fig. 6E) can be explained by the change of distance between donor and acceptor as shown in Figure 6A. The mechanism of sensing by the probe of Morikawa *et al.* (Fig. 6D) is less clear but may occur through destabilization of the folding of the fluorescent protein under condition of high crowding.

The sensors from Boersma *et al.* are mostly sensitive to the excluded-volume effect and less influenced by other forces. Additionally, as the sensors are genetically encoded, they do not require perturbation of the living cell other than effects caused by their expression. Moreover, the genetically encoded FRET sensors can be widely applied in different types of cells. One disadvantage of these sensors is that the fluorescent proteins are less photostable than the synthetic fluorophores used by Gnutt *et al.* Other points that are inherent to genetically encoded sensors will be addressed in this thesis: The maturation of fluorescent proteins, incomplete sensor synthesis and sensor degradation (Chapter 3), and the pH sensitivity of the fluorescent proteins (Chapter 4).

Conclusion

The high density of macromolecules causes the crowded nature of cytoplasm. The quantification of macromolecular crowding under varying conditions is important for understanding the physicochemical homeostasis of the cell, and consequently an array of techniques that sense crowding has been developed.

Thesis outline

In this thesis, I shed light on the mechanism of crowding sensing and the development of FRET-based crowding probes; I use these sensors to determine the significance of macromolecular crowding in bacterial cells. We show that 1) the effect of macromolecular crowding on the sensor in the living cells displays polymer-type behavior and its compression scales with the biopolymer volume fraction and sensor size, and depends *in vivo* on its structure (Chapter 2); 2) the maturation of fluorescent proteins can influence the ratiometric FRET, which can be minimized by constitutive expression of the sensor (Chapter 3); and 3) by perturbing the crowding by hyperosmotic stress and leaving the cells to adapt, I show that macromolecular crowding remains at a lower level compared to unstressed cells upon adaptation (chapter 4). Additionally, we present the first sensors to determine the ionic strength in living cells. The ionic strength sensors

allow observation of spatiotemporal changes in the ionic strength on the single-cell level in mammalian cells.

Reference

1 Madigan, Michael T., John M. Martinko, and Jack Parker. Brock biology of microorganisms. 4th edition, Vol. 13. Pearson, (2017)

2 Hajdu, S. I. A note from history: Introduction of the cell theory. *Annals of Clinical and Laboratory Science* **32**, 98-100 (2002).

3 Parry, B. R. *et al.* The Bacterial Cytoplasm Has Glass-like Properties and Is Fluidized by Metabolic Activity. *Cell* **156**, 183-194, doi:10.1016/j.cell.2013.11.028 (2014).

4 van den Berg, J., Boersma, A. J. & Poolman, B. Microorganisms maintain crowding homeostasis. *Nature Reviews Microbiology* **15**, 309-318, doi:10.1038/nrmicro.2017.17 (2017).

5 Yu, I. *et al.* Biomolecular interactions modulate macromolecular structure and dynamics in atomistic model of a bacterial cytoplasm. *Elife* **5**, doi:10.7554/eLife.19274 (2016).

6 Marenduzzo, D., Finan, K. & Cook, P. R. The depletion attraction: an underappreciated force driving cellular organization. *Journal of Cell Biology* **175**, 681-686, doi:10.1083/jcb.200609066 (2006).

7 Soranno, A. *et al.* Single-molecule spectroscopy reveals polymer effects of disordered proteins in crowded environments. *Proceedings of the National Academy of Sciences of the United States of America* **111**, 4874-4879, doi:10.1073/pnas.1322611111 (2014).

8 Minton, A. P. Excluded volume as a determinant of macromolecular structure and reactivity. *Biopolymers* **20**, 2093-2120, doi:10.1002/bip.1981.360201006 (1981).

9 Zhou, H.-X., Rivas, G. & Minton, A. P. Macromolecular crowding and confinement: Biochemical, biophysical, and potential physiological consequences. *Annual Review of Biophysics* **37**, 375-397, doi:10.1146/annurev.biophys.37.032807.125817 (2008).

10 Volkmer, B. & Heinemann, M. Condition-Dependent Cell Volume and Concentration of Escherichia coli to Facilitate Data Conversion for Systems Biology Modeling. *Plos One* **6**, doi:10.1371/journal.pone.0023126 (2011).

11 Kubitschek, H. E. CELL-VOLUME INCREASE IN ESCHERICHIA-COLI AFTER SHIFTS TO RICHER MEDIA. *Journal of Bacteriology* **172**, 94-101 (1990).

12 Werner, E. An introduction to systems biology: Design principles of biological circuits. *Nature* **446**, 493-494, doi:10.1038/446493a (2007).

13 Milo, R., Jorgensen, P., Moran, U., Weber, G. & Springer, M. BioNumbers-the database of key numbers in molecular and cell biology. *Nucleic Acids Research* **38**, D750-D753, doi:10.1093/nar/gkp889 (2010).

14 Erickson, H. P. Size and shape of protein molecules at the nanometer level determined by sedimentation, gel filtration, and electron microscopy." Biological procedures online *Biol Proced Online* Vol. 11 32-51 (2009).

15 Milo, R. What is the total number of protein molecules per cell volume? A call to rethink some published values. *Bioessays* **35**, 1050-1055, doi:10.1002/bies.201300066 (2013).

16 Tartaglia, G. G., Pechmann, S., Dobson, C. M. & Vendruscolo, M. Life on the edge: a link between gene expression levels and aggregation rates of human proteins. *Trends in Biochemical Sciences* **32**, 204-206, doi:10.1016/j.tibs.2007.03.005 (2007).

17 Ciryam, P., Kundra, R., Morimoto, R. I., Dobson, C. M. & Vendruscolo, M. Supersaturation is a major driving force for protein aggregation in neurodegenerative diseases. *Trends in Pharmacological Sciences* **36**, 72-77, doi:10.1016/j.tips.2014.12.004 (2015).

18 Milo, Ron, and Rob Phillips. Cell biology by the numbers. Garland Science (2015).

19 Stagg, L., Zhang, S. Q., Cheung, M. S. & Wittung-Stafshede, P. Molecular crowding enhances native structure and stability of alpha/beta protein flavodoxin. *Proceedings of the National Academy of Sciences of the United States of America* **104**, 18976-18981, doi:10.1073/pnas.0705127104 (2007).

20 Balchin, D., Hayer-Hartl, M. & Hartl, F. U. In vivo aspects of protein folding and quality control. *Science* **353**, doi:10.1126/science.aac4354 (2016).

21 Murata, S., Yashiroda, H. & Tanaka, K. Molecular mechanisms of proteasome assembly. *Nature Reviews Molecular Cell Biology* **10**, 104-115, doi:10.1038/nrm2630 (2009).

22 Ali, Mayssam H., and Barbara Imperiali. Protein oligomerization: how and why. *Bioorganic & medicinal chemistry* **13**.17 (2005): 5013-5020

23 Helenius, A. *et al.* Protein folding and oligomerization in the endoplasmic reticulum. *Journal of Cellular Biochemistry*, 46-46 (1993).

24 Hurtley, S. M. & Helenius, A. Protein oligomerization in the endoplasmic-reticulum. *Annual Review of Cell Biology* **5**, 277-307 (1989).

25 Squier, T. C. Oxidative stress and protein aggregation during biological aging. *Experimental Gerontology* **36**, 1539-1550, doi:10.1016/s0531-5565(01)00139-5 (2001).

26 Winkler, J. *et al.* Quantitative and spatio-temporal features of protein aggregation in Escherichia coli and consequences on protein quality control and cellular ageing. *Embo Journal* **29**, 910-923, doi:10.1038/emboj.2009.412 (2010).

27 Blattner, F. R. *et al.* The complete genome sequence of Escherichia coli K-12. *Science* **277**, 1453-&, doi:10.1126/science.277.5331.1453 (1997).

28 Cohen, R. D. & Pielak, G. J. Electrostatic Contributions to Protein Quinary Structure. *Journal of the American Chemical Society* **138**, 13139-13142, doi:10.1021/jacs.6b07323 (2016).

29 Majumder, S. *et al.* Probing Protein Quinary Interactions by In-Cell Nuclear Magnetic Resonance Spectroscopy. *Biochemistry* **54**, 2727-2738, doi:10.1021/acs.biochem.5b00036 (2015).

30 Biswas, N. *et al.* Phase separation in crowded micro-spheroids: DNA-PEG system. *Chemical Physics Letters* **539**, 157-162, doi:10.1016/j.cplett.2012.05.033 (2012).

31 Bakshi, S., Choi, H., Mondal, J. & Weisshaar, J. C. Time-dependent effects of transcription- and translation-halting drugs on the spatial distributions of the Escherichia coli chromosome and ribosomes. *Molecular Microbiology* **94**, 871-887, doi:10.1111/mmi.12805 (2014).

32 Stiehl, O., Weidner-Hertrampf, K. & Weiss, M. Macromolecular crowding impacts on the diffusion and conformation of DNA hairpins. *Physical Review E* **91**, doi:10.1103/PhysRevE.91.012703 (2015).

33 Akabayov, B., Akabayov, S. R., Lee, S. J., Wagner, G. & Richardson, C. C. Impact of macromolecular crowding on DNA replication. *Nature Communications* **4**, doi:10.1038/ncomms2620 (2013).

34 Tan, C. M., Saurabh, S., Bruchez, M. P., Schwartz, R. & LeDuc, P. Molecular crowding shapes gene expression in synthetic cellular nanosystems. *Nature Nanotechnology* **8**, 602-608, doi:10.1038/nnano.2013.132 (2013).

35 Yamamoto, T., Izumi, S. & Gekko, K. Mass spectrometry of hydrogen/deuterium exchange in 70S ribosomal proteins from E-coli. *Febs Letters* **580**, 3638-3642, doi:10.1016/j.febslet.2006.05.049 (2006).

36 Pathak, B. K., Mondal, S., Banerjee, S., Ghosh, A. N. & Barat, C. Sequestration of Ribosome during Protein Aggregate Formation: Contribution of ribosomal RNA. *Scientific Reports* **7**, doi:10.1038/srep42017 (2017).

37 Fromont-Racine, M., Senger, B., Saveanu, C. & Fasiolo, F. Ribosome assembly in eukaryotes. *Gene* **313**, 17-42, doi:10.1016/s0378-1119(03)00629-2 (2003).

38 Ramakrishnan, V. Ribosome structure and the mechanism of translation. *Cell* **108**, 557-572, doi:10.1016/s0092-8674(02)00619-0 (2002).

39 Kaczanowska, M. & Rydén-Aulin, M. in *Microbiol Mol Biol Rev* Vol. 71 477-494 (2007).

40 Delarue, M. *et al.* mTORC1 controls cytoplasmic crowding by regulating ribosome concentration. doi:10.1101/073866 (2017).

41 Zimmerman, S. B. & Trach, S. O. Effects of macromolecular crowding on the association of *Escherichia coli* ribosomal particles. *Nucleic Acids Research* **16**, 6309-6326, doi:10.1093/nar/16.14.6309 (1988).

42 Bennett, B. D. *et al.* Absolute metabolite concentrations and implied enzyme active site occupancy in Escherichia coli. *Nature Chemical Biology* **5**, 593-599, doi:10.1038/nchembio.186 (2009).

43 Patel, A. *et al.* ATP as a biological hydrotrope. *Science* **356**, 753-756, doi:10.1126/science.aaf6846 (2017).

44 Demchenko, A. P., Mely, Y., Duportail, G. & Klymchenko, A. S. Monitoring Biophysical Properties of Lipid Membranes by Environment-Sensitive Fluorescent Probes. *Biophysical Journal* **96**, 3461-3470, doi:10.1016/j.bpj.2009.02.012 (2009).

45 Janmey, P. A. & Kinnunen, P. K. J. Biophysical properties of lipids and dynamic membranes. *Trends in Cell Biology* **16**, 538-546, doi:10.1016/j.tcb.2006.08.009 (2006).

46 Cremesti, A. E., Goni, F. M. & Kolesnick, R. Role of sphingomyelinase and ceramide in modulating rafts: do biophysical properties determine biologic outcome? *Febs Letters* **531**, 47-53, doi:10.1016/s0014-5793(02)03489-0 (2002).

47 Matalon, S. & O'Brodovich, H. Sodium channels in alveolar epithelial cells: Molecular characterization, biophysical properties, and physiological significance. *Annual Review of Physiology* **61**, 627-661, doi:10.1146/annurev.physiol.61.1.627 (1999).

48 Salamon, Z., Macleod, H. A. & Tollin, G. Surface plasmon resonance spectroscopy as a tool for investigating the biochemical and biophysical properties of membrane protein systems .1. Theoretical principles. *Biochimica Et Biophysica Acta-Reviews on Biomembranes* **1331**, 117-129, doi:10.1016/s0304-4157(97)00004-x (1997).

49 Webb, M. S. & Green, B. R. Biochemical and biophysical properties of thylakoid acyl lipids. *Biochimica Et Biophysica Acta* **1060**, 133-158 (1991).

50 Hall, D. & Minton, A. P. Macromolecular crowding: qualitative and semiquantitative successes, quantitative challenges. *Biochimica Et Biophysica Acta-Proteins and Proteomics* **1649**, 127-139, doi:10.1016/s1570-9639(03)00167-5 (2003).

51 Heinen, M. *et al.* Viscosity and Diffusion: Crowding and Salt Effects in Protein Solutions. doi:10.1039/C1SM06242E (2011).

52 Mika, J. T. & Poolman, B. Macromolecule diffusion and confinement in prokaryotic cells. *Current Opinion in Biotechnology* **22**, 117-126, doi:10.1016/j.copbio.2010.09.009 (2011).

53 Dix, J. A. & Verkman, A. S. Crowding effects on diffusion in solutions and cells. *Annual Review of Biophysics* **37**, 247-263, doi:10.1146/annurev.biophys.37.032807.125824 (2008).

54 Konopka, M. C., Shkel, I. A., Cayley, S., Record, M. T. & Weisshaar, J. C. Crowding and confinement effects on protein diffusion in vivo. *Journal of Bacteriology* **188**, 6115-6123, doi:10.1128/jb.01982-05 (2006).

55 Dauty, E. & Verkman, A. S. Molecular crowding reduces to a similar extent the diffusion of small solutes and macromolecules: measurement by fluorescence correlation spectroscopy. *Journal of Molecular Recognition* **17**, 441-447, doi:10.1002/jmr.709 (2004).

56 Tsao, D., Minton, A. P. & Dokholyan, N. V. A Didactic Model of Macromolecular Crowding Effects on Protein Folding. *Plos One* **5**, 8, doi:10.1371/journal.pone.0011936 (2010).

57 Cheung, M. S., Klimov, D. & Thirumalai, D. Molecular crowding enhances native state stability and refolding rates of globular proteins. *Proceedings of the National Academy of Sciences of the United States of America* **102**, 4753-4758, doi:10.1073/pnas.0409630102 (2005).

58 Zhou, H. X., Rivas, G. N. & Minton, A. P. in *Annual Review of Biophysics* Vol. 37 *Annual Review of Biophysics* 375-397 (2008).

59 Minton, A. P. Implications of macromolecular crowding for protein assembly. *Current Opinion in Structural Biology* **10**, 34-39, doi:10.1016/s0959-440x(99)00045-7 (2000).

60 Flaugh, S. L. & Lumb, K. J. Effects of macromolecular crowding on the intrinsically disordered proteins c-Fos and p27(Kip1). *Biomacromolecules* **2**, 538-540, doi:10.1021/bm015502z (2001).

61 Gnutt, D. & Ebbinghaus, S. The macromolecular crowding effect - from in vitro into the cell. *Biological Chemistry* **397**, 37-44, doi:10.1515/hsz-2015-0161 (2016).

62 Marion, D. An Introduction to Biological NMR Spectroscopy. *Molecular & Cellular Proteomics* **12**, 3006-3025, doi:10.1074/mcp.O113.030239 (2013).

63 Bothwell, J. H. F. & Griffin, J. L. An introduction to biological nuclear magnetic resonance spectroscopy. *Biological Reviews* **86**, 493-510, doi:10.1111/j.1469-185X.2010.00157.x (2011).

64 Kleckner, I. R. & Foster, M. P. An introduction to NMR-based approaches for measuring protein dynamics. *Biochimica Et Biophysica Acta-Proteins and Proteomics* **1814**, 942-968, doi:10.1016/j.bbapap.2010.10.012 (2011).

65 Li, C. *et al.* Protein 19F NMR in Escherichia coli. *J Am Chem Soc* **132**, 321, doi:10.1021/ja907966n (2010).

66 Wang, G.-F., Li, C. & Pielak, G. J. F-19 NMR studies of alpha-synuclein-membrane interactions. *Protein Science* **19**, 1686-1691, doi:10.1002/pro.449 (2010).

67 Luchinat, E. & Banci, L. A Unique Tool for Cellular Structural Biology: In-cell NMR. *Journal of Biological Chemistry* **291**, 3776-3784, doi:10.1074/jbc.R115.643247 (2016).

68 Maldonado, A. Y., Burz, D. S. & Shekhtman, A. In-cell NMR spectroscopy. *Progress in Nuclear Magnetic Resonance Spectroscopy* **59**, 197-212, doi:10.1016/j.pnmrs.2010.11.002 (2011).

69 Axelrod, D., Koppel, D. E., Schlessinger, J., Elson, E. & Webb, W. W. Mobility measurement by analysis of fluorescence photobleaching recovery kinetics *Biophysical Journal* **16**, 1055-1069 (1976).

70 Koppel, D. E., Axelrod, D., Schlessinger, J., Elson, E. L. & Webb, W. W. Dynamics of fluorescence marker concentration as a probe of mobility. *Biophysical Journal* **16**, 1315-1329 (1976).

71 Ishikawa-Ankerhold, H. C., Ankerhold, R. & Drummen, G. P. C. Advanced Fluorescence Microscopy Techniques-FRAP, FLIP, FLAP, FRET and FLIM. *Molecules* **17**, 4047-4132, doi:10.3390/molecules17044047 (2012).

72 Mika, J. T. *et al.* Molecular sieving properties of the cytoplasm of Escherichia coli and consequences of osmotic stress. *Molecular Microbiology* **77**, 200-207, doi:10.1111/j.1365-2958.2010.07201.x (2018).

73 Machan, R. & Wohland, T. Recent applications of fluorescence correlation spectroscopy in live systems. *Febs Letters* **588**, 3571-3584, doi:10.1016/j.febslet.2014.03.056 (2014).

74 Tsekouras, K., Siegel, A. P., Day, R. N. & Presse, S. Inferring Diffusion Dynamics from FCS in Heterogeneous Nuclear Environments. *Biophysical Journal* **109**, 7-17, doi:10.1016/j.bpj.2015.05.035 (2015).

75 Enderlein, J., Gregor, I., Patra, D. & Fitter, J. Art and artefacts of fluorescence correlation spectroscopy. *Current Pharmaceutical Biotechnology* **5**, 155-161, doi:10.2174/1389201043377020 (2004).

76 Lavis, L. D. & Raines, R. T. Bright ideas for chemical biology. *Acs Chemical Biology* **3**, 142-155, doi:10.1021/cb700248m (2008).

77 Owicki, J. C. Fluorescence polarization and anisotropy in high throughput screening: Perspectives and primer. *Journal of Biomolecular Screening* **5**, 297-306, doi:10.1177/108705710000500501 (2000).

78 Soleimaninejad, H., Chen, M. Z., Lou, X., Smith, T. A. & Hong, Y. Measuring macromolecular crowding in cells through fluorescence anisotropy imaging with an AIE fluorogene. *Chemical Communications* **53**, 2874-2877, doi:10.1039/c6cc09916e (2017).

79 Sekar, R. B. & Periasamy, A. Fluorescence resonance energy transfer (FRET) microscopy imaging of live cell protein localizations. *Journal of Cell Biology* **160**, 629-633, doi:10.1083/jcb.200210140 (2003).

80 Ha, T. Single-molecule fluorescence resonance energy transfer. *Methods* **25**, 78-86, doi:10.1006/meth.2001.1217 (2001).

81 Kenworthy, A. K. Imaging protein-protein interactions using fluorescence resonance energy transfer microscopy. *Methods* **24**, 289-296, doi:10.1006/meth.2001.1189 (2001).

82 Lakowicz, J. R. & Masters, B. R. *Principles of Fluorescence Spectroscopy*. 3rd edn, (2006).

83 Loura, L. M. S. Simple Estimation of Forster Resonance Energy Transfer (FRET) Orientation Factor Distribution in Membranes. *International Journal of Molecular Sciences* **13**, 15252-15270, doi:10.3390/ijms131115252 (2012).

84 Hanley, Q. S. Spectrally resolved fluorescent lifetime imaging. *Journal of the Royal Society Interface* **6**, S83-S92, doi:10.1098/rsif.2008.0393.focus (2009).

85 Merzlyak, E. M. *et al.* Bright monomeric red fluorescent protein with an extended fluorescence lifetime. *Nature Methods* **4**, 555-557, doi:10.1038/nmeth1062 (2007).

86 Boersma, A. J., Zuhorn, I. S. & Poolman, B. A sensor for quantification of macromolecular crowding in living cells. *Nature Methods* **12**, 227–229, doi:10.1038/nmeth.3257 (2015).

87 Gnutt, D., Gao, M., Brylski, O., Heyden, M. & Ebbinghaus, S. Excluded-Volume Effects in Living Cells. *Angewandte Chemie-International Edition* **54**, 2548-2551, doi:10.1002/anie.201409847 (2015).

88 Morikawa, T. J. *et al.* Dependence of fluorescent protein brightness on protein concentration in solution and enhancement of it. *Scientific Reports* **6**, doi:10.1038/srep22342 (2016).

89 Konopka, M. C., Weisshaar, J. C. & Record, M. T., Jr. Methods of changing biopolymer volume fraction and cytoplasmic solute concentrations for in vivo biophysical studies. *Methods Enzymol* **428**, 487-504, doi:10.1016/s0076-6879(07)28027-9 (2007).

90 Kisley, L. *et al.* Direct Imaging of Protein Stability and Folding Kinetics in Hydrogels. *Acs Applied Materials & Interfaces* **9**, 21606-21617, doi:10.1021/acsami.7b01371 (2017).

91 Sukenik, S., Ren, P. & Gruebele, M. Weak protein-protein interactions in live cells are quantified by cell-volume modulation. *Proceedings of the National Academy of Sciences of the United States of America* **114**, 6776-6781, doi:10.1073/pnas.1700818114 (2017).

92 Gnutt, D., Brylski, O., Edengeiser, E., Havenith, M. & Ebbinghaus, S. Imperfect crowding adaptation of mammalian cells towards osmotic stress and its modulation by osmolytes. *Molecular bioSystems*, doi:10.1039/c7mb00432j (2017).

93 Pedersen, M., Carmosino, M. & Forbush, B. Intramolecular and intermolecular fluorescence resonance energy transfer in fluorescent protein-tagged na-k-cl cotransporter (NKCC1) - Sensitivity to regulatory conformational change and cell volume. *Journal of Biological Chemistry* **283**, 2663-2674, doi:10.1074/jbc.M708194200 (2008).

94 Groen, J. *et al.* Associative Interactions in Crowded Solutions of Biopolymers Counteract Depletion Effects. *Journal of the American Chemical Society* **137**, 13041-13048, doi:10.1021/jacs.5b07898 (2015).

95 Dhar, A. *et al.* Structure, function, and folding of phosphoglycerate kinase are strongly perturbed by macromolecular crowding. *Proceedings of the National Academy of Sciences of the United States of America* **107**, 17586-17591, doi:10.1073/pnas.1006760107 (2010).

96 Liu, B. Q. *et al.* Design and Properties of Genetically Encoded Probes for Sensing Macromolecular Crowding. *Biophysical Journal* **112**, 1929-1939, doi:10.1016/j.bpj.2017.04.004 (2017).

CHAPTER 2

Design and Properties of Genetically-Encoded Probes for Sensing Macromolecular Crowding

Boqun Liu,[1] Christoffer Åberg,[1] Floris J. van Eerden,[1] Siewert J. Marrink,[1] Bert Poolman,[1,*] and Arnold J. Boersma[1,*]

[1]Department of Biochemistry, Groningen Biomolecular Sciences and Biotechnology Institute & Zernike Institute for Advanced Materials, University of Groningen, Groningen, the Netherlands

A.J.B. designed research. B.L., C. Å., F.J.v.E., and A.J.B. performed research. B.L., C. Å., F.J.v.E., and S.J.M. contributed new reagents/analytical tools. All authors analyzed data and wrote the paper.

*Correspondence: b.poolman@chem.rug.nl or a.j.boersma@rug.nl

Boqun Liu, Christoffer Åberg, and Floris J. van Eerden contributed equally to this work.

Published in Biophysical journal 112.9 (2017): 1929-1939.

Abstract

Cells are highly crowded with proteins and polynucleotides. Any reaction that depends on the available volume can be affected by macromolecular crowding, however the effects of crowding in cells are complex and difficult to track. Here, we present a set of Förster resonance energy transfer (FRET)-based crowding-sensitive probes and investigate the role of the linker design. We investigate the sensors in vitro and in vivo and by molecular dynamics simulations. We find that in vitro all the probes can be compressed by crowding, with a magnitude that increases with the probe size, the crowder concentration, and the crowder size. We capture the role of the linker in a heuristic scaling model, and we find that compression is a function of size of the probe and volume fraction of the crowder. The FRET changes observed in the cell are more complicated, where FRET-increases and scaling behavior are observed solely with probes that contain the helices in the linker. The probe with the highest sensitivity to crowding in vivo yields the same macromolecular volume fractions as previously obtained from cell dry weight. The collection of new probes provides more detailed readouts on the macromolecular crowding than a single sensor.

Introduction

The high macromolecule content in the cell, 300-400 mg/mL[1], influences the physicochemical properties in its interior. A protein in this crowded environment will endure forces due to excluded volume and nonspecific chemical interactions with the other macromolecules[2–4]. Its thermodynamic activity will furthermore be affected by the solvent properties. When introducing a protein in a crowded solution, the excluded volume reduces the entropy of the system, by reducing the number of possibilities the crowders can be arranged. The entropic penalty can be relieved by reducing the volume of the introduced protein. In the cell, other interactions are able to attenuate this entropic effect, resulting in net effects that are often different to what would be predicted solely due to steric exclusion[5–12]. This makes that crowding effects are unpredictable in cells, and can be overshadowed by other nonspecific interactions if the excluded volume effects are small.

To isolate excluded volume effects from other effects we developed previously a sensor for quantification of macromolecular crowding[13], based on Förster resonance energy transfer (FRET). The original probe consists of mCitrine (YFP, yellow fluorescent protein) and mCerulean3[14] (CFP, cyan fluorescent protein), which form a FRET pair, and are connected by a flexible linker (Fig. 1A). Upon placement in a crowded environment the probe will populate more condensed conformations, leading the FRET pair to be closer to each other. This crowding-induced compression of the whole protein is quantified by an increase in FRET efficiency between the fluorescent proteins. We validated the sensor in bacterial and mammalian cells, and observed FRET efficiencies comparable to ~20% w/w Ficoll in bacterial cells.

Other sensors have been developed, including a synthetic sensor based on polyethylene glycol that is compressed by macromolecular crowding[15], and a genetically-encoded sensor that is based on protein-induced destabilization of an impaired YFP[16]. The PEG-based sensor may function via a similar mechanism as our sensor, while the mechanism behind the destabilization of the YFP sensor is not yet clear. Crowding can also be inferred from diffusion measurements, among other methods[17], but these are strongly dependent on other parameters such as confinement, viscosity, and nonspecific attractive interactions.

Given the multiplicity of parameters that act on a crowding sensor, we argued that a set of sensors would yield a more informative readout of the macromolecular crowding in cells compared to a single sensor. This is especially relevant when *in cell* calibration of the sensor is prohibited, for example during time-lapse recordings. The structural simplicity of the original crowding sensor allows for a relatively straightforward design process to i) determine the effect of structural variations in the linker on the quantification of macromolecular

crowding, and ii) to uncover potential linker-induced artifacts interfering with the *in cell* readouts.

We designed a set of 9 probes (Table 1). We varied the linker and kept the fluorophores the same to exclude effects specific to the fluorescent proteins[18]. The length of the helices and the random coil domains are varied to allow assessment if the linker flexibility and the distance between the fluorophores are affected by crowding[19,20]. In here, we find that the compression of the sensors scales with probe size and volume fraction of crowder. In the cell, only probes with an α-helix in the linker are compressed, pointing to additional contributions to the FRET besides excluded volume when the helix is absent. This set of probes provides more detailed information on the effect of crowding in the cell than a single sensor.

Materials and methods

Plasmid preparation

The gene encoding the crcrGE probe was obtained from GeneArt and subcloned into the pACYC vector in the *Sal*I and *Bam*HI sites. DNA encoding the linker region of crE6G6, crE6G2, crE4G6, crE4G2, crG12, or crG24 (PMK plasmid, GeneArt) was subcloned in the *Xho*I and *Sac*I of pACYC carrying the gene for the crGE probe. Genes encoding the crE6, CRGE, and the crGE probe with the fluorescent proteins swapped (crGEs probe), all in pRSET A, were obtained from GeneArt. The gene encoding the crG18 linker in the PMK plasmid (GeneArt) was subcloned in between the *Bam*HI and *Nco*I sites in the crGE gene in pRSET A. To place the crE6G2 and crG12 genes from pACYC into pRSET A, the genes encoding crE6G2 and crG12 in pACYC plasmid were amplified by PCR (Forward primer: CAAAGGTGAAGAGCTCTTTACCGGTGTTGTTCCGATTC and reverse primer: TTATTTGTACAGCTCGTCCATGCCCAGTG) and digested with *Sac*I and *Eco*RI, and subsequently ligated into pRSET-A containing the crGE gene. *E. coli* MG1655 was transformed with the pACYC plasmids, while *E. coli* BL21(DE3) pLysS (Promega) was transformed with the pRSET A plasmids.

Protein expression

E. coli BL21 (crGES, crGE, crE6, crG18, crG12, or crE6G2 in pRSET A) or E. coli MG1655 (crG24, crE6G6, crE4G2, or crE4G6 in pACYC) were grown to OD_{600} 0.6 in LB medium (10 g/L tryptone, 5 g/L yeast extract, 10 g/L NaCl), and induced with 0.1 mM isopropyl β-D-1-thiogalactopyranoside (IPTG) (pRSET A) or 0.1% rhamnose (pACYC).

After incubation at 25 °C overnight, the cells were spun down at 3000 g for 30 min, resuspended in buffer A (10 mM sodium phosphate (NaP_i), 100 mM NaCl, 0.1 mM phenylmethylsulfonyl fluoride (PMSF), pH 7.4) and lysed in a tissue lyser. The lysate was cleared by centrifugation, supplemented with 10 mM imidazole and the proteins were purified by nickel-nitrilotriacetic acid Sepharose chromatography (wash/elution buffer: 20/250 mM imidazole, 50 mM NaPi, 300 mM NaCl, pH 7.4). The constructs were further purified by Superdex 200 10/300GL size-exclusion chromatography (Amersham Biosciences) in 10 mM NaP_i, pH 7.4. The expression and purification were analyzed by 12% SDS-PAGE, and the bands were visualized by in-gel fluorescence and subsequent Coomassie staining. Fractions containing pure protein were aliquoted and stored at −80 °C.

Fluorometry

The crowding agent was dissolved in 10 mM NaPi, 100 mM NaCl, 2 mg/mL BSA, pH 7.4. The pH was checked after dissolution of crowding agent; crowding agents such as lysozyme and ovomucoid decreased the pH significantly and, considering the pH sensitivity of mCitrine (13), were not tested further. A 1.0-mL solution was placed in a quartz cuvette, and its fluorescence emission spectrum after excitation at 420 nm (for mCitrine and mCerulean3) and 515 nm (for mCitrine as control) were recorded at 20 °C on a Fluorolog-3 (Jobin Yvon) spectrofluorometer. Subsequently, the constructs were added, mixed by pipette and measured. The background spectrum from before the addition of the probe was subtracted.

FRET efficiency determination

The fluorescence emission spectrums were recorded as before[13]: 2.0 µL of Proteinase K (Aldrich, 5.0 mg/mL in water) was added and the solution was mixed by pipette. After incubation at 20 °C for 1 min, the reaction was quenched by addition of 2.0 µL PMSF (100 mM in isopropanol). Longer incubation times before quenching did not alter the spectra. The fluorescence emission spectrum was subsequently recorded. The fluorescence spectra did not change after addition of PMSF. The FRET efficiency was calculated using[21]:

$$\text{FRET efficiency} = 1 - \frac{F_{DA}}{F_D} \quad (1)$$

in which F_{DA} is the intensity of mCerulean3 before the cleavage, and F_D the intensity of mCerulean3 after proteolytic cleavage of the linker.

Confocal fluorescence microscopy

Ratiometric fluorescence emission measurements of *E. coli* by scanning confocal fluorescence microscopy were carried out as reported previously (13). In short, *E. coli* strain BL21(DE3) pLysS containing pRSET-A with the gene encoding the probe (crGE, crG18, crE6, crG12, or crE6G2) was inoculated from a glycerol stock into 10 mL of filter-sterilized MOPS minimal medium supplemented with 20 mM glucose. The culture was grown to OD_{600} = 0.1–0.2. In parallel, the same *E. coli* strain with the pRSET-A plasmid with a gene encoding for a non-fluorescent protein (monomeric streptavidin), functioning as a control and background, was grown to the same OD_{600}. For both cultures the proteins were expressed in the absence of added inducer. The fluorescent cells were mixed with the non-fluorescent cells so as to obtain equal amounts of each cell-type. The combined cells were washed by centrifugation and resuspension in MOPS minimal medium with the desired amount of NaCl, in the absence of K_2HPO_4 and glucose to prevent adaptation of the cells. 10 µL of this mixture was added to a coverslip modified with (3-aminopropyl) triethoxysilane (Aldrich). For imaging, the coverslip was mounted on a laser-scanning confocal microscope (Zeiss LSM 710), the FRET pair was excited using a 405-mm diode laser, and the emission were split into a 450–505 nm channel and a 505–797 nm channel.

For each cell, the 505–797 nm channel (mCitrine) intensity was plotted versus the 450–505 nm channel (mCerulean3) intensity (see *e.g.* Fig. S9). The brightest cells were not analyzed, to minimize artifacts from intermolecular FRET, influences of high expression levels on cell contents, or incomplete maturation of the fluorescent proteins. The data was fitted to a linear equation using a least squares approach, using the slope as the average FRET ratio.

The microscope was calibrated as described previously[13], briefly: A solution of the desired concentration Ficoll PM70 (20 µL, 10 mM NaP_i, 2 mg/mL BSA, 100 mM NaCl, pH 7.4.) was placed onto a coverslip. The microscope settings were the same as the *in vivo* measurement. Three pictures were taken from different locations in the same drop, and this was repeated in 3 different drops. The intensities were determined for the complete image. The same procedure was followed for drops without fluorescent proteins for the background measurement. The ratios were calculated by simple linear regression, using the same methodology as for the *in vivo* measurements. These ratios were plotted versus the ratios obtained in fluorometry, to obtain a conversion relation and hence provide direct comparison between fluorescence microscopy and fluorometry.

Molecular Dynamics Simulations

The coordinates of CPF and YPF were obtained by homology modeling with SWISS-MODEL[22]. For both CFP and YFP the PDB ID: 4en1 was used as a template structure. In Pymol[23] the two proteins were connected by the two different linkers, creating two different sensors: crGE and crG18. The systems were coarse grained and solvated using respectively the martinize.py and insane tools[24,25]. NaCl was added to a concentration of approximately 160 mM and on top of that extra sodium ions were added to neutralize the systems. In the PEG systems, the concentration of PEG was approximately 20% (w/w) (excluding the ions and the sensor); the PEG polymers consist of 136 monomers. The ubiquitin (UBQ) structure was taken from PDB ID: 1UBQ. In the EG and crG18 systems the concentration of ubiquitin was approximately 27% and 20% (w/w), respectively. The composition of the various simulated systems is given in Table S1.

The systems were simulated using Martini 2.2[26] in conjunction with ElNeDyn[26] to restrain the secondary structural motifs. For PEG, the parameterization by Lee *et al.* was used[27]. Test simulations indicated that the fluorescent proteins showed a high tendency to stick together, a known problem of the Martini force field[28]. To increase the kinetics of the opening-closing transition of the sensor, the sensor was therefore made less 'sticky'. This was done by decreasing the Lennard-Jones epsilon value by 0.6 kJ/mol for all interactions between all protein beads (sensor and ubiquitin) and between the protein beads and the PEG beads. No other interactions were modified, i.e. water-water, water-protein, PEG-PEG. Note, decreasing the Lennard-Jones interactions does not result in denaturation of the fluorophores because of the use of ElNeDyn. The ElNeDyn bonds were only placed on the fluorophores and on the alpha helical parts of the sensor, i.e. there were no elastic bonds between the two different α-helices, the two fluorophores or between a fluorophore and an α-helix.

All simulations were performed using GROMACS 4.5.5[29] with the standard Martini parameters[26], at 310 K and at 1 bar pressure. A time step of 20 fs was used for the simulations without PEG, but a 10 fs time step had to be used in the simulations containing PEG for numerical stability. The systems were run for 15 μs and the trajectory was saved every 1 ns. The first 1 μs simulation time was discarded as equilibration time. This results in a total analysis time of 14 μs per simulation.

The simulations were analyzed by calculating the FRET efficiencies. For the calculation of the FRET efficiencies, Eq. S3 was used, with r as the distance between the backbone (BB) beads of the fluorophores. The Förster radius R_0 in Eq. S3 was calculated from $R_0 = 0.211^*(\kappa^2 QnJ)^{1/6}$. We assumed that $R_0 = 5.4$ nm is correct for $\kappa^2 = 2/3$[30], and calculated the remaining factor QnJ based on this.

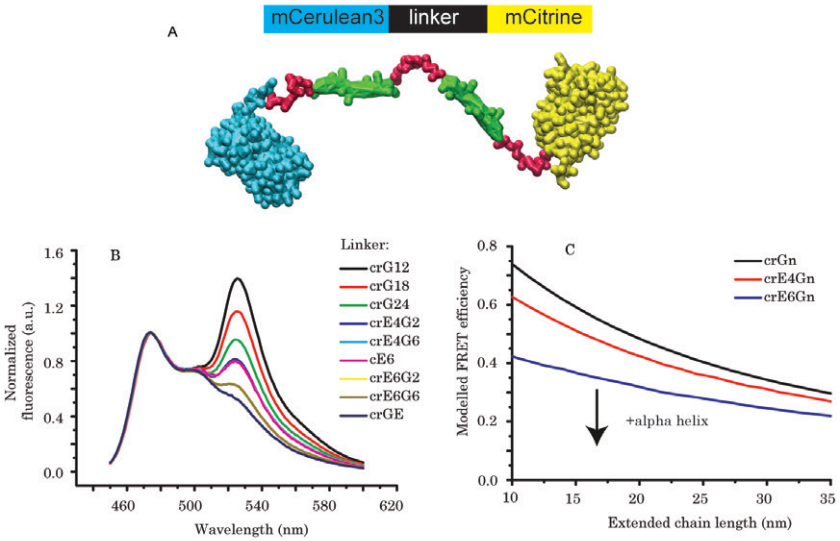

Fig. 1. Characterization of the probes. A: *The previously developed crGE probe served as a template for structural variation in the linker region.* ***B:*** *Normalized fluorescence emission spectra of the probes in dilute buffer (10 mM NaPi, 100 mM NaCl, 2 mg/mL BSA, pH 7.4), showing the range of FRET efficiencies covered.* ***C:*** *The ideal chain model predicts that the FRET efficiencies of the probes in the absence of crowder decrease when α-helices are included in the linker region, as observed experimentally (Table S3 and Fig. S2). Arrow shows direction of increasing α-helix content.*

Subsequently, we calculated the real R_0 for each conformation based on QnJ being known, with the orientation factor κ determined for each conformation from the transition dipole moments of the fluorophores as calculated by Ansbacher *et al.*[31], mapped to the vector between the BB and the SC1 bead. The resulting data are presented in Table S2. From the FRET efficiencies the 'apparent distance' between the fluorophores was calculated. Note, for a more elaborate comparison of simulation data and FRET efficiencies, see the work of Hoefling *et al.*[32]. For the calculation of the density maps (Fig. 3C), the tools developed by Castillo *et al.* were used[33].

Results

Design and in vitro characterization

The probes were designed in a stepwise manner with the parent crGE probe serving as a starting point (Table 1). We removed the outer $(GSG)_6$ sections to decrease the probe size (the crE6Gn family), and

Table 1. *Probe Design and properties*

Acronym	Linker sequence	FRET efficiency[a] (%)	Distance from FRET[b] (nm)
	with α-helix		
crGE	-$(GSG)_6$A$(EAAAK)_6$A$(GSG)_6$A$(EAAAK)_6$A$(GSG)_6$-	11±1	7.6±0.2
crE6G6	-A$(EAAAK)_6$A$(GSG)_6$A$(EAAAK)_6$A-	14.0±0.2	7.3±0.1
crE6G2	-A$(EAAAK)_6$A$(GSG)_2$A$(EAAAK)_6$A-	14.2±0.5	7.3±0.1
crE4G6	-A$(EAAAK)_4$A$(GSG)_6$A$(EAAAK)_4$A-	22.0±0.4	6.7±0.1
crE4G2	-A$(EAAAK)_4$A$(GSG)_2$A$(EAAAK)_4$A-	22.8±0.4	6.6±0.1
crE6	-$(GSG)_6$A$(EAAAK)_6$A$(GSG)_6$-	22.4±0.5	6.6±0.1
	without α-helix		
crG24	-$(GSG)_{24}$-	28.4±0.5	6.3±0.1
crG18	-$(GSG)_{18}$-	34.6±0.6	6.0±0.1
crG12	-$(GSG)_{12}$-	40.9±0.2	5.7±0.1

[a] *Efficiencies determined from the increase in mCerulean3 emission upon proteolytic cleavage as described in Materials and Methods.* [b] *Distances determined from FRET efficiencies using the Förster equation. See Table S3 for more linker properties. Errors are standard deviations based on three independent repeats.*

varied the length of the inner $(GSG)_n$ section, resulting in the crE6G2 and crE6G6 probes. We shortened the α-helix (the crE4Gn family), and again varied the internal $(GSG)_n$ section, resulting in the crE4G2 and crE4G6 probes. To assess whether the two helices interact with each other, we also removed one $(EAAAK)_6$ helix and a $(GSG)_6$ coil from the crGE probe to obtain the crE6 probe. Finally, we removed the α-helices and varied the size of the $(GSG)_n$ linker, the Gn family.

These probes were first characterized in detail in the absence of crowders. We expressed and purified the probes and determined their properties in phosphate buffer by fluorometry (Fig. 1b). The probes exhibit a wide range of FRET efficiencies as observed from the fluorescence emission intensities of mCitrine at 525 nm. For a direct quantification, we measured the increase in mCerulean3 emission upon proteolytic cleavage of the probes (Fig. S1), from which the FRET efficiencies and the corresponding distances (*r0*) between the fluorophores were determined (Table 1). The wide range of FRET efficiencies from 11±1 to 40.9±0.2% (n = 3) correspond to distances between the fluorophores of 7.6±0.2 and 5.7±0.1 nm, respectively. These average distances obtained from FRET are likely smaller than the real average distance between the fluorophores (see Table S2).

The FRET efficiencies vary with length and rigidity of the linker: The FRET efficiency of the Gn family is clearly higher than those of the crE4Gn family, which, in turn, is higher than the crE6Gn family (see also Table S3 and Fig. S2). We can understand these observations qualitatively using simple models from polymer physics (Fig. 1C) (Supporting Material)[34,35]. These models predict that replacing part of

a flexible linker with a more rigid structure will increase the probability that the two ends are far apart, explaining the lower FRET efficiencies of the helix-containing probes. Furthermore, the probability of the two ends being far apart is higher the longer the rigid part of the linker, thus explaining the difference between the crE4Gn and crE6Gn families. A quantitative comparison is more complicated because the persistence length is not known, it is not clear where precisely the helices end, and the fluorescent proteins also need to be considered. Nevertheless, this simple analysis suggests that the probes exhibit polymer-like behavior. These findings are in line with previous findings on random coil and α-helix containing linkers[19,20].

Compression relates to probe size and Ficoll concentration

The effect of crowding on the probes was first studied by addition of the crowding agent Ficoll 70. In all cases the mCitrine/mCerulean3 ratio increased with Ficoll 70 (Fig. 2A). With the exception of crG12, the ratio increased stronger with shorter linkers, which is caused by their proximity to the Förster radius (5.4 nm)[30], where the distance dependence of the FRET efficiency is highest.

We determined the distances (*r*) between the fluorophores in all cases from the FRET efficiency (Fig. S3) and quantified the relative compression by dividing with the distance in the absence of crowder (*r0*). The addition of crowder changes the refractive index, inducing a small deviation in FRET efficiency (36). It would be extremely complicated to correct for the refractive index, because the intervening medium between the fluorophores contains on average less crowder, and the linker contributes to the refractive index. Assuming that the refractive index is 1.4, we underestimate crowding-induced FRET increases by 1-2%. To verify that fluorophore orientation has a negligible effect on the FRET efficiency, we constructed a probe with a circular permuted YFP. Ficoll compresses this probe in the same manner as the crGE probe (Fig. S4), indicating that we only probe the distance changes. When comparing all the probes, we found that all probes are compressed with Ficoll, but that the larger probes also show a larger compression (Fig. 2B,C), of up to 85% of their original size.

Compression is related to crowder radius

Next, we determined compression of the probes with different crowding agents. We selected the crGE, crE6, and crG18 probes, which represent the extreme and intermediate length scales and rigidities of

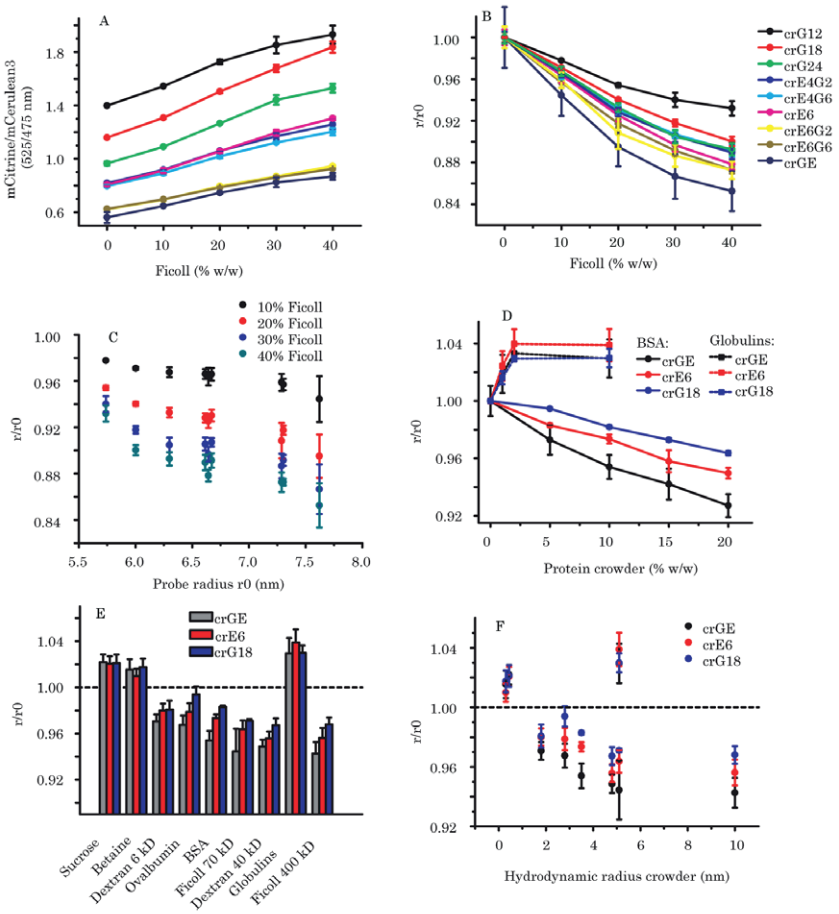

Fig. 2. Determination of in vitro crowding-induced compression of the probes. A: *Ratiometric fluorescence change of the probes upon titration with Ficoll 70.* ***B:*** *Compression (r/r0) of the probes upon addition of Ficoll 70. r0 is the probe radius without crowder, r with crowder, both calculated from the FRET efficiencies.* ***C:*** *The dependence of the compression r/r0 on the probe radius r0, at different Ficoll concentrations; the same data as in panel B.* ***D:*** *The effect of BSA and γ-Globulins at different weight% on r/r0.* ***E:*** *The effect of various small molecules and macromolecular crowders, all at 10 % w/w, on r/r0.* ***F:*** *The compressions obtained for the various crowders plotted versus their hydrodynamic radius (Table S4). All experiments in 10 mM NaPi, 100 mM NaCl, 2 mg/mL BSA, pH 7.4. Data represent the mean ± SD of three independent experiments.*

the other probes well. Bovine serum albumin (BSA) induced compression of the probes with a similar trend and concentration dependence as Ficoll 70 (Fig. 2D). The probes expanded in the presence of small amounts (1% w/w) of γ-Globulins, which suggests that γ-Globulins bind the probes. The probes did not expand further by addition of

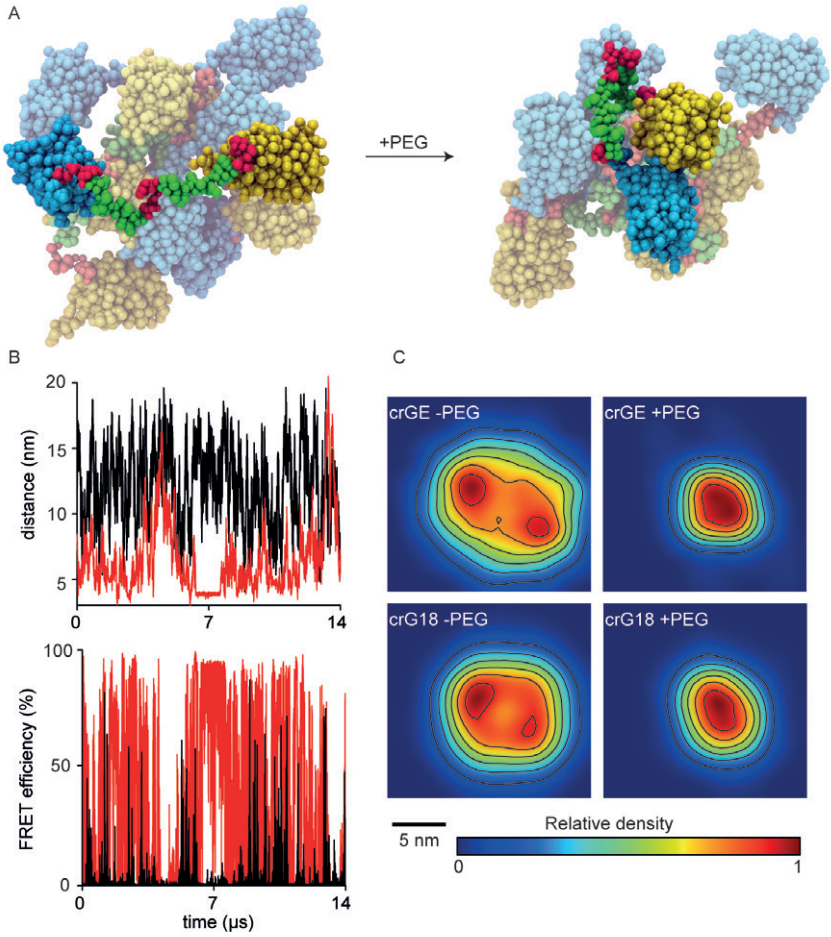

Fig. 3. Coarse-grained molecular dynamic simulations of the crGE and crG18 probes. ***A:*** *Snapshots of conformations of the crGE probe without crowder and in the presence of polyethylene glycol 6000 (PEG). For clarity, only one probe conformation is highlighted.* ***B:*** *Time traces of the distance and calculated FRET efficiency of the crGE probe with (red) and without (black) PEG.* ***C:*** *Normalized number densities of the crGE and crG18 probes projected in 2D space, plotted on distance coordinates, with and without crowding with PEG. The scale bar applies to the x- and y-axis.*

10% w/w γ-Globulins, which could be due to saturation of binding sites, balancing excluded volume effects[9], or the decrease of attractive interactions of concentrated antibodies[37,38]. We observed compression of the three probes in the presence of a variety of macromolecular crowders based on the carbohydrates Ficoll 70 kD and 400 kD, Dextran 40 kD and 6 kD, and the proteins BSA and ovalbumin, all at 10% w/w (Fig. 2E). In all these cases the probes compressed with a

magnitude that depended on the probe and the crowder (Fig. 2F): Compression followed probe size (crGE>crE6>crG18), while the dependence on the crowder hydrodynamic radius (Table S5), for fixed crowder weight%, seemed to level off at ~2-4 nm. We have previously observed the same behavior for crGE in the presence of PEGs of varying weight[13]. Small molecules such as sucrose and glycine betaine (each at 10% w/w) did not compress the probes (Fig. 2E). The small apparent expansion of the probes of ~1-2% can at least partially be explained by the increase in refractive index upon dissolution of these solutes. Application of a mix of the four most abundant metabolites in *Escherichia coli* at their *in vivo* concentrations (potassium salts of 100 mM glutamate, 20 mM glutathione, 15 mM fructose bisphosphate, and 10 mM ATP)[39], or the application of high concentrations of salt (up to 500 mM NaCl) did not lead to an appreciable change in the FRET value (Fig. S5 and S6).

In summary, these experiments show that the probes respond to macromolecular crowding by compression, which is related to the weight percent of crowder, the probe radius, and the crowder radius. The compression is absent for small molecules and crowders with associative interactions.

Molecular dynamics simulations confirm dependence on radii

To verify our experimental observations on the probe- and crowder-size dependent compression, we performed coarse grained molecular dynamics simulations[40,41]. We simulated the crGE and crG18 probes in the absence and presence of PEG 6000 or ubiquitin (Fig. 3, Table 2), which represent a polymer- and a protein-based crowder. In experiment, we found that 20 %w/w PEG 6000 compresses crG18 to an r/r_0 of ~0.88, and we previously[13] found for crGE an r/r_0 of ~0.80. The simulations showed qualitative agreement with these experimental

Table 2. *FRET Efficiencies and distances obtained from 14 μs molecular dynamic simulations. Errors are standard errors calculated from the means of blocks of 3.5 μs.*

	FRET Efficiency (%)	Distance from FRET (nm)
crGE		
No crowder	2.7±0.4	9.8±0.2
Ubiquitin	4.3±1.6	9.1±0.5
PEG 6000	36.6±4.4	5.9±0.2
crG18		
No crowder	13.8±0.4	7.3±0.04
Ubiquitin	18.4±2.6	6.9±0.2
PEG 6000	54.9±15.7	5.2±0.9

results: in both cases the addition of PEG resulted in compression of the probes, as was clearly apparent from the densities (Fig. 3C), leading to higher FRET efficiencies. The compression r/r_0 obtained from the simulations was ~0.60 for crGE, and ~0.71 for crG18, which confirmed the probe-size dependence qualitatively. The compression in the simulations was higher than in the experiments, which may relate to the difference in timeframe or the simulation parameters. Note, due to the coarse-graining of the interactions, the MD results are qualitative rather than quantitative. The behavior of the probes both with and without crowder could be described by a single population of FRET efficiencies on this timescale, albeit that in the presence of PEG both in the case of crG18 and the crGE probe an additional population appeared that represented one long-term event (at ~7 μs for crGE in Fig. 3B) where the two fluorophores dimerize. Although such events could indeed occur in experiment, the average FRET in the simulations increased upon addition of PEG without this additional population in a similar manner, and hence was not required to explain compression of the probes. The addition of ubiquitin (Table 2) lead to a smaller compression of the sensor, r/r_0 ~0.93, which is consistent with the smaller radius of ubiquitin. These data show that crowding-induced compression can be mimicked by simulation, and that the radii dependence is also observed in the simulations.

Probe compression in living cells depends on the linker composition

We selected 5 probes for *in vivo* assessment of probe performance. We expressed the probes in *E. coli* BL21(DE3) and analyzed the cells in the exponential growth phase in MOPS minimal media at OD 0.1–0.2. Under these conditions the concentration of the probes is constant over time (Fig. S7). *In gel* fluorescence of lysed cells under measurement condition show that the probes are intact (Fig. S8). The intensities of the fluorophore emissions were determined by scanning confocal microscopy after excitation of mCerulean3 at 405 nm and subsequent determination of the mCitrine/mCerulean3 emission ratio (Fig. S9). As a further control, we constructed a probe in which the mCitrine and the mCerulean3 are swapped. The swapped probe has similar fluorescent ratios as the parent crGE probe (1.03±0.01 versus 1.06±0.02), further confirming the presence of intact probes.

Fig. 4A shows that the *in cell* mCitrine/mCerulean3 ratios of the probes followed the same order as *in vitro*. We imposed osmotic upshifts by adding NaCl to the medium to test whether the probes are sensitive to crowding in cells[13]. The osmotic upshift was performed in the absence of potassium and glucose to prevent (rapid) recovery

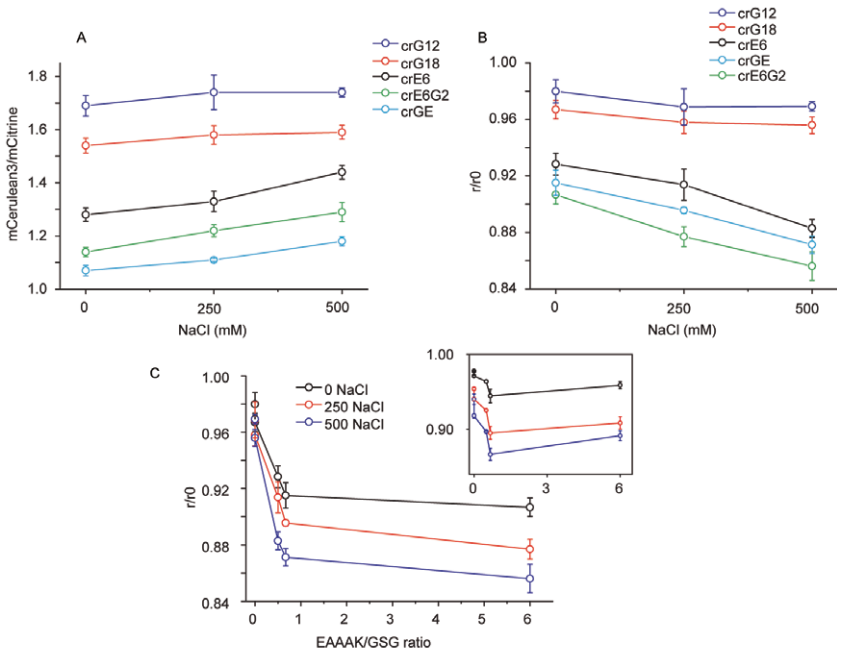

Fig. 4. Analysis of the compression of the probes in E. coli cells. A: *YFP/CFP ratios of the different probes, and change in YFP/CFP ratio upon osmotic upshift. Data represent the mean ± SD of three independent experiments.* ***B:*** *Compression (r/r0) of the probes in cells and effect of osmotic upshift.* ***C:*** *Dependence of the compression on the (EAAAK)/(GSG) ratio in the linker. Inset: In vitro dependence on the (EAAAK)/(GSG) ratio in the presence of 10 (black), 20 (red), and 30 (blue) % w/w Ficoll 70. Data taken from Fig. 2B.*

of the cell volume, and the cells were measured within 10 minutes to prevent alterations of the proteome. Furthermore, because the probes are less sensitive to small molecules (*vide supra*), we expect that the increase in crowding will dominate the readouts. Only a small transient increase of the cytoplasmic pH from ~7.9 to ~8.2 will occur upon a 500 mM NaCl-induced osmotic upshift[42], and hence the pH is unlikely to influence our measurements. The osmotic upshift increased the mCitrine/mCerulean3 ratio of the helix-containing probes (crE6, crE6G2), similar to the increase of the crGE probe we reported previously[13]. The ratios of the Gn family, on the other hand, barely increase. The crGE and crG18 probes diffuse roughly as rapid as GFP (Fig. S10), which diffuses without binding to slow moving cell components, showing that the difference in response between families is not due to binding to a slow diffusing cell component that alters FRET efficiency.

We calibrated the YFP/CFP ratios in cells with the ratios of purified probes in the presence of Ficoll in microscopy. Next, we relate this microscopy data to fluorometry ratios (Fig. S11). This allowed

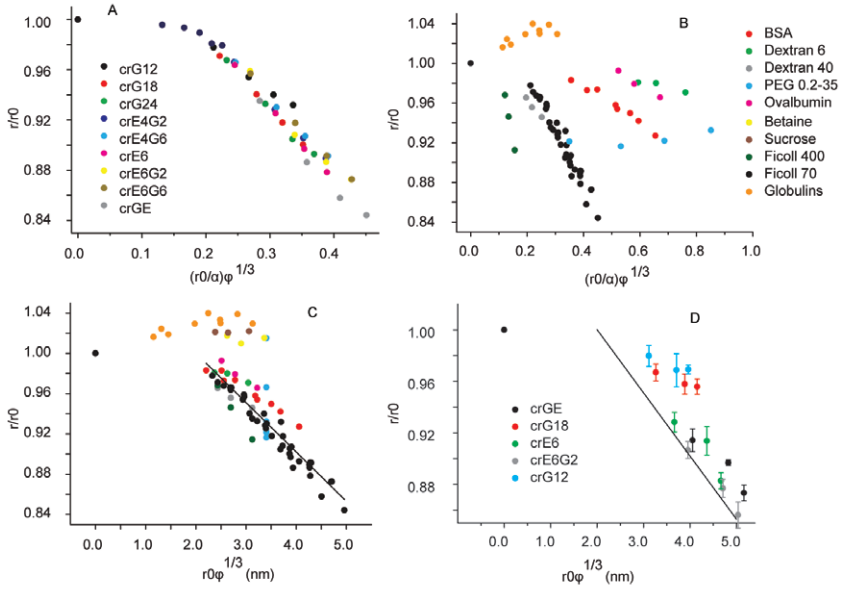

Fig. 5. Scaling behavior of crowding-induced probe compression. ***A:*** *Compression of the probes by Ficoll 70 fulfills a scaling relation, involving the probe size, the crowding agent radius, σ, (Table S5) and the crowder volume fraction, Φ (determined from the partial specific volume; Table S4). Data reproduced from Fig. 2B, with additional data for the crGE probe with 1, 2, 3, 4, 5 % w/w Ficoll 70 to show the plateau at low volume fractions.* ***B****: Scaling relation of the compression for a range of crowding agents. Data reproduced from Fig. 2E; additionally, the PEG data of 0.2, 1.5, 4, 6, 10, 20, 35 kD at 10% w/w with the crGE probe is taken from ref. 13, and displayed in more detail in Fig. S12. The values for the small molecules sucrose, betaine, and PEG 0.2 kD are off scale and not displayed.* ***C:*** *Plotting the data of panel B against r0φ1/3 rather than (r0/σ)φ1/3 results in a collapse of the data onto a single master curve. The line is a linear fit of the probes with all crowding agents that are within the stated boundary conditions (hence excluding small molecules and γ-globulins), and excluding the data point without crowder that is not in the linear regime.* ***D:*** *Comparison of in cell compression with the modified scaling relation of Fig. 5C, using reported volume fractions for E. coli (34). The line is from Fig. 5C, and experimental data from Fig. 4B.*

converting *in cell* data to *in vitro* fluorescence ratios, and thereby determination of FRET efficiencies and subsequent FRET distances (Fig. 4B). The conversion emphasizes the observed trends of Fig. 4A: The Gn probes were much less compressed in the cell and their FRET distances are within ~4% of the distances in dilute buffer. However, the presence of α-helices (crE6, crE6G2 and crGE) gave rise to a significant compression of over 10%. The compression relates with the helical content of the probes, described as the (EAAAK)/(GSG) ratio (Fig 4C). The compression did not follow the (EAAAK)/(GSG) ratio in the case of Ficoll crowding *in vitro* (Fig. 4C, inset). Indeed, in the cell

the crE6G2 probe was more compressed than the larger crGE probe, which relates to a higher (EAAAK)/(GSG) ratio of 6.0 versus 0.67, respectively. This data shows that, contrary to the *in vitro* conditions, the helices in the linker region are required for the compression of this set of probes by macromolecular crowding in living cells.

Compression follows a scaling relation

Next, we developed a description that could capture our observations. We first noticed that the *in vitro* compressions are qualitatively similar to those obtained for intrinsic disordered proteins in the presence of PEG as reported by Schuler and coworkers[43]. They explained the behavior of intrinsic disordered proteins by a renormalized Flory-Huggins theory, and hence this theory would likely fit the results of the probes used here upon adjustment of the fitting parameters. Scaled particle theory, Gaussian cloud scaled particle theory and Flory-Huggins theory did not fit their data, suggesting these theories would also not fit our data.

Kang *et al*. proposed to explain the data of Schuler and coworkers using an alternative approach[44]. Although their approach is not microscopic, we find that it gives a surprisingly accurate description that is simple enough to use on *in cell* data, something a truly microscopy description would not allow. The work of Kang *et al.* is based on the idea of two competing length scales, namely the size of the probe in the absence of crowding, *r0*, and the distance between crowders, *D*. If these are the only important length-scales, then the compression of the probe in the presence of crowding would fulfill a scaling relation, that is, $r/r_0 = f(r_0/D)$; r/r_0 depends on the ratio of the size of the probe under dilute conditions (r_0) to the distance between crowders (D). The distance between crowders can be readily estimated from the volume fraction of crowder (φ, Table S4) and the radius of the crowder (σ, Table S5) as $D \propto \sigma/\varphi^{1/3}$. We tested this *ansatz* on the measured compression of the probes by Ficoll 70 (Fig. 2A), by plotting r/r_0 *versus* $(r_0/\sigma)\varphi^{1/3}$. Interestingly, the results for all probes collapse onto a single master curve (Fig. 5A), showing that the probes are well described by this scaling relation.

The relation works well when comparing different probes, but the data no longer falls onto a single master curve when comparing different crowding agents (Fig. 5B). However, we find empirically that by excluding the size of the crowder the results again largely fall upon a single master curve (Fig. 5C). The residual dependence on the crowder size (Fig. S12) is much smaller than that in Fig. 5B. The heuristic master curve describes the compression of a large number of probes by several crowding agents. Importantly, we make the same observation

when re-analyzing the data of Schuler and coworkers on crowding effects on a set of intrinsically disordered proteins (Fig. S13)[43]. Thus, the same scaling relation is fulfilled by two independent experimental data sets. A potential justification for our modification of the original scaling *ansatz* may be that other distances than the two originally included (probe size and distance between crowders) could have a compensating effect. Notably, the crowder size is not explicitly included in the original *ansatz* but only enters implicitly through converting the distance between crowders to volume fraction; including this length scale explicitly could compensate for the implicit dependence from the distance between crowders. The volume fraction itself is a function of crowder size and number density and hence these parameters do influence probe compression. Furthermore, the crowder size is not constant throughout the concentration regime, as crowding agents such as Ficoll and PEG compress.

We prefer to use our modified scaling relation because of its simplicity and predictive nature. However, we stress that three important boundary conditions must be satisfied to use this empirical scaling relation as a "calibration curve" (Fig. 5C; line) for interpretation of *in cell* measurements: i) compression occurs at values of $r_0\varphi^{1/3} > 2$ nm; ii) for crowder sizes < 1–2 nm the compression becomes less; and iii) attractive interactions expand the probes. In our dataset, Ficoll 70 contributes most to the curve, and small deviations may occur when using crowders with a different radius. A range of other factors including the shape of the crowder, interactions of the crowders with itself, solvent properties, and intramolecular interactions were apparently not strong enough to change the scaling behavior.

We next apply the relation to interpret the dependence of *in cell* compression on the probe structure. We use previously determined macromolecule volume fractions inside cells from dry weight[45], and can thereby test the scaling *ansatz* also on *in cell* data, using osmotic upshifts to increase the intracellullar crowding. We find that, even though the cytoplasm provides a vastly more complicated environment than the artificial crowding agents, the helix-containing probes (here crGE, crE6, and crE6G2) follow the master curve measured with artificial crowders reasonably well, both without and with osmotic upshift (Fig. 5D, Fig S14). Especially the *in cell* data for the crE6G2 probe collapses very well onto the calibration line. The Gn family yields smaller compressions inside cells than predicted on the basis of the calibration line, also with osmotic upshift. This behavior can also be seen directly by comparing the lack of increase in ratio of the Gn after osmotic upshift (Fig. 4A) versus the addition of Ficoll (Fig. 2A). When we perform the same analysis but instead use the calibration curve to *calculate* the volume fraction, we see that the volume fractions reflect the (EAAAK)/(GSG) ratio in the linker (Fig S15): The crE6G2 probe yields the highest

volume fractions, followed by crGE and crE6, while crG18 and crG12 sense the lowest volume fractions. As expected based on Fig. 5D, good agreement with the volume fractions obtained from cell dry weight is obtained for those determined with the crE6G2 probe.

Thus, compression of this set of probes follows a scaling behavior involving the size of the probe and the volume fraction of crowder, while in the cell deviation from the scaling behavior occurs for linkers that do not contain the helices.

Discussion

In this paper, we describe a set of FRET-based compression-sensitive protein probes. We find that (a) all probes sense macromolecular crowding, with a magnitude that depends on the probe size and crowder volume fraction (which is a function of crowder radius and concentration), and (b) the *in cell* sensitivity depends on the linker composition, where only the α-helix containing probes show an increase in FRET efficiency.

This set of probes provides more detailed information on macromolecular crowding effects. It also highlights the difference between *in cell* and *in vitro* readouts of FRET-based probes, and warrants care when quantitatively interpreting *in cell* data. We calibrate the sensors by means of osmotic upshift, and comparison with known macromolecule volume fractions and *in vitro* crowding. This is currently the best approach to vary the internal crowding, because other methods such as overexpression of proteins take longer and would lead to adaptation of cells. We previously showed that the volume fraction increase as determined with the crGE probe corresponds well to the cell volume decrease induced with an osmotic upshift[13]. *In vitro* compression is eventually limited by the solubility of crowding agent, because the probes can be compressed continuously, and hence it is not possible to saturate the probe readout in a cell. The absence of a FRET increase with osmotic upshift for the Gn family makes it less likely that the higher FRET in cells for the other probes are due to photophysical artifacts such as maturation or stability.

It is not directly clear from the data why the Gn family is not compressed in the cell. In lieu of direct evidence, we can hypothesize that nonspecific chemical interactions with the linker region occur, which can be prevented by the (EAAAK)n peptides. More specifically, the shielding of the peptide backbone by the helical conformation could prevent interactions between the backbone and the crowder. This would also explain the dependence on the (EAAAK)/(GSG) ratio. Additionally, the helices contain ion-paired lysines and glutamates, which are preferentially hydrated over interactions with other amino acids, and are the most common paired amino acids on cytosolic protein

surfaces[46]. The incorporation of paired lysines and glutamates would prevent interactions, allowing steric effects to govern the conformation. In general, the observation that *in cell* behavior is different compared to *in vitro* crowding is not very surprising: Chemical nonspecific interactions seem to dominate over the steric crowding for most reported small proteins[6–12]. Hence this is the most likely explanation, and it is remarkable that the steric compression appears to be regained by the presence of these helices. Various other explanations can be put forward, such as specific interactions with the helices or helix destabilization. However, considering the high stability of the (EAAAK) helix[47], and the absence of precedence of helix destabilization inside cells, we deem these explanations less likely. Specific autocleavage of the (EAAAK) helix has been reported[48], but we do not see new bands appearing after cell lysis, nor do we see fluorescence changes in long term *in vitro* experiments. Another possibility would be repulsive charge-charge interactions of the helices with their environment. However, we do not see the same trends *in vitro* with the negatively charged bovine serum albumin. Small molecules such as betaine, sucrose, and PEG 0.2 kD compensate the readout, but do so to a very small extent in the presence of crowders (data not shown), and do not allow the distinction between the families that we see in the cell.

It is highly encouraging that the crE6G2 probe yields volume fractions equal to previous determined volume fractions from dry weight measurements[45]. Both our experiments and the dry-weight determination have been performed under the same conditions. However, the *in cell* readout should not only depend on the volume fraction (or weight% of macromolecules), but also on how well a cytoplasm is mixed. If for example higher crowded regions (due to an increased affinity between the cytosolic proteins, possibly combined with size-sorting by the depletion interaction) or regions with only smaller crowders exist[49,50], it may induce inhomogeneous distribution of the sensor to the less crowded regions. Inhomogeneous distribution could potentially occur under for example starvation conditions, or when other stresses are imposed on the cell[51–53]. In these cases the probes may indicate changes in the superstructure of the cytoplasm, especially when combined with classical volume fraction determinations from cell dry weight and probe diffusion measurements[45,17].

Conclusions

We present a new set of crowding-sensitive probes, which we characterize extensively with a variety of methods and conditions. We show that the compression induced by crowding agents fulfills a scaling relation involving the volume fraction of crowder and the radius

of the probe. In the cell, we find that (EAAAK) repeat units in the linker region of the proteins are required to compress the probes and to obtain the same scaling behavior as *in vitro*. The Gn family of probes serves as a control that is not compressed, while the crE6G2 probe is compressed most in *E. coli*. We encourage to use this set of sensors to observe possible effects other than steric repulsion, and also because the new probes provide higher sensitivity.

References

1. Zimmerman, S. B., and S. O. Trach. Estimation of macromolecule concentrations and excluded volume effects for the cytoplasm of Escherichia coli. *J. Mol. Biol.* **222**:599-620. (1991).
2. Zhou, H. X., G. Rivas, and A. P. Minton. Macromolecular crowding and confinement: biochemical, biophysical, and potential physiological consequences. *Annu. Rev. Biophys.* **37**:375-397. (2008).
3. Gnutt, D., and S. Ebbinghaus. The macromolecular crowding effect--from in vitro into the cell. *Biol. Chem.* **397**:37-44. (2016).
4. Guo, M., and M. Gruebele. Spatiotemporal fluctuations of protein folding in living cells. In Molecular Science of Fluctuations Toward Biological Functions. M. Terazima, M. Kataoka, R. Ueoka, and Y. Okamoto, editors. Springer, Tokyo, Japan, pp. 205-219, (2015).
5. Rivas, G., and A. P. Minton. Macromolecular crowding in vitro, in vivo, and in between. *Trends Biochem. Sci.* **41**:970-981. (2016).
6. Smith, A. E., L. Z. Zhou, A. H. Gorensek, M. Senske, and G. Pielak. In-cell thermodynamics and a new role for protein surfaces. *Proc. Natl. Acad. Sci. U. S. A.* **113**:1725-1730. (2016).
7. Monteith, W. B., R. D. Cohen, A. E. Smith, E. Guzman-Cisneros, and G. J. Pielak. Quinary structure modulates protein stability in cells. *Proc. Natl. Acad. Sci. U. S. A.* **112**:1739-1742. (2015).
8. König, I., A. Zarrine-Afsar, M. Aznauryan, A. Soranno, B. Wunderlich, F. Dingfelder, J. C. Stüber, A. Plückthun, D. Nettels, and B. Schuler. Single-molecule spectroscopy of protein conformational dynamics in live eukaryotic cells. *Nat. Methods* **12**:773-779.(2015).
9. Groen, J., D. Foschepoth, E. te Brinke, A. J. Boersma, H. Imamura, G. Rivas, H. A. Heus, and W. T. Huck. Associative interactions in crowded solutions of biopolymers counteract depletion effects, *J. Am. Chem. Soc.* **137**:13041-13048. (2015).
10. Guzman, I., H. Gelman, J. Tai, and M. Gruebele. The extracellular protein VlsE is destabilized inside cells. *J. Mol. Biol*. **423**:11-20. 2014.
11. Guo, M., Y. Xu, and M. Gruebele. Temperature dependence of protein folding kinetics in living cells. *Proc. Natl. Acad. Sci. U. S. A.* **109**:17863-17867. (2012).
12. Danielsson, J., X. Mu, L. Lang, H. Wang, A. Binolfi, F. X. Theillet, B. Bekei, D. T. Logan, P. Selenko, H. Wennerström, and M. Oliveberg. Thermodynamics of protein destabilization in live cells. *Proc. Natl. Acad. Sci. U. S. A.* **112**:12402-12407. (2015).

13. Boersma, A. J., I. S. Zuhorn, and B. Poolman. A sensor for quantification of macromolecular crowding in living cells. *Nat. Methods* **12**:227-229. (2015).
14. Markwardt, M. L., G. J. Kremers, C. A. Kraft, K. Ray, P. J. C. Cranfill, K. A. Wilson, R. N. Day, R. M. Wachter, M. W. Davidson, and M. A. Rizzo. An improved cerulean fluorescent protein with enhanced brightness and reduced reversible photoswitching. *Plos One* **6**:e17896. (2011).
15. Gnutt D, M. Gao, O. Brylski, M. Heyden, and S. Ebbinghaus. Excluded-volume effects in living cells. Angew. Chem. Int. Ed. Engl. 54:2548-2551. (2015).
16. Morikawa, T. J., H. Fujita, A. Kitamura, T. Horio, J. Yamamoto, M. Kinjo, A. Sasaki, H. Machiyama, K. Yoshizawa, T. Ichimura, K. Imada, T. Nagai, and T. M. Watanabe. Dependence of fluorescent protein brightness on protein concentration in solution and enhancement of it. *Sci. Rep*. *6*: 22342. (2016).
17. van den Berg, J., A. J. Boersma, and B. Poolman. Microorganisms maintain crowding homeostasis. Nature Rev. Microbiol. doi:10.1038/nrmicro.2017.17. (2017).
18. Dave, K., H. Gelman, C. T. Thu, D. Guin, and M. Gruebele. The effect of fluorescent protein tags on phosphoglycerate kinase stability is nonadditive. *J. Phys. Chem. B* **120**:2878-2885. (2016).
19. Li, G., Z. Huang, C. Zhang, B. J. Dong, R. H. Guo, H. W. Yue, L. T. Yan, and X. H. Xing. Construction of a linker library with widely controllable flexibility for fusion protein design. *Appl. Microbiol. Biotechnol*. **100**:215-225. (2016).
20. Evers, T. H., E. M. van Dongen, A. C. Faesen, E. W. Meijer, and M. Merkx. Quantitative understanding of the energy transfer between fluorescent proteins connected via flexible peptide linkers. *Biochemistry* **45**:13183-13192. (2006).
21. Lakowicz, J. R. Principles of Fluorescence Spectroscopy, 3rd edition, Springer, New York, NY, p. 446. (2006)
22. Biasini, M., S. Bienert, A. Waterhouse, K. Arnold, G. Studer, T. Schmidt, F. Kiefer, T. Gallo Cassarino, M. Bertoni, L. Bordoli, and T. Schwede. SWISS-MODEL: modelling protein tertiary and quaternary structure using evolutionary information. *Nucleic Acids Res*. **42**:W252–8. (2014)
23. Schrödinger, L. L. C. The PyMOL Molecular Graphics System. Version 1.7.0.0. (2010).
24. de Jong, D. H., G. Singh, W. F. D. Bennett, C. Arnarez, T. A. Wassenaar, L. V. Schäfer, X. Periole, D. P. Tieleman, and S. J. Marrink. Improved parameters for the Martini coarse-grained protein force field. *J. Chem. Theory Comput*. **9**:687–697. (2013).
25. Wassenaar, T. A., H. I. Ingólfsson, R. A. Böckmann, D. P. Tieleman, and S. J. Marrink. Computational lipidomics with insane: a versatile tool for generating custom membranes for molecular simulations. *J. Chem. Theory Comput*. **11**:2144–2155. (2015).
26. Periole, X., M. Cavalli, S. J. Marrink, and M. A. Ceruso. Combining an elastic network with a coarse-grained molecular force field: Structure, dynamics, and intermolecular recognition. *J. Chem. Theory Comput.* **5**:2531–2543. (2009).
27. Lee, H., A. H. de Vries, S. J. Marrink, and R. W. Pastor. A coarse-grained model for polyethylene oxide and polyethylene glycol: conformation and hydrodynamics. *J. Phys. Chem. B* **113**:13186–13194. (2009).
28. Stark, A. C., C. T. Andrews, and A. H. Elcock. Toward optimized potential functions for protein-protein interactions in aqueous solutions: osmotic second virial

coefficient calculations using the MARTINI coarse-grained force field. *J. Chem. Theory Comput*. **9**:4176–4185. (2013).

29. Hess, B., C. Kutzner, D. van der Spoel, E. Lindahl. 2008. GROMACS 4: Algorithms for highly efficient, load-balanced, and scalable molecular simulation. *J. Chem. Theory Comput*. **4**:435–447.
30. Rizzo, M. A., G. Springer, K. Segawa, W. R. Zipfel, and D. W. Piston. Optimization of pairings and detection conditions for measurement of FRET between cyan and yellow fluorescent proteins. *Microsc. Microanal.* **12**:238-254. (2006).
31. Ansbacher, T., H. K. Srivastava, T. Stein, R. Baer, M. Merkx, and A. Shurki. Calculation of transition dipole moment in fluorescent proteins--towards efficient energy transfer. *Phys. Chem. Chem. Phys*. **14**:4109–4117. (2012).
32. Hoefling, M., N. Lima, D. Haenni, C. A. M. Seidel, B. Schuler, and H. Grubmüller. Structural heterogeneity and quantitative FRET efficiency distributions of polyprolines through a hybrid atomistic simulation and Monte Carlo approach. *Plos One* **6**:e19791. (2011).
33. Castillo, N., L. Monticelli, J. Barnoud, and D. P. Tieleman. Free energy of WALP23 dimer association in DMPC, DPPC, and DOPC bilayers. *Chem. Phys. Lipids* **169**:95–105. (2013).
34. de Gennes, P. G. Scaling Concepts in Polymer Physics. Cornell University Press, Ithaca, N.Y. (1979).
35. Doi, M. Introduction to Polymer Physics. Clarendon Press, Oxford, UK. (1996).
36. Knox, R. S., and H. van Amerongen. Refractive Index Dependence of the Förster Resonance Excitation Transfer Rate. *J. Phys. Chem. B* **106**:5289-5293. (2002).
37. Yadav, S., T. M. Laue, D. S. Kalonia, S. N. Singh, and S. J. Shire. The influence of charge distribution on self-association and viscosity behavior of monoclonal antibody solutions. *Mol. Pharm*. **9**:791-802. (2012).
38. Yearley, E. J., I. E. Zarraga, S. J. Shire, T. M. Scherer, Y. Gokarn, N. J. Wagner, and Y. Liu. Small-angle neutron scattering characterization of monoclonal antibody conformations and interactions at high concentrations. *Biophys. J.* **105**:720-731 (2013).
39. Bennett, B. D., E. H. Kimball, M. Gao, R. Osterhout, S. J. Van Dien, and J. D. Rabinowitz. Absolute metabolite concentrations and implied enzyme active site occupancy in Escherichia coli. *Nat. Chem. Biol.* **5**:593-599. (2009).
40. Ingólfsson, H. I., C. A. Lopez, J. J. Uusitalo, D. H. de Jong, S. M. Gopal, X. Periole, and S. J. Marrink. The power of coarse graining in biomolecular simulations. Wiley Interdiscip. *Rev. Comput. Mol. Sci*. **4**:225-248. (2014).
41. de Jong, D. H., G. Singh, W. F. Bennett, C. Arnarez, T. A. Wassenaar, L. V. Schäfer, X. Periole, D. P. Tieleman, and S. J. Marrink. Improved parameters for the martini coarse-grained protein force field. *J. Chem. Theory Comput*. **9**:687-697. (2013).
42. Dinnbier, U., E. Limpinsel, R. Schmid, and E. P. Bakker. Transient accumulation of potassium glutamate and its replacement by trehalose during adaptation of growing cells of Escherichia coli K-12 to elevated sodium chloride concentrations. *Arch. Microbiol.* **150**:348-357. (1988).
43. Soranno, A., I. König, M. B. Borgia, H. Hofmann, F. Zosel, D. Nettels, and B. Schuler. Single-molecule spectroscopy reveals polymer effects of disordered proteins in crowded environments. *Proc. Natl. Acad. Sci. U. S. A.* **111**:4874-4879. (2014).

44. Kang, H., P. A. Pincus, C. Hyeon, and D. Thirumalai. Effects of macromolecular crowding on the collapse of biopolymers. *Phys. Rev. Lett.* **114**:068303. (2015).
45. Konopka, M. C., K. A. Sochacki, B. P. Bratton, I. A. Shkel, M. T. Record, and J. C. Weisshaar. Cytoplasmic protein mobility in osmotically stressed Escherichia coli. *J. Bacteriol.* **191**:231-237. (2009).
46. White, A. D., A. K. Nowinski, W. Huang, A. J. Keefe, F. Sun, and S. Jiang. Decoding nonspecific interactions from nature. *Chem. Sci.* **3**:3488-3494. (2012).
47. Marqusee, S., V. H. Robbins, and R. L. Baldwin. Unusually stable helix formation in short alanine-based peptides. *Proc. Natl. Acad. Sci. U. S. A.* **86**:5286-5290. (1989).
48. Wu, Y. J., C. Y. Fan, and Y. K. Li. Protein purification involving a unique auto-cleavage feature of a repeated EAAAK peptide. *J. Chromatogr. B Analyt. Technol. Biomed. Life Sci.* **877**:4015-4021. (2009).
49. Spitzer, J., and B. Poolman. The role of biomacromolecular crowding, ionic strength, and physicochemical gradients in the complexities of life's emergence. *Microbiol. Mol. Biol. Rev.* **73**:371-388. (2009).
50. Spitzer, J., and B. Poolman. How crowded is the prokaryotic cytoplasm? *FEBS Lett.* **587**:2094-2098. (2013).
51. Munder, M. C., D. Midtvedt, T. Franzmann, E. Nüske, O. Otto, M. Herbig, E. Ulbricht, P. Müller, A. Taubenberger, S. Maharana, L. Malinovska, D. Richter, J. Guck, V. Zaburdaev, and S. Alberti. A pH-driven transition of the cytoplasm from a fluid- to a solid-like state promotes entry into dormancy. *Elife* **5**:09347. (2016).
52. Joyner, R. P., J. H. Tang, J. Helenius, E. Dultz, C. Brune, L. J. Holt, S. Huet, D. J. Müller, and K. Weis. A glucose-starvation response regulates the diffusion of macromolecules. *Elife* **5**:09376. (2016).
53. Parry, B. R., I. V. Surovtsev, M. T. Cabeen, C. S. O'Hern, E. R. Dufresne, and C. Jacobs-Wagner. The bacterial cytoplasm has glass-like properties and is fluidized by metabolic activity. *Cell* **156**:183-194. (2014).
54. Mika, J. T., P. E. Schavemaker, V. Krasnikov, and B. Poolman. Impact of osmotic stress on protein diffusion in Lactococcus lactis. *Mol. Microbiol.* **94**:857-870. (2014).
55. Mika, J. T., V. Krasnikov, G. van den Bogaart, F. de Haan, and B. Poolman. Evaluation of pulsed-FRAP and conventional-FRAP for determination of protein mobility in prokaryotic cells. *Plos One* **6**:e25664. (2011).
56. Christiansen, A., Q. Wang, A. Samiotakis, M. S. Cheung, and P. Wittung-Stafshede. Factors defining effects of macromolecular crowding on protein stability: an in vitro/in silico case study using Cytochrome C. *Biochemistry* **49**:6519-6530. (2010).
57. Mika, J. T., and B. Poolman. Macromolecule diffusion and confinement in prokaryotic cells. *Curr. Opin. Biotechnol.* **22**:117-126. (2011).

Supporting information: Design and Properties of Genetically-Encoded Probes for Sensing Macromolecular Crowding

Boqun Liu, Christoffer Åberg, Floris J. van Eerden, S. J. Marrink, Bert Poolman, and Arnold J. Boersma.

Department of Biochemistry, Groningen Biomolecular Sciences and Biotechnology Institute & Zernike Institute for Advanced Materials, University of Groningen, Nijenborgh 4, 9747 AG Groningen, the Netherlands

Materials.

Chemicals were obtained from Sigma-Aldrich at the highest available purity, and used without further purification, unless noted otherwise.

2

Fluorescence recovery after photobleaching (FRAP)

Cells were grown as for the FRET measurements in confocal microscopy. The cells were harvested by centrifugation and washed by MOPS minimal medium without glucose and potassium phosphate. The cells were subsequently resuspended with desired concentration NaCl in MOPS minimal medium without glucose and potassium phosphate and immediately placed on a coverslip. Both photobleaching and excitation were carried out using a 480 nm laser (with different intensities). The emission was collected from 493 nm to 797 nm. We focused on a cell using low laser intensity, and an area at one side of the bacterium was bleached using a diffraction-limited laser beam of high intensity. Immediately after that a series of images was collected using the low intensity laser beam to capture the fluorescence recovery process. The resolution of the images was 16×16 pixels. The diffusion coefficients were calculated as reported previously.[1,2]

Modeling effect of linker length and flexibility on FRET efficiency in the absence of crowding

Because of the linker being rather flexible and because we are interested in qualitative features, we may approximate the Gn family as simple ideal chains[3,4]. Assuming an ideal chain, the probability, $P(r)\mathrm{d}r$, of a given end-to-end distance, r, is given by

$$P(r)\mathrm{d}r = \left(\frac{3}{2\pi Ll}\right)^{3/2} \exp\left(-\tfrac{3}{2}r^2/(Ll)\right) 4\pi r^2 \mathrm{d}r \qquad \text{(S2)}$$

where L is the extended length of the linker and l is the length of a Kuhn segment.

The FRET efficiency can then be evaluated as the average

$$\left\langle \frac{1}{1+(r/R_0)^6} \right\rangle = \int \frac{P(r)\mathrm{d}r}{1+(r/R_0)^6} \qquad \text{(S3)}$$

where R_0 is the Förster radius. With a Förster radius of $R0$ = 5.4 nm and a Kuhn length of l = 2 nm this results in the relation between FRET efficiency and linker length shown in Fig. 1C (black).

For the EmGn families we approximate the linker by an ideal chain and two completely rigid rods, randomly oriented, in succession. The probability, *P(r)*d*r*, of a given end-to-end distance is readily found by stochastic numerical simulation: choosing a length of the ideal chain part from the distribution in Eq. S2 and choosing the orientations of the two rigid rods uniformly over the surface of the sphere, followed by calculating the FRET efficiency from the first equality of Eq. S3. Using a rigid rod length of 3.01 nm (E4Gn) and 4.35 nm (E6Gn), respectively, results in the relation shown in Fig. 1C (red and blue, respectively).

Using these simple models it may be observed how, for a given length of the linker, replacement of part of a flexible linker with a completely rigid part lowers the observed FRET efficiency (Fig. 1C arrow). Furthermore, the FRET efficiency is lowered more the longer the rigid part of the linker. All in all, the same qualitative observations as made experimentally (Table 1). More sophisticated models (potentially also including the fluorescent proteins) will give different parameters and may yield better quantitative agreement. However, most likely this would not change the qualitative picture.

Table S1. *Composition of simulated systems. Type of sensor and crowding agent, number of CG water beads (note, the corresponding number of real water molecules is four times bigger), amount of PEG136 polymer chains, number of ubiquitin proteins, and number of Na+ and Cl- ions, respectively.*

System	Water	PEG	UBQ	Na^+	Cl^-
crGE	205617	0	0	2334	2317
crGE UBIQ	174913	0	311	1986	1969
crGE PEG	145588	441	0	1826	1809
crG18	90943	0	0	1037	1020
crG18 UBIQ	75205	0	161	859	842
crG18 PEG	64401	189	0	817	800

***Table S2**: Comparison of the actual distance between fluorophores, and the apparent distance calculated from the FRET efficiencies using the Förster equation. Both distances were determined from molecular dynamics simulations as described above.*

	crGE		crG18	
	Distance from MD (nm)	Distance from FRET[a] (nm)	Distance from MD (nm)	Distance from FRET[a] (nm)
No crowder	12.1±0.2	9.8±0.2	8.1±0.05	7.3±0.04
Ubiquitin	11.4±0.7	9.1±0.5	7.6±0.4	6.9±0.2
PEG 6 kD	6.4±0.6	5.9±0.2	4.9±0.8	5.2±0.9

[a] Calculated with the Förster equation from the FRET efficiencies, which in turn are determined by the molecular dynamics simulations as described in the materials and methods section. To understand the reason behind the difference between these distances we note that the distance from FRET is from a large set of conformations. Within the population of conformations, the smaller distances contribute more to this average FRET due to the dependence of the FRET efficiency on the distance. Hence calculating the distance from FRET from a population of conformations will give a separation that is different from the average distance. Because the efficiencies are rather low, the direction of the deviation is mostly the same. This reasoning also applies to our "wet" experiments where there are always a large number of conformations sampled at a given time interval. If we were to correct for this deviation, it would require knowledge of the distribution of states that the sensor populates. In molecular dynamics simulations we can measure all states in one molecule individually; this allowed us to compare the "real" radius with an "ensemble" FRET.

***Table S3**. Detailed characteristics of the linkers.*

Acronym	Amino acids in linker	Extended linker length (nm)[a]	Measured distance from FRET (nm)	EAAAK/GSG ratio
GE	114	34.71	7.6±0.2	0.67
E6G6	78	22.13	7.3±0.1	2
E6G2	66	17.97	7.3±0.1	6
E4G6	58	19.45	6.7±0.1	1.3
E4G2	46	15.29	6.6±0.1	4
E6	66	23.92	6.6±0.1	0.5
G24	72	32.0	6.3±0.1	0
crG18	54	25.71	6.0±0.1	0
G12	36	19.42	5.7±0.1	0

[a] Extended linker length was determined by model building in Pymol, with α-helical backbone conformations for the helical regions and parallel β-sheet for the random coil domains. The C- to N-terminus distance was measured with the distance measuring tool in Pymol.

***Table S4**: Partial specific volumes used to calculate crowder volume fractions. Especially for Ficolls and dextrans various values, generally between 0.61 and 0.67 mL/g, have been reported in the literature. Despite these different values (that are often within the measurement error of the reported methods), the differences are small and would hence only induce small shifts in Fig. 5. These values have also been shown to be fairly independent of concentration.*[5]

Crowder	Partial specific volume (mL/g)	Reference
Ficoll 70	0.65	Christiansen, A., Wang, Q., Samiotakis, A., Cheung, M. S., Wittung-Stafshede, P. *Biochemistry* **2010**, *49*, 6519.
Ficoll 400	0.65	
Dextran 6	0.65	
Dextran 40	0.65	
BSA	0.733	Aldrich product specification sheet
Ovalbumin	0.750	Gagen, W.L. Biochemistry 1966, 5, 2553

***Table S5**: Hydrodynamic radii (σ) used in the scaling models.*

Crowder	Hydrodynamic radius (nm)	Reference
Ficoll 70	5.1	GE Life Sciences product information sheet
Ficoll 400	10	
Dextran 6	1.8	Aldrich product information sheet, and Armstrong, J. K.; Wenby, R. B.; Meiselman, H. J.; Fisher, T. C. *Biophys. J.* **2004**, *87*, 4259.
Dextran 40	4.8	
BSA	3.5	Axelsson, I. *J. Chromatography A* **1978**, *152*, 21.
Ovalbumin	2.8	Bio-rad product information sheet
γ-Globulins	5.1	

Figures:

For control experiments on the crowding sensing and general properties of the GE probe we refer to ref. 9.

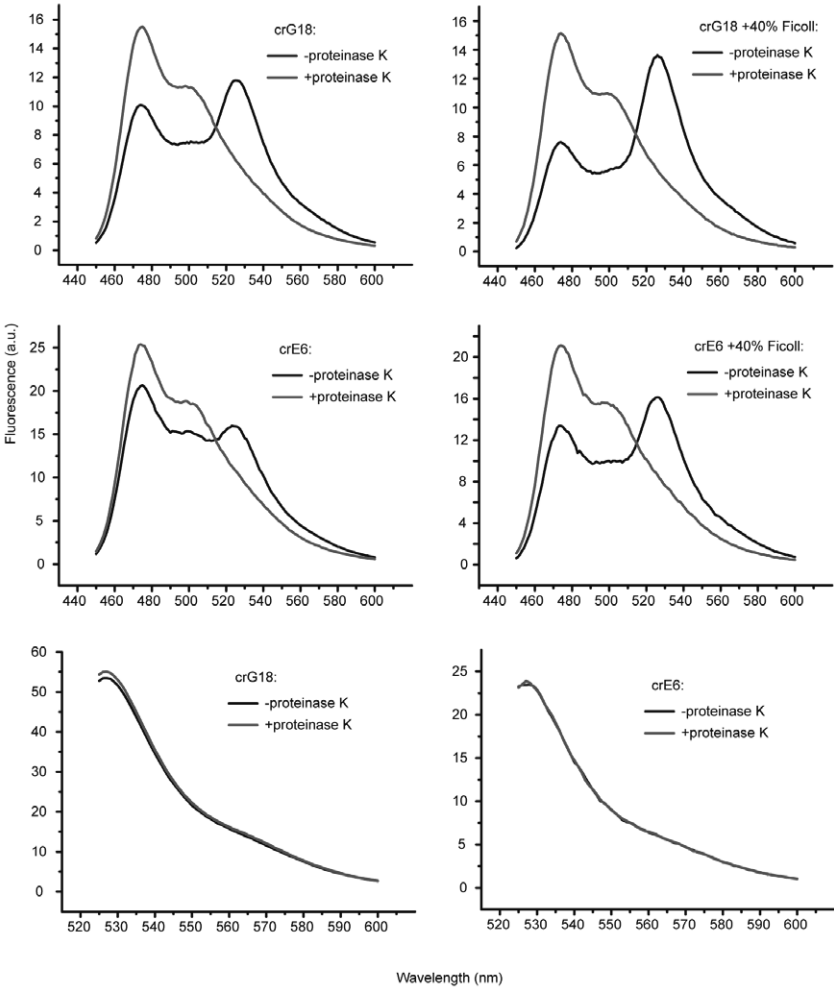

Fig. S1. Fluorescence spectra of the crG18 and E6 probes before and after proteinase K treatment, both with and without 40% w/w Ficoll 70. *After treatment, FRET disappears leaving only the spectrum of mCerulean3. The increase in mCerulean3 fluorescence was used to determine the FRET efficiency using Eq. 1. The lower two graphs are the direct excitation of the mCitrine, as a control to confirm intact fluorophores after treatment. Furthermore, direct excitation of YFP after cleavage and comparison of the intensities with the CFP intensity after cleavage shows that all the probes give the same YFP/CFP ratio of 3.2±0.4 (also in the presence of Ficoll), and hence the linker does not influence the maturation efficiency of YFP and/or CFP.*

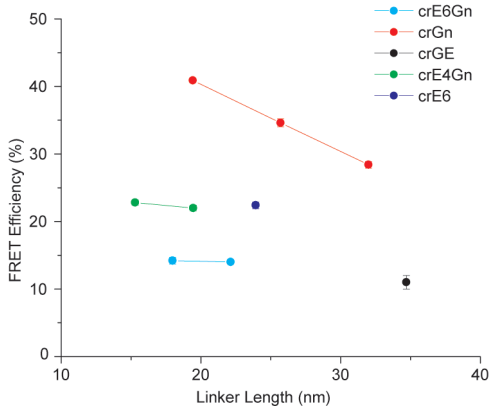

Fig. S2. FRET efficiency as a function of linker length for the different families. *It is clear that the FRET efficiency depends on the presence and length of α-helices in the linker. Data was taken from Table 1 and Table S3.*

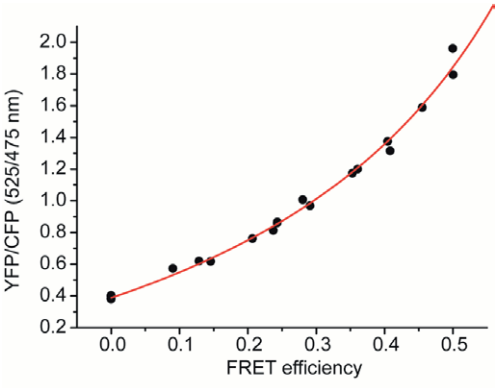

Fig. S3. Empirical relation between YFP/CFP ratios and FRET efficiencies*. Data correspond to the GE, E6G6, E6G2, E4G6, E4G2, E6, G24, crG18, and G12 probes, at 0 and 40 % w/w Ficoll 70 in 10 mM NaPi, 100 mM NaCl, 2 mg/mL BSA, pH 7.4. All data points are evaluated using cleaving with proteinase K (see methods, as in Fig. S1 and Table 1). The 0.0 FRET efficiency data points (which includes data from all 9 probes, but which are virtually indistinguishable) correspond to the YFP/CFP ratios of the cleaved probes. (Solid line) Fit to data, resulting in the relation y = -1.455/(x - 1) - 1.068.*

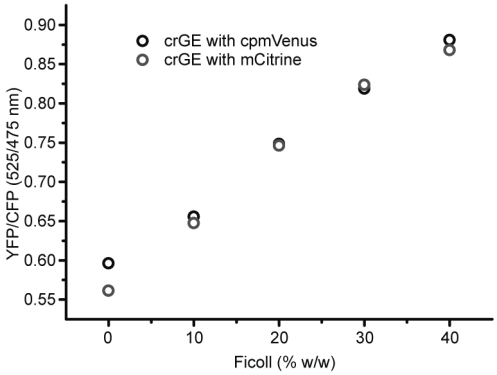

Fig. S4. Comparison of the effect of Ficoll on the GE probes with different YFPs, i.e. mCitrine or circular permuted mVenus (cpmVenus). *In cpmVenus the native N- and C-terminus are fused with a GGSGG linker, and a new N- and C-terminus is introduced in a loop on the other side of the barrel (the amino acid sequences can be found below). This results in the fluorescent protein to be upside down. In principle placing a fluorescent protein upside down would give the same FRET efficiency because the dipole of the fluorophore is unchanged (the fluorophore is perpendicular to the axis of the barrel, hence the direction of the dipole will not change). If changes are seen with circular permuted proteins it is due to fluorophore dimerization (GFPs also crystallize as antiparallel dimers), or other interactions that prevent free tumbling of the protein. The proteins in our case contain the A206K mutation to ensure monomeric fluorescent proteins. The YFPs do not have a similar brightness, with the cpmVenus excited at 515 nm being 30% more bright than mCitrine. The brightness levels do not change by addition of Ficoll. The increase in brightness gives a marginal increase in YFP/CFP ratio, which is small due to the cross talk of CFP emission into the YFP channel.9 It can be seen that the results for both probes are nearly superimposable, indicating that the fluorescent proteins move freely in all cases.*

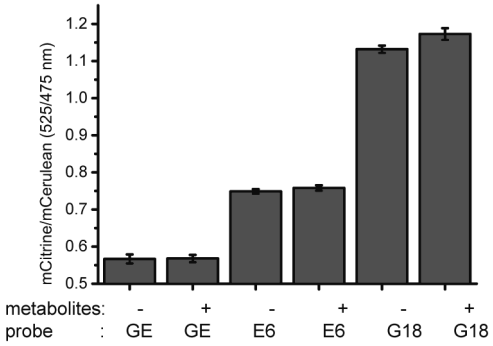

Fig. S5. Effects of a mixture of the four most common metabolites in E. coli on the mCitrine/mCerulean3 emission ratio of the probes. We used a freshly prepared mixture of 100 mM glutamate, 20 mM glutathione, 15 mM fructose bisphosphate, and 10 mM ATP, in 10 mM NaPi, and the pH was set to pH 7.4 with NaOH after dissolution of all solutes. Error bars represent the standard deviation of three independent experiments.

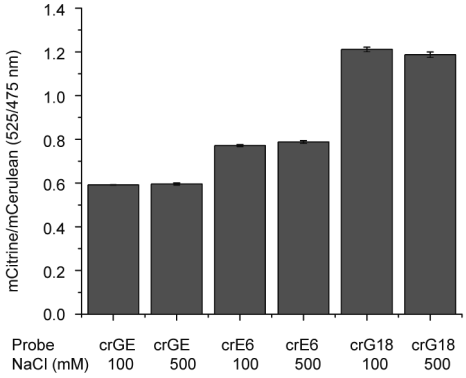

Fig. S6. Addition of up to 500 mM NaCl did not influence the mCitrine/mCerulean3 ratios *of purified GE, E6, and crG18 probes; measurements were done in 10 mM NaPi, 2 mg/mL BSA, pH 7.4.*

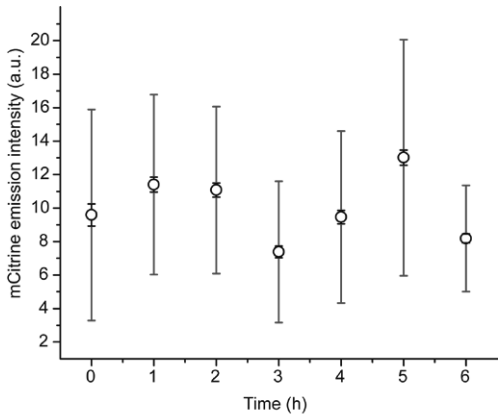

Fig. S7. Expression of the crG18 probe over time determined from mCitrine emission in fluorescence confocal microscopy *(excitation 405 nm, emission 505-750 nm). The cells are grown at 30 °C in MOPS minimal medium. The OD was kept between 0.1 – 0.2 by dilution. The averages of over >100 cells are given, the red error bars are the standard deviations denoting the spread of intensities found within a single population of cells; the black error bars are the standard error of the mean. The data shows that the expression of the probes is balanced with the growth rate of the cells, maintaining similar concentrations over time.*

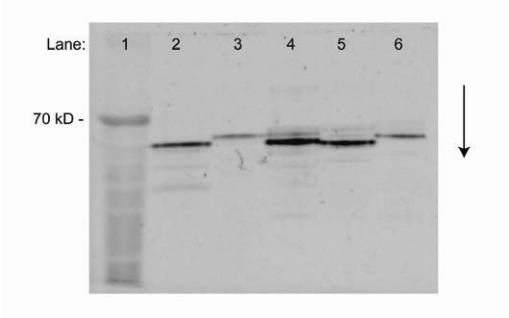

Fig. S8. In-gel fluorescence SDS-PAGE analysis of the expression quality of the probes. *Cells were grown in MOPS minimal medium at 30 °C and harvested at an OD600 of 0.1-0.2. Cells were spun down and the cell pellet resuspended in 10 mM NaPi, 100 mM NaCl, pH 7.4, supplemented with PMSF. The cells were lysed by tissue lyser and the lysate was directly loaded on the SDS-PAGE (10% polyacrylamide) gel. The gel was imaged by fluorescence using excitation at 460 nm, filter 515 nm. Integration of the fluorescent bands by ImageJ shows >95% purity. Lane 1: Marker, lane 2: crG18, lane 3: G12, lane 4: E6, lane 5: E6G2, lane 6: GE.*

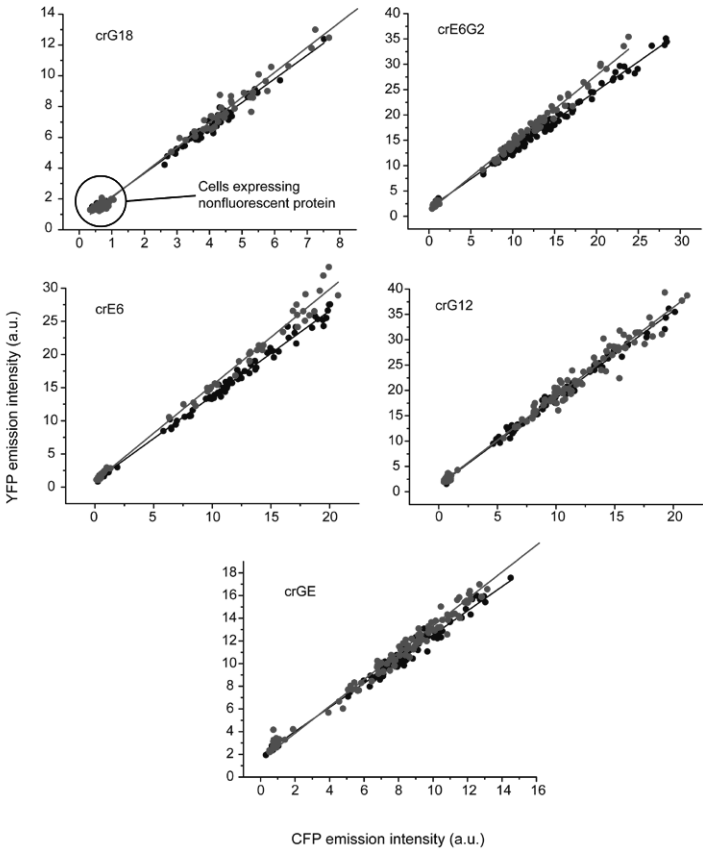

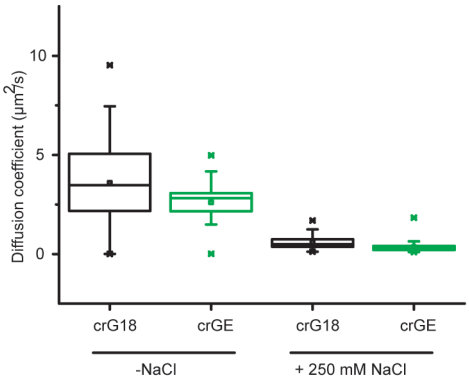

Fig. S10. Diffusion coefficients of the G18 and crGE probes in E. coli BL21*, growing in MOPS minimal medium, with and without added 250 mM NaCl, as determined by FRAP. The diffusion coefficient at 500 mM NaCl was too slow to be observed. Under similar conditions in E. coli, GFP diffuses with a diffusion coefficient of 6-12 µm2/s.8 The difference in lateral diffusion constant can be explained by the larger size (and shape) of the sensors as compared to GFP.10*

Previous page:

Fig. S9. Representative examples of in cell YFP emission intensity versus CFP emission intensity acquired by confocal microscopy to determine YFP/CFP ratios*. The low fluorescence population is E. coli cells expressing a non-fluorescent protein under the same conditions added to the full population. Each data point represents a single cell, and the results from all cells were fit to a line. The black data corresponds to cells before osmotic upshift; the red data corresponds to cells after 500 mM NaCl upshift. The R2 values are in all cases > 0.985. The linear fit shows that the FRET ratio is independent on the emission intensity in the measured range.*

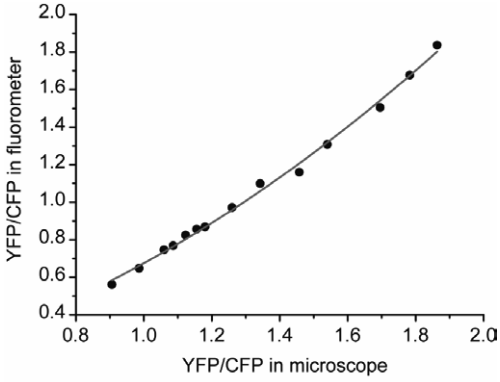

Fig. S11. Empirical relation between YFP/CFP ratios determined by fluororescence spectrophotometer and by fluorescence microscope*. The experimental data is the G18, E6, and crGE probes, with 0, 10, 20, 30, and 40% w/w Ficoll 70, in 10 mM NaPi, 100 mM NaCl, 2 mg/mL BSA, pH 7.4. These ratios span the whole range of ratios that we measure in the experiments. The data fits a polynomial y = 0.02733 + 0.29485x + 0.35293x2, with R2 = 0.995. The fit depends on multiple parameters that may not scale linearly: 1) The detection sensitivities of the two instruments over the whole spectrum range are not the same. 2) For the fluorometer it is the maximum intensity (at 475 and 525), while for the microscope it is a large wavelength range intensity that is measured (450-505 and 505-700). 3) Different contributions of emission bleed-through (CFP into YFP, and YFP into CFP) because the emission is determined differently on the two instruments.*

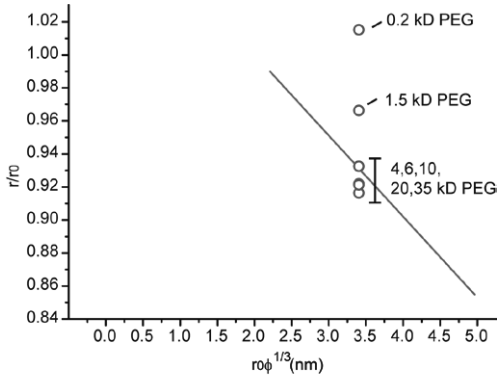

Fig. S12. Dependence of compression on PEG size*: For weights >4 kD, the compression no longer dependence on the size of the PEG and converges to the "calibration line" of Fig. 5C. Data is at 10% w/w PEG with the crGE probe.*

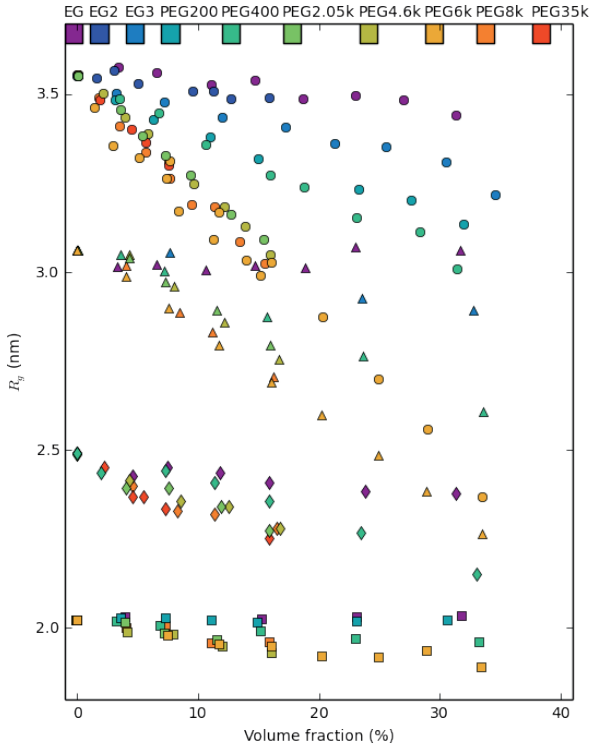
EG EG2 EG3 PEG200 PEG400 PEG2.05k PEG4.6k PEG6k PEG8k PEG35k
3.5
3.0
2.5
2.0
R_g (nm)
0
10
20
30
40
Volume fraction (%)

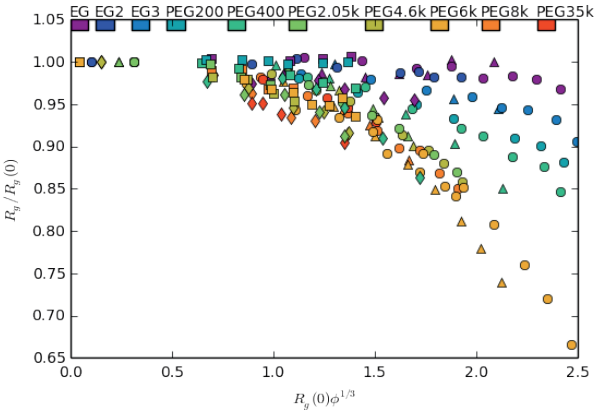
EG EG2 EG3 PEG200 PEG400 PEG2.05k PEG4.6k PEG6k PEG8k PEG35k
1.05
1.00
0.95
0.90
0.85
0.80
0.75
0.70
0.65
$R_g / R_g(0)$
0.0
0.5
1.0
1.5
2.0
2.5
$R_g(0)\phi^{1/3}$

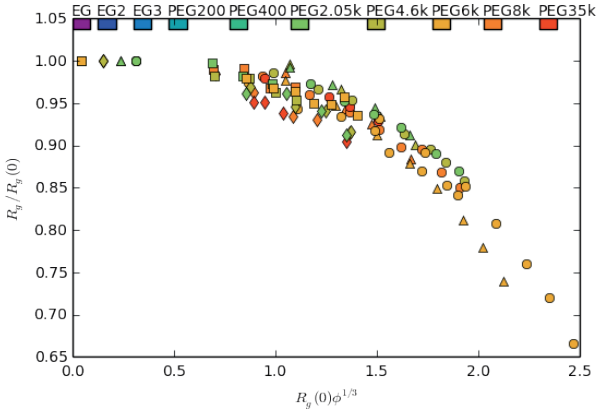

Fig. S13. Reanalysis of measurement data of Schuler and coworkers6 using the scaling ansatz from Kang et al.7 A: *Radii of gyration (Rg) of four intrinsic disordered proteins ProTα-C (circles), ProTα-N (triangles), ACTR (diamonds), and IN (squares) in the presence of PEGs of varying molecular weight versus the volume fraction of PEG (φ). Data directly reproduced from ref. 19.* ***B:*** *Data plotted as the relative compression Rg(φ)/Rg(0) versus Rg(0)φ1/3, that is, according to the scaling ansatz as described in the main text.* ***C:*** *Same as panel B, but with the PEGs <1.5 kD omitted showing how the data follows a master curve with striking similarity to the probes used in this work, depicted in Fig. 5C.*

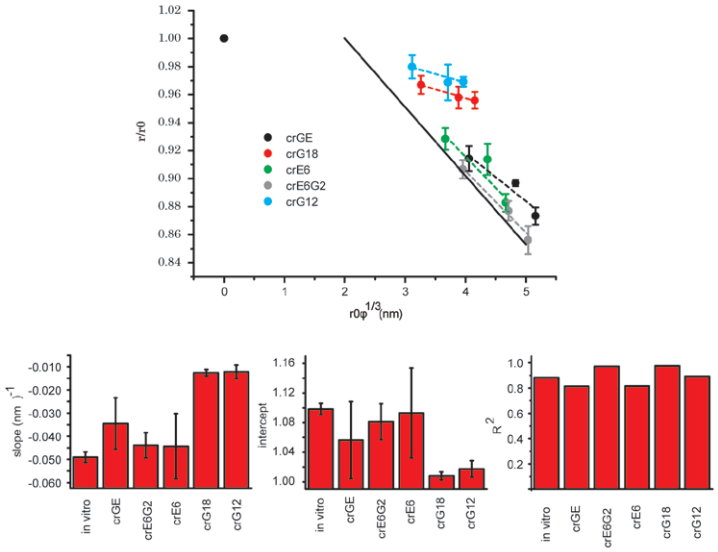

Fig. S14. Comparison of the in vitro calibration with in cell compressions of the helix containing probes *(E6, crGE, and E6G2) and the probes that do not contain a helix (G18 and crG12). The data is from Fig. 5D and the individual probes fitted to a linear function. The bar graphs show the comparison of the slopes, intercepts and R2 of the linear fits. Clearly, helix-lacking probes deviate inside the cells. The errors in the bar graphs are the standard errors from the fits.*

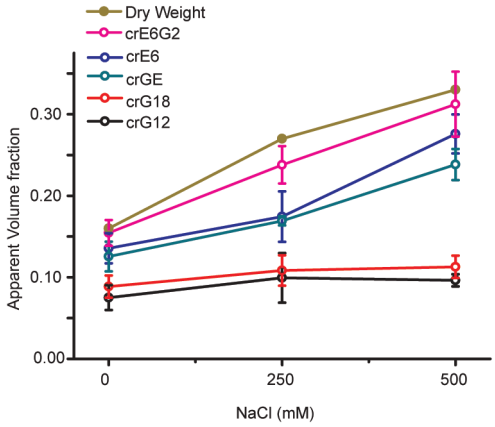

Fig. S15. Apparent volume fraction sensed by the probes calculated with the calibration line of Fig. 5C*, and comparison with volume fractions determined from literature8 (φ = 0.16, 0.27, 0.33, for 0, 250, 500 mM added NaCl respectively).*

Supporting references

1. J.T. Mika, P.E. Schavemaker, V. Krasnikov, B. Poolman, Impact of osmotic stress on protein diffusion in Lactococcus lactis, *Mol. Microbiol.* **94** 857-870. (2014)
2. J.T. Mika, V. Krasnikov, G. van den Bogaart, F. de Haan, B. Poolman, Evaluation of pulsed-FRAP and conventional-FRAP for determination of protein mobility in prokaryotic cells, *Plos One* **6** e25664. (2011)
3. Doi, M. In Introduction to Polymer Physics, Clarendon Press, Oxford, UK. (1996)
4. de Gennes, PG (1979) In Scaling Concepts in Polymer Physics, Cornell University Press, Ithaca, N.Y.
5. A. Christiansen, Q. Wang, A. Samiotakis, M.S. Cheung, P. Wittung-Stafshede, Factors defining effects of macromolecular crowding on protein stability: an in vitro/ in silico case study using Cytochrome C, *Biochemistry* **49** 6519-6530. (2010)
6. A. Soranno, I. König, M.B. Borgia, H. Hofmann, F. Zosel, D. Nettels, B. Schuler, Single-molecule spectroscopy reveals polymer effects of disordered proteins in crowded environments, Proc. Natl. Acad. Sci. U. S. A. 111 4874-4879. (2014)
7. H. Kang, P.A. Pincus, C. Hyeon, D. Thirumalai, Effects of macromolecular crowding on the collapse of biopolymers, *Phys. Rev. Lett*. 114 068303(2015)
8. M.C. Konopka, K.A. Sochacki, B.P. Bratton, I.A. Shkel, M.T. Record, J.C. Weisshaar, Cytoplasmic protein mobility in osmotically stressed Escherichia coli, *J. Bacteriol.* **191** 231-237. (2009)
9. A.J. Boersma, I.S. Zuhorn, B. Poolman, A sensor for quantification of macromolecular crowding in living cells, **12** Nat. *Methods* 227-229. (2015)
10. J.T. Mika, B. Poolman, Macromolecule diffusion and confinement in prokaryotic cells, *Curr. Opin. Biotechnol*. **22** 117-126. (2011)

Chapter 3

Comparison of fluorescent proteins in a crowding sensor and the importance of efficient maturation in *Escherichia coli*

Boqun Liu,[1] Sara N. Mavrova,[1]
Sebastian K. Kristensen, Jonas van den Berg,
Liesbeth M. Veenhoff, Bert Poolman,*
and Arnold J. Boersma*

Abstract

The high macromolecular crowding in the intracellular environment can be quantified with FRET-based sensors. To assess the influence of fluorophore maturation on FRET, we varied both the protein expression conditions and the pairs of fluorescent proteins. We built a model to quantify the influence of the maturation efficiency on the measured FRET efficiency. Our findings show that artifacts from slow maturing fluorescent proteins can be significant in case of rapid increasing fluorescent protein levels (induced expression) but can be minimized by expression with stable protein levels (constitutive expression). The model indicates that the ratiometric FRET relates to the maturation of the fluorescent proteins and depends mostly on the maturation of mCitrine (acceptor), while the maturation of mCerulean3 (donor) influences the ratiometric FRET at very low level of maturation. These results demonstrate that the maturation efficiency has significant effect on the measured FRET efficiency. Similar outcomes should apply to other fluorescent protein-based FRET sensors described in the literature, and it shows the need for characterizing the maturation of fluorescent proteins to minimize artifacts.

Introduction

Fluorescence resonance energy transfer (FRET) is a powerful tool that enables real-time measurements of processes in living cells.[1–3] Researchers have developed sensors to detect e.g. the redox and energy status[4] and metabolite and ion[5–12] concentrations in bacterial, fungal, plant and mammalian cells. Typically, protein-based FRET sensors for intracellular measurements consist of two fluorescent proteins linked by a conformational switchable domain that provides specificity for an analyte. The fluorescent protein is essential and its properties affect the application of the sensor.

The synthesis of GFP-type fluorescent proteins goes through several stages of processing, including, cyclization, dehydration, and aerial oxidation of the fluorophore, which is termed maturation[13,14]. The oxidation step limits the maturation of GFP-type proteins. Bajar *et al*.[15] summarized that the maturation half-life of commonly used fluorescent proteins range from 15 min to 150 min, depending on the fluorescent protein and the organism in which it is expressed. Hebisch *et al.*[16] found that doubling the growth rate of *E. coli* results in a longer maturation time by a factor of 1.4, which might be due to the oxygen availability in the cell. Considering the doubling time of *E. coli* varies from 30–120 min[17], we assume that the fluorescent proteins of FRET sensors are not always fully mature in living cells.

Due to the presence of immature fluorescent protein, one obtains a mixture of three types of FRET sensor (Fig. 1) in the cells: the fully matured, only donor-matured, and only acceptor-matured. These different types of FRET sensors will influence the ratiometric FRET by bleed-through and cross-excitation artifacts. The bleed-through artifact is caused by the emission of donor that is detected in the acceptor channel, and the cross-excitation is due to direct excitation of acceptor at the donor excitation wavelength.

Our recently developed FRET-based crowding sensor (crGE, containing mCerulean3 and mCitrine) is excited at 405nm under the microscope and the emission is split at 505 nm. The 405-505 nm channel gives the emission of the donor (*Idonor*, mCerulean3), and the 505–786 nm channel gives the emission of the acceptor (*Iacceptor*, mCitrine). The emission in the acceptor channel is composed of three components: the cross-excitation of mCitrine (Fig. 1B), the bleed through of mCerulean3 (Fig. 1C) and the actual FRET signal. The spectrum of the sensor is complicated because it is a sum of the three species. When sensor with only matured mCitrine ($crGE_{cit}$) is present in excess, the intensity of *Iacceptor* is relatively high due to cross-excitation of mCitrine, which causes an apparent increase in ratiometric FRET. When mature mCerulean3 ($crGE_{cer}$) is in excess, *Iacceptor* is relatively low due to a fraction of sensor that does not have acceptors

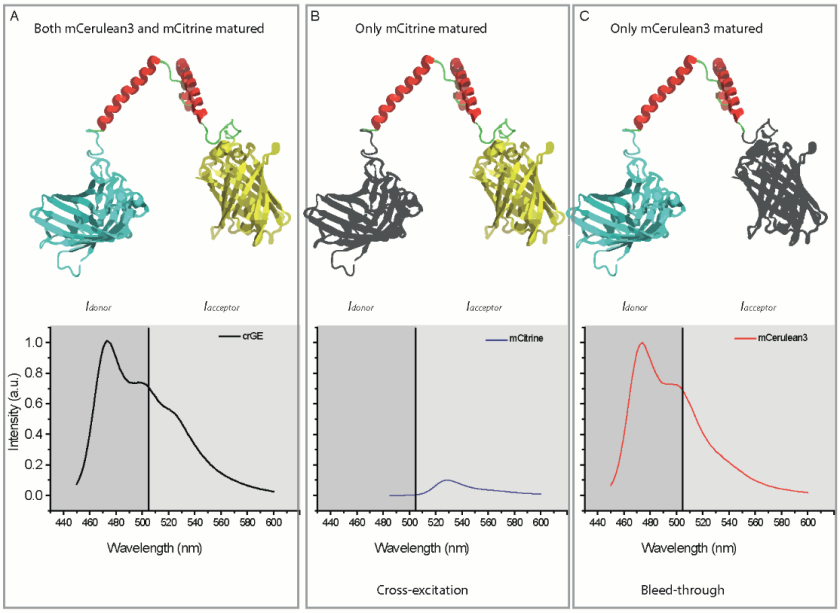

Fig. 1. Structures of FRET sensors with either the donor or acceptor or both fluorephores fully matured. ***A****: Structure and fluorescence emission spectra of both mCerulean3 and mCitrine matured (crGEcercit) (λEx = 420 nm).* ***B****: Structure and fluorescence emission spectra of mCitrine matured (crGEcit) (λEx = 405 nm).* ***C****: Structure and fluorescence emission spectra of mCerulean3 matured (crGEcer) (λEx = 405nm), which shows the bleed-though. The 450-505 nm channel is the donor emission channel (Idonor). The 505-786 nm channel is the acceptor emission channel (Iacceptor). The spectra show that Iacceptor of crGE can be influenced by cross-excitation and bleed-through. The spectra serve as examples and are qualitative.*

and there is no FRET possible, which causes a lower ratiometric FRET. Hence, the maturation of fluorescent protein has an influence on the measured ratiometric FRET[15,18].

In the current study, we investigate the influence of maturation on the ratiometric FRET on our recently developed FRET-based crowding sensors in *E. coli*[19,20]. With the crowding sensor crGE as starting point, we varied the fluorescent proteins (Table 1) and the expression vector. We find that artifacts can arise from the slow maturing FRET donor, and that the FRET donor maturation can be maximized by constitutive expression (stable protein levels), leading to accurate ratiometric FRET readouts. We built a model for quantification of the influence of fluorescent protein maturation on the read-out of the FRET signal. Our results show that maturation influences the ratiometric FRET. For crGE sensor, artifacts from slower maturing fluorescent proteins depend strongly on the maturation of mCitrine, while the maturation of mCerulean3 mostly influences the ratiometric FRET at low levels of maturation.

Materials and method

Plasmid and protein preparation

The genes encoding crGE, crGE$_{switch}$, crGEu, crGO and crYCY in pRSET A were obtained from GeneArt. DNA encoding mTurquoise2 (PMK plasmid, GeneArt) was cloned with *Nsi*I and *Bam*HI into pRSET A, carrying the gene for the crGE probe. crGEL201K (pMA-T, Eurofins) was subcloned in the *Nsi*I and *Bam*HI sites of pRSET A, carrying the gene for the crGE probe. DNA encoding crGR in pBAD from GeneArt was subcloned into pRSET A, carrying the gene for the crGE probe, using the *Sac*I and *Hind*III endonuclease restriction sites. All plasmids with sensor genes were transformed into *E. coli* BL21(DE3) pLysS (Promega).

E. coli BL21(DE3) pLysS with the pRSET A vector containing the desired sensor (Table 1) was grown to OD_{600} = 0.6 in LB medium (10 g/L tryptone, 5 g/L yeast extract, 10 g/L NaCl), and induced with 1mM isopropyl β-D-1-thiogalactopyranoside (IPTG) overnight at 25 °C. The cells were spun down at 3000g for 30min, resuspended in buffer A (10 mM sodium phosphate (NaPi), 100 mM NaCl, 0.1 mM phenylmethylsulfonyl fluoride (PMSF), pH 7.4) and lysed in TissueLyser LT (QIAGEN). The lysate was cleared by centrifugation (5 min, 10000 g), and the supernatant was supplemented with 10 mM imidazole, and, subsequently, the proteins were purified by nickel-nitrilotriacetic acid Sepharose (NTA-Sepharose) chromatography (wash/elution buffer: 20/250 mM imidazole, 50 mM NaPi, 300 mM NaCl, pH 7.4). The constructs were further purified by Superdex 200 10/300GL size-exclusion chromatography (Amersham Biosciences) in 10 mM NaPi 100 mM NaCl, pH 7.4. The expression and purification were analyzed by 12% SDS-PAGE, and the bands were visualized by in-gel fluorescence and subsequent Coomassie staining. Fractions containing pure protein were aliquoted and stored at −80 °C.

To obtain mCerulean3 and mCitrine separately, the crGE sensor, bound to NTA-Sepharose, was treated on-column with proteinase K (Sigma) for 5 min. The mixture was first washed with 20 mM imidazole, 50 mM NaPi, 300 mM NaCl, pH 7.4 to collect mCitrine, and then washed with 250 mM imidazole, 50 mM NaPi, 300 mM NaCl, pH 7.4 to collect mCerulean3. The fractions containing a single fluorescent protein were further purified by size-exclusion chromatography and analyzed as above.

Fluorescence spectroscopy

The required amount of Ficoll 70 was dissolved in 10 mM NaPi, 100 mM NaCl, 2 mg/mL BSA, pH 7.4. To obtain background spectra,

1.0 mL of the Ficoll solution was added in a quartz cuvette and its fluorescence emission spectrum was recorded after excitation at 488 nm for crGO and crGR, and at 420 nm for all the other sensors. Subsequently, the purified sensor was added, mixed by pipette, and the spectra were recorded again. The background spectrum prior addition of the probe was subtracted to obtain the sensor spectrum.

Maturation measurement

E. coli BL21(DE3) strain, without pLysS, with pRSET A containing the gene encoding the probe, was inoculated in 10 mL of filter-sterilized MOPS minimal[21] medium containing 20 mM glucose. The culture was grown to OD_{600} to 0.1–0.2, and treated with 200 µg/mL chloramphenicol to stop protein synthesis. The fluorescence emission spectra (λ_{Ex} = 420 nm) were recorded every 30 min after the addition of chloramphenicol, and the spectra were corrected for OD_{600}. The fluorescence emission of the same strain without plasmid was treated in the same manner (in the absence of ampicillin) and the corresponding spectra were subtracted from those of cells carry the FRET probe. The data were fit to an exponential model to predict the maturation time.

Confocal fluorescence microscopy

Ratiometric FRET measurements of *E. coli* by scanning confocal fluorescence microscopy were carried out as reported previously[20]. Briefly, the culture was grown in MOPS minimal[21] medium containing 20 mM glucose to OD_{600} to 0.1–0.2. In parallel, the same *E. coli* strain with the pRSET A plasmid containing monomeric streptavidin served as background. For both cultures, the proteins were constitutively expressed, *i.e.* in the absence of inducer. The cells were combined in a 1:1 ratio and washed by centrifugation and resuspension in MOPS minimal medium with the desired amount of NaCl, but without K_2HPO_4 and glucose to minimize adaptation of the cells to the osmotic stress imposed by the addition of NaCl. 10 µL of this mixture was added to a coverslip modified with (3-aminopropyl) triethoxysilane (Aldrich) as described in chapter 2. The coverslip was placed on a 40× water immersion objective lens on a laser-scanning confocal microscope (Zeiss LSM 710).

For imaging, the cells expressing the crGE, crGEs, crGEu, crYCY and crTC sensors, we used a 405 nm diode laser for excitation and the emission was split into a 450-505 nm and 505-797 nm channel. The cells with the crGO sensor were excited at 488 nm and the emission of mEGFP and mKO2 was split into a 500-540 nm and 540-797 nm

channel. To correct for bleed through and cross excitation, a droplet (20 µL, 10 mM NaP_i, 2 mg/mL BSA, 100 mM NaCl, pH 7.4.) containing the same concentration of either crGE, mCerulean3, or mCitrine was placed on the coverslip, and excited by 405 nm and the emission was split into a 405-505 nm channel and a 505-797 nm channel. Then, the fluorescent proteins were excited at 488 nm and the emission was collected between 505-797 nm.

The model

To quantify the influence of maturation on the observed ratiometric FRET, a model consisting of the maturation efficiency of the donor and the acceptor was build. The model is based on Eq. 1:

$$Ratiometric\ FRET = \frac{I_{acceptor}}{I_{donor}} \quad \text{Eq. 1}$$

Ratiometric FRET is the ratio of intensity of acceptor ($I_{acceptor}$) divided by intensity of donor (I_{donor}). For crGE sensor, I_{donor} is the fluorescent emission from the 450-505 nm channel and $I_{acceptor}$ is the fluorescent emission from the 505-797nm channel.

We then dissected the composition of Eq. 1. I_{donor} depends on the donor fluorescent protein and is decreased by FRET (Fig. 1A and C). $I_{acceptor}$ includes three parts (Eq. 2, Fig. 1): $I_{donor\ bleed\ through}$ is bleed through from donor. I_{FRET} is the donor's fluorescence emission from FRET by FRET. $I_{acceptor\ cross\text{-}excitation}$ is the direct excitation of the acceptor at 405 nm.

$$I_{acceptor} = I_{donor\ bleed\ through} + I_{FRET} + I_{acceptor\ cross\ \mathrm{excitation}} \quad \text{Eq. 2}$$

Now we quantify these three parts, with the assumption that crGE is fully matured. First, we quantify the donor bleed through ($I_{donor\ bleed\ through}$), which is proportional to the intensity in the donor channel (Eq. 3).

$$I_{donor\ bleed\ through} = \alpha \cdot I_{donor} \quad \text{Eq. 3}$$

To calculate *IFRET*, we start with the FRET efficiency, Eq. 4[22]. I_{donor} is the intensity of donor in the presence of acceptor. $I_{donor\ only}$ is the intensity of donor in the absence of acceptor. The difference between I_{donor} and $I_{donor\ only}$ is ΔI_{donor} (Eq. 5), which is due to FRET. With Eq. 6, we can rewrite Eq. 4 into Eq. 6.

$$E = 1 - \frac{I_{donor}}{I_{donor\ only}} \quad \text{Eq. 4}$$

$$\Delta I_{donor} = I_{donor\ only} - I_{donor} \quad \text{Eq. 5}$$

$$\Delta I_{donor} = \frac{E}{1-E} \cdot I_{donor} \quad \text{Eq. 6}$$

When considering the difference in brightness between donor and acceptor, we introduce coefficient γ (Eq. 7).

$$I_{FRET} = \gamma \cdot \Delta I_{donor} \quad \text{Eq. 7}$$

We quantified $I_{acceptor\ cross\text{-}excitation}$, which is proportional to the amount of acceptor. The number of donors and acceptors is the same in fully matured sensor, which means that the cross-excitation part ($I_{acceptor\ cross\text{-}excitation}$) is proportional to the intensity of the donor in the absence of acceptor ($I_{donor\ only}$). Hence, we introduce to obtain the relation between cross excitation of acceptor and $I_{donor\ only}$. The relation is shown in Eq. 8. With Eq. 4, we can rewrite Eq. 8 to Eq. 9.

$$I_{acceptor\ cross\ excitation} = \beta \cdot I_{donor\ only} \quad \text{Eq. 8}$$

$$I_{acceptor\ cross\ excitation} = \frac{\beta \cdot I_{donor}}{1-E} \quad \text{Eq. 9}$$

Now we can insert Eq. 2, 3, 7, and 9 into Eq. 1, resulting in Eq. 10 which need to further simply:

$$Ratiometric\ FRET = \frac{I_{acceptor}}{I_{donor}} = \frac{\alpha \cdot I_{donor} + \gamma \cdot \frac{E}{1-E} \cdot I_{donor} + \frac{1}{(1-E)} \cdot \beta \cdot I_{donor}}{I_{donor}} \quad \text{Eq. 10}$$

Next, we introduced the degree of maturation to obtain Eq. 11, in which m_{donor} is the maturation percentage of donor, $m_{acceptor}$ is the maturation percentage of acceptor, and I^0 indicates the intensity of fully matured protein. The bleed through only relates to the maturation of donor and can be calculated with Eq. 12. FRET requires that both donor and acceptor are matured. Cross-excitation is only related to the maturation of acceptor.

Lastly, to predict the effect of maturation on ratiometric FRET, we determined the coefficients α, β and γ, and FRET efficiency (*E*). We quantified these parameters with purified fluorescent proteins (mCerulean3 and mCitrine) and purified, fully matured crGE. Coefficient α is related to the emission of mCerulean3 (Fig. 1C). It was determined by excitation of purified mCerulean3 (λ_{Ex} = 405 nm) and measurement of the emission in channel 405–505 and channel 505–797 nm. The coefficient β is employed to build the relation between the ratio of emission upon cross excitation of acceptor, and donor emission in the absence of acceptor ($I_{donor\ only}$). To determine coefficient β, we need to know the emission intensity of mCitrine (Ex 405 and 488 nm) and the emission intensity of mCerulean3 (λ_{Ex} = 405 nm).

We excited purified mCitrine and mCerulean at 405nm and 488 nm, respectively. We did not observe emission of mCerulean3 when excited at 488 nm, which indicates that we can quantify the amount of mCitrine in crGE with 488 nm excitation. We excited crGE sensor at 405 and 488 nm separately and recorded the intensity.

$$Ratiometric\ FRET = \frac{m_{donor} \cdot \alpha \cdot I^0_{donor} + m_{donor} \cdot m_{acceptor} \cdot \gamma \cdot I^0_{donor} \cdot \frac{E}{1-E} + \frac{1}{(1-E)} m_{acceptor} \cdot \beta \cdot I^0_{donor}}{m_{donor} \cdot I^0_{donor}}$$

$$= \frac{m_{donor} \cdot \alpha \cdot I^0_{donor}}{m_{donor} \cdot I^0_{donor}} + \frac{m_{donor} \cdot m_{acceptor} \cdot \gamma \cdot I^0_{donor} \cdot \frac{E}{1-E}}{m_{donor} \cdot I^0_{donor}} + \frac{\frac{1}{(1-E)} m_{acceptor} \cdot \beta \cdot I^0_{donor}}{m_{donor} \cdot I^0_{donor}} \quad \text{Eq. 11}$$

$$I_{donor} = m_{donor} \cdot I^0_{donor} \quad \text{Eq. 12}$$

$$I_{acceptor} = m_{acceptor} \cdot I^0_{acceptor} \quad \text{Eq. 13}$$

Equation 11 can be simplified to Equation 14:

$$Ratiometric\ FRET = \alpha + m_{acceptor} \cdot \gamma \cdot \frac{E}{1-E} + \frac{1}{(1-E)} \cdot \frac{m_{acceptor} \cdot \beta}{m_{donor}} \quad \text{Eq. 14}$$

Results

In vitro characterization of FRET-based sensors

We initially set out to vary the fluorescent proteins in the crGE sensor in order to improve its performance, and to understand the influence of the fluorescent proteins on crowding sensing. To determine the influence of the order of translation on maturation, we switched the order of mCitrine and mCerulean3 on the gene encoding crGE yielding $crGE_{switch}$. To determine the influence of the orientation of mCitrine on the ratiometric FRET, we employed a circular permitted fluorescent protein (cpmVenus), yielding the crGEu sensor. Then, to investigate the influence of intramolecular hydrophobic interactions, we mutated a hydrophobic patch that we identified in mCerulean3 and mCitrine to a repulsive electrostatic interaction, yielding crGEL201K To minimize the effect of maturation, we replaced slow-maturation mCerulean3 with mTurquoise2 which is a brighter and faster maturing fluorescent protein[23], yielding crTC. To obtain a red-shifted FRET pair, we employed mEGFP and TagRFP, yielding crGR. To increase the pH stability of the sensor, we combined EGFP with mKO2, which was previously stated pH insensitive[24], yielding crGO. To increase the size of the sensor, we linked a second mCitrine fused to the N-terminus of the crGE, yielding the crYCY sensor, and lastly, we fused non-fluorescent GFPs to both the C- and N-terminus of the crGE sensor,

Table 1. Different crowding sensors

Acronym	Donor	Acceptor	Vector	Properties
crGE	mCerulean3	mCitrine	pRSET A	
crGE	mCerulean3	mCitrine	pACYC	Rhamnose inducible
$crGE_{switch}$ [1]	mCerulean3	mCitrine	pRSET A	switched position donor and acceptor
crGEu [2]	mCerulean3	cpmVenus [25]	pRSET A	acceptor orientation change
crTC	mTurquoise2	mCitrine	pRSET A	Fast maturing donor
crGEL201K [3]	mCerulean3	mCitrine	pRSET A	reduced donor/acceptor association
crGR	mEGFP	TagRFP	pBAD	Red-shifted
crGO	mEGFP	mKO2	pRSET A	pH insensitive
crYCY [4]	mCerulean3	mCitrine(2x)	pRSET A	Increased size
crNon-GFP [5]	mCerulean3	mCitrine	pRSET A	Increased size

1. *The order of mCitrine and mCerulean3 was switched to first mCitrine and then mCerulean3 (crGEswitch).* ***2.*** *cpmVenus is a circularly permuted variant of yellow fluorescent proteins see [ref 25] for detail.* ***3.*** *The crGEL201K sensor is crGE sensor with two mutations L201K and L557K.* ***4.*** *An additional mCitrine fused to the N-terminus of the crGE sensor* ***5.*** *Additional non-fluorescent GFPs were linked to both the C-terminus and the N-terminus of the crGE, which compromised the folding of sensor in E. coli.*

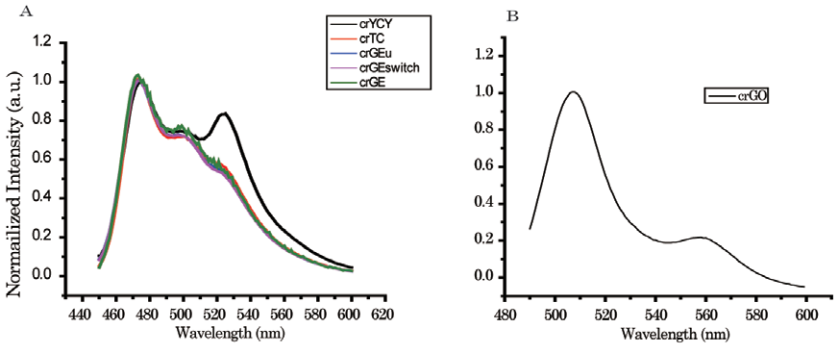

Fig. 2. Spectral characterization of the probes. A: *Fluorescent spectra of the sensors with CFP-YFP (= 420nm).* ***B:*** *Fluorescent spectra for the crGO sensor (= 488nm).*

yielding crNon-GFP. We anticipated that these larger constructs would be more crowding-sensitive due to the size-dependence of crowding effects (Table 1).

All sensors (Table 1 and Fig. 2) were purified by size-exclusion chromatography. To determine the purity of the sensors, we ran SDS-PAGE gels and identified the proteins by Coomassie staining and in-gel fluorescence (**Fig. 3**). For crTC, crGEswitch, and crGEu, we saw a small fraction of more slowly migrating proteins, which could reflect a different folding state of the fluorescent proteins in SDS [26] (**Fig. 3A**). For the crGO sensor, a more intense band migrating with apparent molecular weight about 10 kDa higher than that of the main protein,

which is indicative of a significant fraction of the crGO sensor that is not folding/maturing correctly. For the crYCY sensor (**Fig. 3B**), we find multiple bands, indicating that the additional mCitrine causes incomplete protein synthesis in *E. coli*.

All the sensors are characterized by fluorometry with Ficoll 70 as crowder. All the sensors respond to crowding (**Fig.** 4A); the acceptor/donor ratio increases when the weight percentage of Ficoll 70 is increased. The crYCY sensor with an additional mCitrine has a higher FRET efficiency and cross-excitation compared to the crGE. The crGO has a low acceptor/donor ratio, which is caused by the low brightness and maturation of mKO2 in *E. coli* (Fig. 2). The tagRFP in crGR does not give emission (data not shown), which could be due to the instability of TagRFP or absence of maturation. Neither mCerulean3 nor mCitrine in crNon-GFP gives any emission, which could be due to the misfolding of both donor and acceptor or aggregation of the sensors in vivo (Fig. 3C). Further, it is known that misfolding of a fusion protein can hamper proper folding of fluorescent proteins[27].

Characterization of the sensors in E. coli

We characterized all the sensors in terms of ratiometric FRET and maturation in *E. coli*. The plasmids carrying the genes for the various crowding sensors were transformed into *E. coli* BL21(DE3) pLysS, and the cells were grown in MOPS medium at 30 °C and shaking at 200rpm. The ratiometric FRET of sensors in the cells was quantified by confocal microscopy. Similar to our *in vitro* data, the cyan-yellow sensors crGE, crGEs, crGEu, crTC, and crGEL201K, yield comparable acceptor/donor ratios, the crYCY shows a higher acceptor/donor ratio, and the crGO gives the lowest acceptor/donor ratio (Fig. 4B). Similar to the purified sensors in fluorescence spectroscopy, the sensors show an increase in ratiometric FRET by osmotic upshift of the media in which the cells are incubated (Fig. 4C).

To compare the different FRET ratios, we calibrated the purified sensors with Ficoll 70 as crowder and converted the ratiometric FRET *in vivo* to %w/w equivalents of Ficoll 70. The results are shown in Fig. 4. In MOPS medium, the ratiometric FRET of the sensors (crGE, crGEs, crGEu, crTC, and crGEL201K) is equivalent to ~19% w/w Ficoll 70. The equivalent fraction for crYCY is only ~8%, which may due to truncation of crYCY sensor *in cell*. The crGO does not give a realistic value with the equivalents of Ficoll 70 lower than 0%, likely due to the low maturation of mKO2. The difference in %w/w equivalents of Ficoll 70 could be due to the difference in maturation, which may relate to the expression condition, the concentration of the sensors which may result in formulating dimer, and other factors.

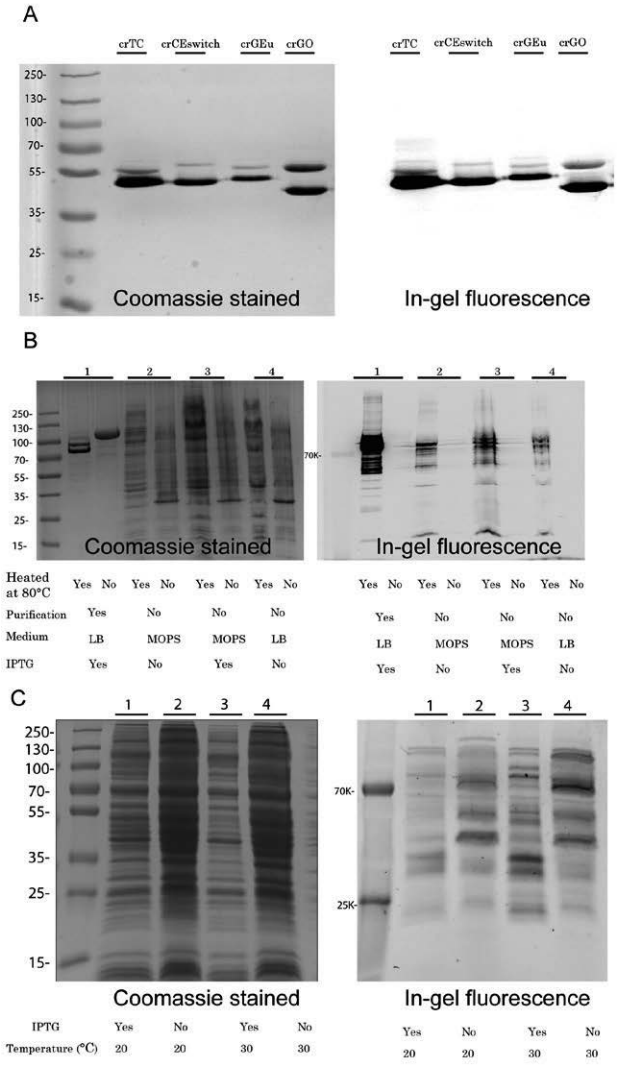

Fig. 3. SDS-PAGE of different FRET sensors. *The left panels are stained with Coomassie Brilliant Blue and the right panels are in gel fluorescent images at an excitation of 535nm.* ***A:*** *SDS-PAA gels showing the purity of crTC, crGEswitch, and crGEu after Ni-Sepharose and size-exclusion chromatography.* ***B:*** *Characterization of crYCY under different expression conditions by SDS-PAGE; (-) indicates sample buffer at room temperature and (+) indicates incubation in sample buffer at 80°C for 10 min. Lane 1: Purified CrYCY purified by size exclusion chromatography, LB medium, shaking at 25°C. Lane 2: Cell lysate from E. coli BL21(DE3) with constitutively expressed crYCY, MOPS mineral medium, shaking at 30°C. Lane 3: As in B, with 1 mM IPTG induction, MOPS mineral medium, shaking at 30°C. Land 4: Cell lysate form E. coli BL21(DE3) under constitutive expression (slow expression), LB medium, shaking at 25°C.* ***C:*** *SDS-PAGE gel electrophoresis of crNon-GFP isolated from E. coli BL21(DE3) pLysS. Characterization of crNon-*

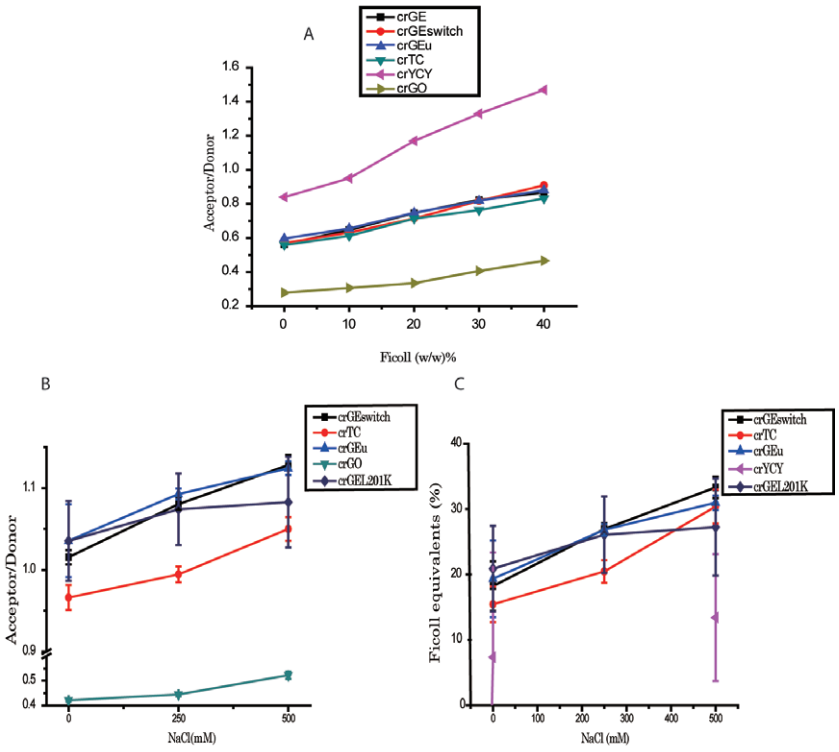

Fig. 4. Characterization of FRET-based crowding sensors. *The donor and acceptor pairs are shown in Table 1.* ***A:*** *Effect of Ficoll 70 on the purified crowding sensors.* ***B:*** *Acceptor/Donor ratio of different sensors in exponential growing (MOPS-glucose medium) E. coli.* ***C:*** *The same as B but after osmotic upshift (NaCl, 250 and 500 mM).* ***D:*** *% w/w Ficoll equivalents for the different sensors expressed in in exponential growing E. coli. E: C: The same as B but after osmotic upshift (NaCl, 250 and 500 mM). Error bars are the standard deviation of data from >100 cells.*

To figure out the difference in %w/w equivalents of Ficoll 70 for different sensors, we initially tried to control the sensor concentration *in vivo*. We transferred the crGE gene from pRSET A to pACYC, with expression controlled by a rhamnose-inducible promoter. Interestingly, the crGE sensor in the low-copy number pACYC vector gives a much higher acceptor/donor ratio compared to the same sensor in the high-copy number pRSET A plasmid.

The increase in FRET efficiency is also observed when the sensor is induced by IPTG with the pRSET A plasmid. To explain the

GFP sensor under different expression conditions. Lane 1: The cells were incubated at 20°C, 200rpm, under IPTG induction. Lane 2: The cells were incubated at 20°C, 200rpm, constitutive expression (slow expression). Lane 3: The cells were incubated at 30°C, 200rpm, IPTG induction. Lane 4: The cells were incubated at 30°C, 200rpm, constitutive expression (slow expression).

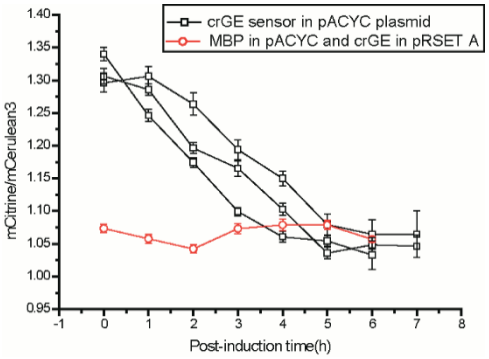

Fig. 5. The mCitrine/mCerulean3 ratio of crGE in pACYC decreases in the post-induction period and approaches the ratios obtained with constitutive expression. *Black squares: crGE sensor in pACYC after induction with 0.1% rhamnose overnight, and the induction was halted at t = 0. Red circles; cells expressing MBP in pACYC, induced overnight and stopped at t = 0, and crGE in pRSET A, which is constitutively expressed. All the experiments were performed in E. coli BL21DE3 incubated in MOPS mineral medium at 30 °C and 200rpm of shaking. Error bars are the standard error over 100 E. coli cells.*

unexpected increase in acceptor/donor ratios of induced expression as compared to constitutive expression, we tracked mCitrine/mCerulean3 during a post-induction period. We incubated *E. coli* BL21DE3 with crGE sensor in pACYC in MOPS mineral medium (at 30 °C and 200 rpm of shaking), and induced expression with 0.1% rhamnose overnight. The next day, we stopped induction by spinning down the cells and resuspending them in MOPS medium without rhamnose. We determined the mCitrine/mCerulean3 ratio over time (Fig. 5). At t = 0, after induction overnight, the acceptor/donor ratio of crGE in pACYC was ~1.32. The ratio dropped to 1.05 at 6 h post-induction. This ratio is comparable to that of cells constitutively expressing crGE with pRSET A.

To confirm that induced expression itself does not cause overcrowding of the cell, and hence change the sensor readout, control cells with pACYC containing the gene for maltose-binding protein (MBP, a non-fluorescent protein) and crGE in pRSET A were tested. Overexpression (induced/high expression) of MBP in the cytoplasm with 0.1% rhamnose did not lead to changes in the FRET ratio of the constitutively expressed crGE sensor, indicating that intracellular crowding does not change during induced expression.

The high ratiometric FRET ratio of crGE in pACYC could be caused by incomplete maturation of mCerulean3 when produced from the pACYC vector, rather than crowding changes. When we stop induction, the cells stop synthesizing the protein and the immature mCerulean3 continues to mature. The newly matured mCerulean3

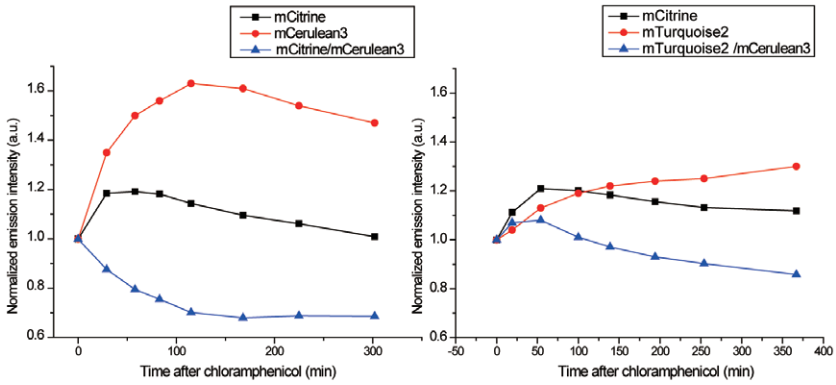

Fig. 6. The maturation of fluorescent proteins in E. coli. A: *the maturation of mCitrine (excited at 505 nm) and mCerulean3 (excited at 405 nm) in crGE expressed in E. coli.* ***B:*** *the maturation of mCitrine and mTurquise2 in crTC expressed in E. coli. The E. coli BL21(DE3) strain, without pLysS, with pRSET A containing the gene encoding the probe, was grown in glucose-MOPS mineral medium as described in the Methods section. The intensity of both fluorescent proteins was recorded every half hour after the addition of chloramphenicol. To compare the signal change, the fluorescent intensity was normalized to t = 0.*

significantly increases the intensity of *Idonor*. As a result, the observed ratiometric FRET decreases. Hence, inducible expression of the sensor decreases the fraction of mature mCerulean3; the maturation can be optimized by giving the proteins more to time mature, e.g. as under our conditions of constitutive expression.

The maturation of fluorescent proteins

To investigate the relation between maturation and the FRET ratio of crGE and crTC sensor in *E. coli* further, we determined the kinetics of maturation of the fluorescent proteins in the spectrophotometer. *E. coli* BL21(DE3) cells were grown to OD_{600} of 0.1–0.2, after which they were treated with chloramphenicol to stop protein synthesis. We tracked the fluorescence over time (Fig. 6) and fitted the data with an exponential model. For crGE, it took 30-60 min for mCitrine to reach full maturation with 80% of the mCitrine already matured at t = 0. mCerulean3 was matured in 100-140 min with 50% of the mCerulean3 already matured at t = 0. For crTC sensor, we found the same maturation for mCitrine as mCitrinie in crGE, while the mTurquoise2 matures faster than mCerulean3 (60–90 min with 70% already matured at t = 0). The results demonstrate that crTC shows an improved maturation while neither fluorescent protein in the crTC or crGE is fully matured *in vivo*.

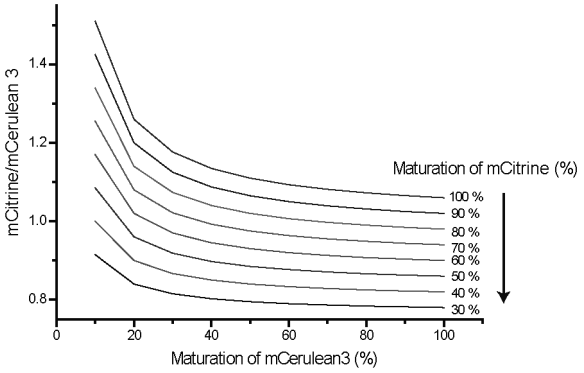

Fig. 7. The effect of maturation of fluorescent proteins on FRET sensor read-out. We assumed the FRET efficiency (E) of crGE in pRSET A is about 12±2% in exponential growing cells in MOPS minimal medium.

The model

We use eq. 15 to quantify the effect of maturation on the FRET ratio. To determine how the bleed-though, the FRET, and the cross-excitation influence the observed ratiometric FRET signal, we quantified the coefficients α, β and γ with purified mCerulean3, mCitrine, and crGE. The value of , which is only related to the emission of mCerulean3, is 0.66. Coefficient γ is the brightness difference between mCerulean3 and mCitrine, and is ~2 according to Cranfill et al.[28]. The coefficient β, which is employed to build the relation between the ratio of emission upon cross excitation of acceptor, and donor emission in the absence of acceptor (*Idonor only*), is 0.05. We know that the FRET efficiency (*E*) of crGE in pRSET A is about 12±2%[19] in exponentially growing *E. coli* cells in MOPS minimal medium. Inserting all parameters into Eq. 15, yields the following relationship.

$$Ratiometric\ FRET = 0.66 + 0.34 \cdot m_{acceptor} + 0.06 \cdot \frac{m_{acceptor}}{m_{donor}} \quad \text{Eq. 15}$$

The data are plotted in Fig. 7 for different degrees of mCitrine and mCerulean3 maturation. We notice that the ratiometric FRET relates to the maturation of fluorescent protein and depends strongly on the maturation of mCitrine, while the maturation of mCerulean3 mostly influences the ratiometric FRET at low levels of maturation. A lower maturation of mCitrine will decrease the mCitrine/mCerulean3, and a lower maturation percentage of mCerulean3 will increase the ratiometric FRET. Hence, the maturation of mCitrine (acceptor) and mCerulean3 (donor) have opposing effects on the ratiometric FRET, and when the maturation of both decreases, the change in ratiometric FRET will be compensated to a certain extent.

Discussion

In this study, we compared a set of fluorescent proteins in the context of their performance as crowding sensors, and observed a strong dependence of the FRET ratios on the expression conditions. We quantified the maturation of the fluorescent proteins of a sensor in *E. coli* and built a model to predict the effect of maturation on the ratiometric FRET values. The maturation of both donor and acceptor influence the ratiometric FRET, while slower expression can maximize the maturation of the fluorescent proteins.

By determining the maturation in *E. coli*, grown in MOPS minimal medium at 30 oC (doubling time of ~ 2h), we find that mCerulean3 matures to about 50% and mCitrine to 80% during constitutive expression from the T7 promoter (Fig. 6). The maturation efficiency decreases during induced expression because synthesis rate will be faster than the maturation rate which increase the fraction of immature protein. Additionally, under these conditions, the concentration of oxygen may be limiting for maturation[16]. Given that maturation times of fluorescent proteins range from 10 min to 500 min[28], we can infer that many will not fully mature under the ambient conditions in the cell, which will influence the ratiometric FRET readout.

To predict the influence of maturation on ratiometric FRET, we quantified the influence of bleed-through, cross-excitation and actual FRET on the ratiometric FRET. We employed crGE as an example and obtained a model for ratiometric FRET as a function of the degrees of maturation of mCerulean3 and mCitrine. The model assumes that the purified crGE sensor is fully matured, while the fluorescent protein mCerulean3 and mCitrine may not be fully mature in reality. Our gel analysis to discriminate fully folded/matured proteins from misfolded proteins, based on Geertsma et al.[26] indicates that the assumption is valid however.

The maturation of both donor and acceptor fluorescence influences the ratiometric FRET. It would be ideal to use an acceptor that is not cross-excited, which would remove the last part of Eq. 16. Then, the ratiometric FRET is only dependent of the acceptor maturation. Hence, a sensor with a fast-matured acceptor that cannot be cross-excited would be the preferred fluorophore for FRET-based readout.

An alternative way to minimize the influence of maturation is to maximize the maturation of both donor and acceptor. We find that constitutive expression (expression with stable protein levels) in MOPS medium yields the most stable ratiometric FRET. Under constitutive expression, the concentration of proteins remains lower than under overexpression (induced/high expression). Furthermore, cells grown in mineral MPOS medium have a longer doubling time compared to cells grown in rich medium.[17]. As a result of these two

factors, the fluorescent protein has more time to mature leading to an increased maturation efficiency.

Conclusion

We delineate the influence of maturation on the ratiometric FRET of a set of crowding-sensitive probes. We show that the maturation of both donor and acceptor fluorophores are key parameters to consider for the interpretation of FRET signals. In *E. coli*, a relatively slow expression of the sensors in MOPS minimal medium yields the most complete maturation and thus a stable ratiometric FRET readout. The choice of fast maturing fluorescent proteins is desirable for FRET-based readout in living cells. Nevertheless, we advise to quantify the maturation of the fluorescent proteins in the FRET sensors when employing the FRET sensors for a given condition *in vivo*.

Reference

1 Joo, C., Balci, H., Ishitsuka, Y., Buranachai, C. & Ha, T. Advances in single-molecule fluorescence methods for molecular biology. *Annual Review of Biochemistry* **77**, 51-76, doi:10.1146/annurev.biochem.77.070606.101543 (2008).

2 Medintz, I. L. & Mattoussi, H. Quantum dot-based resonance energy transfer and its growing application in biology. *Physical Chemistry Chemical Physics* **11**, 17-45, doi:10.1039/b813919a (2009).

3 Merzlyak, E. M. et al. Bright monomeric red fluorescent protein with an extended fluorescence lifetime. *Nature Methods* **4**, 555-557, doi:10.1038/nmeth1062 (2007).

4 Abraham, B. G., Santala, V., Tkachenko, N. V. & Karp, M. Fluorescent protein-based FRET sensor for intracellular monitoring of redox status in bacteria at single cell level. *Analytical and Bioanalytical Chemistry* **406**, 7195-7204, doi:10.1007/s00216-014-8165-1 (2014).

5 Peroza, E. A., Ewald, J. C., Parakkal, G., Skotheim, J. M. & Zamboni, N. A genetically encoded Forster resonance energy transfer sensor for monitoring in vivo trehalose-6-phosphate dynamics. *Analytical Biochemistry* **474**, 1-7, doi:10.1016/j.ab.2014.12.019 (2015).

6 Zhao, F. L., Zhang, C., Tang, Y. & Ye, B. C. A genetically encoded biosensor for in vitro and in vivo detection of NADP(+). *Biosensors & Bioelectronics* **77**, 901-906, doi:10.1016/j.bios.2015.10.063 (2016).

7 Ahmad, M., Ameen, S., Siddiqi, T. O., Khan, P. & Ahmad, A. Live cell monitoring of glycine betaine by FRET-based genetically encoded nanosensor. *Biosensors & Bioelectronics* **86**, 169-175, doi:10.1016/j.bios.2016.06.049 (2016).

8 Ameen, S. et al. Designing, construction and characterization of genetically encoded FRET-based nanosensor for real time monitoring of lysine flux in living cells. *Journal of Nanobiotechnology* **14**, doi:10.1186/s12951-016-0204-y (2016).

9 Mohsin, M. & Ahmad, A. Genetically-encoded nanosensor for quantitative monitoring of methionine in bacterial and yeast cells. *Biosensors & Bioelectronics* **59**, 358-364, doi:10.1016/j.bios.2014.03.066 (2014).

10 Monsin, M., Diwan, H., Khan, I. & Ahmad, A. Genetically encoded FRET-based nanosensor for in vivo monitoring of zinc concentration in physiological environment of living cell. *Biochemical Engineering Journal* **102**, 62-68, doi:10.1016/j.bej.2015.03.012 (2015).

11 Okada, S., Ota, K. & Ito, T. Circular permutation of ligand-binding module improves dynamic range of genetically encoded FRET-based nanosensor. *Protein Science* **18**, 2518-2527, doi:10.1002/pro.266 (2009).

12 Vanoaica, L., Behera, A., Camargo, S. M. R., Forster, I. C. & Verrey, F. Real-time functional characterization of cationic amino acid transporters using a new FRET sensor. *Pflugers Archiv-European Journal of Physiology* **468**, 563-572, doi:10.1007/s00424-015-1754-9 (2016).

13 Remington, S. J. Fluorescent proteins: maturation, photochemistry and photophysics. *Current Opinion in Structural Biology* **16**, 714-721, doi:10.1016/j.sbi.2006.10.001 (2006).

14 Tsien, R. Y. The green fluorescent protein. *Annual Review of Biochemistry* **67**, 509-544, doi:10.1146/annurev.biochem.67.1.509 (1998).

15 Bajar, B. T., Wang, E. S., Zhang, S., Lin, M. Z. & Chu, J. A Guide to Fluorescent Protein FRET Pairs. *Sensors* **16**, doi:10.3390/s16091488 (2016).

16 Hebisch, E., Knebel, J., Landsberg, J., Frey, E. & Leisner, M. High Variation of Fluorescence Protein Maturation Times in Closely Related Escherichia coli Strains. *Plos One* **8**, 9, doi:10.1371/journal.pone.0075991 (2013).

17 Volkmer, B. & Heinemann, M. Condition-Dependent Cell Volume and Concentration of Escherichia coli to Facilitate Data Conversion for Systems Biology Modeling. *Plos One* **6**, doi:10.1371/journal.pone.0023126 (2011).

18 Elder, A. D. et al. A quantitative protocol for dynamic measurements of protein interactions by Forster resonance energy transfer-sensitized fluorescence emission. Journal of the Royal Society Interface 6, S59-S81, doi:10.1098/rsif.2008.0381.focus (2009).

19 Liu, B. Q. et al. Design and Properties of Genetically Encoded Probes for Sensing Macromolecular Crowding. *Biophysical Journal* **112**, 1929-1939, doi:10.1016/j.bpj.2017.04.004 (2017).

20 Boersma, A. J., Zuhorn, I. S. & Poolman, B. A sensor for quantification of macromolecular crowding in living cells. *Nature Methods* **12**, 227-+, doi:10.1038/nmeth.3257 (2015).

21 Neidhard.Fc, Bloch, P. L. & Smith, D. F. CULTURE MEDIUM FOR ENTEROBACTERIA. *Journal of Bacteriology* **119**, 736-747 (1974).

22 Lakowicz, J. R. & Masters, B. R. Principles of Fluorescence Spectroscopy. 3rd edn, (2006).

23 Goedhart, J. et al. Structure-guided evolution of cyan fluorescent proteins towards a quantum yield of 93%. *Nature Communications* **3**, doi:10.1038/ncomms1738 (2012).

24 Nakano, M., Imamura, H., Nagai, T. & Noji, H. Ca2+ Regulation of Mitochondrial ATP Synthesis Visualized at the Single Cell Level. *ACS Chemical Biology* **6**, 709-715, doi:10.1021/cb100313n (2011).

25 Nagai, T. et al. A variant of yellow fluorescent protein with fast and efficient maturation for cell-biological applications. *Nature Biotechnology* **20**, 87-90, doi:10.1038/nbt0102-87 (2002).

26 Geertsma, E. R., Groeneveld, M., Slotboom, D. J. & Poolman, B. Quality control of overexpressed membrane proteins. *Proceedings of the National Academy of Sciences of the United States of America* **105**, 5722-5727, doi:10.1073/pnas.0802190105 (2008).

27 Pedelacq, J. D., Cabantous, S., Tran, T., Terwilliger, T. C. & Waldo, G. S. Engineering and characterization of a superfolder green fluorescent protein. *Nature Biotechnology* **24**, 79-88, doi:10.1038/nbt1172 (2006).

28 Cranfill, P. J. et al. Quantitative assessment of fluorescent proteins. *Nature Methods* **13**, 557-+, doi:10.1038/nmeth.3891 (2016).

Chapter 4

Macromolecular crowding during adaptation to hyperosmotic stress

Manuscript in preparation

Abstract

Cellular macromolecular crowding influences the mobility of biomolecules, protein folding and stability, and the association of macromolecules with each other. To understand how macromolecular crowding changes during adaptation to hyperosmotic stress, we tracked the crowding changes in *Escherichia coli* with previously developed macromolecular crowding sensors (crGE, crE6, and crG18). The results demonstrate that macromolecular crowding increases immediately after osmotic upshift, then decreases to a lower level over 2-5 h, where it remains for several hours. The crowding initially follows cell volume but arrives at a lower value upon adaptation. With these results, in combination with literature observations, we hypothesize that the decrease could be due to an increase in self-association of the macromolecules in the cell upon adaptation. The self-association creates a heterogeneous distribution in the cytoplasm, resulting in some regions experiencing less crowding. This interpretation would be fundamental to the organization of the crowded cellular cytoplasm, and could apply to other species as well.

Introduction

The cellular environment is highly crowded with proteins and other macromolecules[1]. Many biochemical and biophysical processes, such as gene expression[2], macromolecule diffusion[3], protein-DNA interaction[4,5], and protein folding[6,7] are affected by macromolecular crowding. However, the cellular environment is not static and the volume of a cell undergoes changes when unicellular organisms are confronted with changes in the osmolality of the extracellular environment. These changes have consequences for physicochemical parameters such as crowding, ionic strength, pH, viscosity and osmotic pressure.

Cells will adjust their cytoplasm to counteract the consequences of the osmotic stress. Upon osmotic upshift, the cells immediately shrink[8] and many cells counteract this by taking up potassium ions, which is best documented for *E. coli9*. Subsequently, *E. coli* synthesizes or takes up available compatible solutes[10,11], and adjusts the proteome to adapt to the osmotic upshift. Researchers[12–16] showed that in *E. coli* over 300 genes are up- or downregulated by osmotic upshift. Interestingly, Konopka et al.[17] found that the biopolymer fraction increases after adaptation to hyperosmotic shock, while the diffusion coefficient of GFP only shows a small decrease. These findings indicate that there may be significant changes in the molecular crowding and biopolymer organization in the cytoplasm during adaptation of *E. coli*.

Previously, we developed a set of FRET-based crowding sensors[18,19]. The sensors allow one to track temporally the macromolecular crowding during osmotic stress. In this chapter, we employ three sensors, which have different linker structure and sensing properties *in vivo*. The crGE is the largest crowding sensor, which consists of two α-helices three random coils, with fluorescent proteins (donor and acceptor) connected to the N- and C-terminal ends. The crE6G2 sensor consist of two α-helices one small random coil and the fluorescent proteins. The crG18 sensor consist of a single long random coil and is least sensitive to crowding changes in *vivo* (chapter 2). We show that macromolecular crowding increases upon osmotic upshift and returns within 2-5 hours to a level lower than the crowding prior the osmotic shift. We explain the lower apparent crowding with the hypothesis that the macromolecules in adapted cells increasingly associate with each other (perhaps forming areas where the sensor is excluded), which creates regions of lower crowding.

Material and Methods

Cell growth and confocal imaging

The batch culture experiments were performed as described previously[18,19]. The *E. coli* cells with the appropriate plasmids were prepared as described in Chapter 2. Briefly, the pRSET A vector containing the synthetic gene encoding either crGE, crE6G2 or crG18, was transformed into *E. coli* BL21(DE3) pLysS. The cells were incubated at 30 °C, shaking at 200 rpm, in 10 mL MOPS medium[20] with 20 mM glucose and grown overnight. The next day, the cells were diluted into 50 mL of fresh medium to OD_{600} = 0.05. When the OD_{600} reached 0.1–0.2, the cells were exposed to the desired amount of NaCl and imaged under the microscope as described in Chapter 2. In short, 0.5 mL cells, expressing one of the sensors, were combined with 0.5 mL cells without sensor (blank). The combined cells were centrifuged, and resuspended in 100 µL (MOPS minimal medium with 20 mM glucose and the desired amount of NaCl (osmotic upshift). Subsequently, the cells were transferred to a glass slide [coated/treated coverslip modified with (3-aminopropyl) triethoxysilane] and imaged on a laser-scanning microscope (Zeiss LSM 710) immediately after the osmotic upshift.

Imaging in a microfluidics chamber

The microfluidic chamber (CellASIC ONIX Microfluidic Plates) was pre-warmed overnight at 30 °C on the laser-scanning confocal microscope. The *E. coli* BL21(DE3) pLysS strain with desired crowding sensor and the control strain were grown overnight to an OD_{600} of 0.1-0.3, which is still in the exponential growth phase, and they were then diluted to OD_{600} = 0.01 in MOPS minimal medium with 20 mM glucose and subsequently loaded in the microfluidic chamber. After loading, the cells were incubated with 0.1× MOPS-glucose medium (MOPS-glucose medium diluted ten times with 0.16 M NaCl) at 30 °C for 2 h. For the osmotic upshift, 0.3 M NaCl in the 0.1× MOPS-glucose medium was flowed in 2h after the cells were loaded, to allow the cells to adapt to the new environment. Alternatively, we used 600 mM and 1 M sorbitol in 0.1x MOPS-glucose for osmotic upshift in the microfluidic chamber. The images were collected and analyzed as described previously[18,19].

Cell volume determination

The volume of the cytoplasm was determined by PhotoActivated Localization Microscopy (PALM). The gene encoding LacY was fused to YPet which can switch "on" or "off" during imaging in PALM[21]. The gene encoding LacY-Ypet was cloned into pACYC and transfected into *E. coli* BL21(DE3) pLysS. The cells (inoculated from a single colony) were grown at 30 °C, shaking at 200 rpm in 10 mL MOPS medium with 20 mM glucose, overnight. The next day, when OD_{600} reached 0.2, the cells were induced with 0.1% rhamnose. One hour after induction, the cells were imaged by PALM microscopy before and after addition of 300 mM NaCl.

Coverslips were cleaned with 5M KOH in a sonication bath for 30 minutes, and washed with demineralized water and acetone (Aldrich). Next, the coverslips were plasma-cleaned for 10 min, and subsequently coated with 2% (v/v) (3-Aminopropyl) trioxysilane (Aldrich) in acetone for 30 minutes. The coverslips were washed with demineralized water and left drying.

For PALM, a home-built inverted microscope based on an Olympus IX-81 with a high numerical aperture objective (100 X, NA = 1.49, oil immersion, Olympus, UApo) was used. Solid-state lasers were from Coherent (Santa Clara, USA): 514nm (Sapphire 514, 100mW). Imaging was performed in semi-TIRF mode with the angle of light exiting the objective adjusted to create a light sheet restricted to the bottom few micrometers of the specimen. The fluorescence was recorded using an electron multiplying charge-coupled device (EM-CCD camera) from Hamamatsu, Japan, model C9100-13. For data acquisition and analysis, LacY-YPet was continuously illuminated at 517 nm and a total of 3000 frames were recorded with 30 ms for each frame. The data was analyzed with a home-written ImageJ script, in which the reconstructed images of each fluorescent molecule are represented as a single spot at its determined coordinates, with a brightness that corresponds to the localization accuracy [22].

Preparation of cell lysate

The *E. coli* BL21(DE3) pLysS cells were incubated in 10 mL MOPS with 20 mM glucose at 30 °C and shaking at 200 rpm overnight, and then diluted to 1 L of fresh medium to OD_{600} = 0.02. When the OD_{600} reached 0.2, half of the culture was lysed immediately, while the other half was lysed after incubation for 5 h with 300 mM NaCl. To lyse the cells, the cultures were harvested by centrifugation (3000× g, 30 minutes). The pellet was resuspended in phosphate buffer (10 mM NaPi, 100 mM NaCl, pH 7.4) containing proteinase inhibitor (cOmplete™,

Mini, EDTA-free). Cells were lysed by sonication for 2 minutes, with alternating 5 seconds sonication and 5 seconds cooling, and then centrifuged (20,000xg, 10 min). The supernatant was immediately used for the fluorescence measurements.

Fluorometry

Fluorescence emission spectra were measured with a Fluorolog-3 (Jobin Yvon) spectrofluorometer as described in Chapter 2. A 1.0 mL solution (10 mM NaPi, 100 mM NaCl, 2 mg/mL BSA, pH 7.4) was added to a quartz cuvette and its fluorescence emission spectrum was recorded after excitation at 420 nm (A). Subsequently, purified sensor was added, mixed by pipette, and the fluorescence was recorded (B). The desired amount of small molecule or cell lysate was added, mixed by pipette, and the fluorescence was recorded again (C). The background spectrum A, prior to the addition of the probe, was subtracted from B or C.

The influence of small molecules on the read-out of the crowding sensor (crG18) was recorded on a Spark® 10M microplate reader. A 300 µL solution containing the given small molecule (Proline, KCl, ATP, sucrose and aspartic acid) and 10 mM NaPi (adjusted the pH to 7.4 after dissolution of the salts) were added to a 96 well plate (Greiner). The purified sensor was added and the fluorescence intensity at 475 nm and 525 nm were recorded separately with excitation at 420 nm at room temperature. A 20 nm bandwidth for excitation and emission was applied, and the average of 10 measurements of a single well was taken. The background fluorescence (buffer without sensor) was subtracted in all cases.

Results

Temporal changes in apparent crowding upon osmotic upshift

Cells in batch culture

To track the changes in crowding during adaptation to hyperosmotic stress, we grew *E. coli* BL21(DE3) pLysS containing the crGE sensor in a 50 mL MOPS-glucose medium, and exposed the cells to an osmotic stress of 300 mM NaCl when the OD_{600} reached 0.2. We diluted the culture throughout the experiment to maintain the OD_{600} between 0.1 and 0.3, and corrected the OD_{600} for dilution (Fig. 1). We took samples for imaging from the culture to monitor the temporal change of ratiometric FRET of crGE (Fig 1A). The FRET value is 1.06 ± 0.009

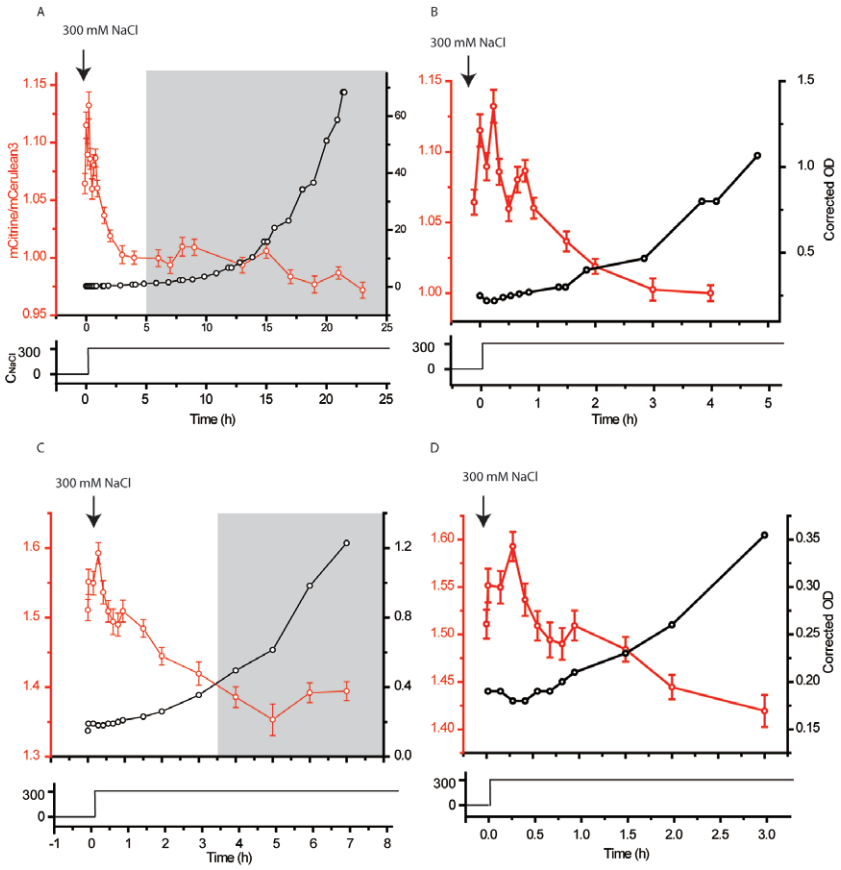

Fig. 1. Crowding changes upon osmotic upshift in cells in batch culture. *The concentration of NaCl is shown in the upper lane of each graph, and the grey shaded area indicates when the crowding remains at a lower level.* ***A:*** *The ratiometric FRET of crGE in E. coli growing in 50 mL culture at 30 °C. The cells were shocked with 300 mM NaCl. We diluted the culture throughout the experiment to maintain the OD600 between 0.1 and 0.3; the corrected OD reflects OD600 times the dilution factor. The point before t = 0 indicates before NaCl addition. Error bars are the standard error (n = ~100 cells).* ***B:*** *The zoom-in of panel A.* ***C:*** *The same as A, except that crG18 was used.* ***D:*** *The zoom-in of C.*

(s.e., n = 98) before the upshift, and immediately increases to 1.12 ± 0.01 (s.e., n = 98) upon addition of NaCl. The ratiometric FRET returns to the level before the osmotic upshift within 1 h and decreases to 1.00 ± 0.006 (s.e., n = 90) over the next 3 h. The ratiometric FRET remains at the lower level for at least 23 h. We observed a similar decrease when the crowding was probed by the crG18 sensor under the same conditions (Fig. 1B). Hence, the observations are independent of the structural properties of the crowding sensor. We found in

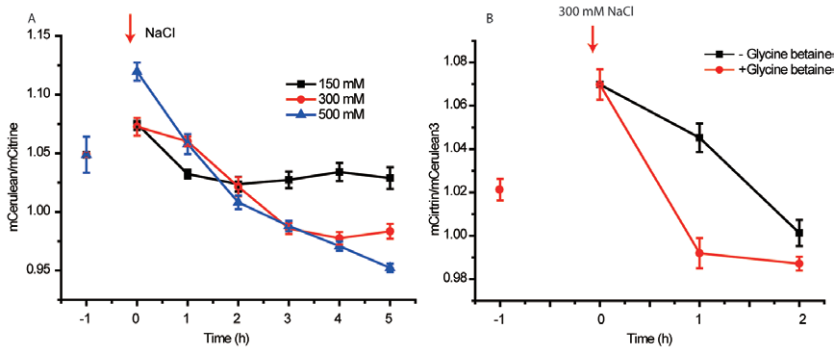

***Fig. 2. Adaptation to osmotic stress at different degrees of upshift. A**: E. coli BL21(DE3) pLysS with crGE sensor was incubated in MOPS-glucose at 30 °C in batch culture. Just before t = 0, the cells were treated with different concentrations of NaCl. **B:** The same as panel A, except that 1 mM glycine betaine was present in the medium. Errors bars show the standard error over ~100 cells.*

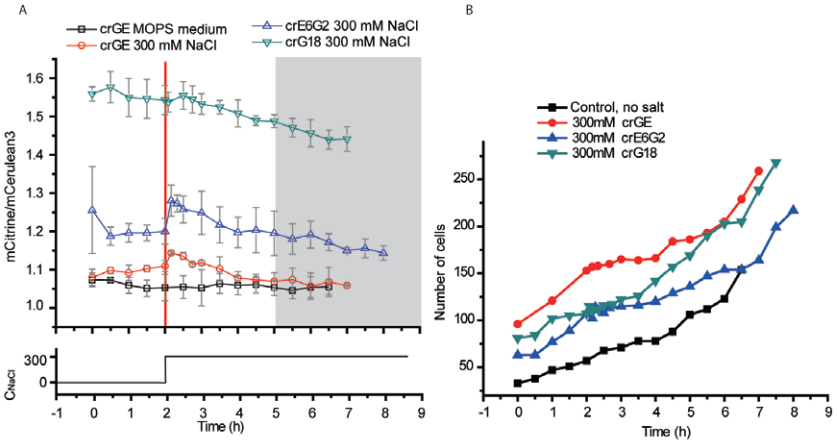

***Fig. 3. Crowding changes upon osmotic upshift in cells in the microfluidic chamber. A**: Ratiometric FRET of different sensors in the microfluidic chamber. Cells were grown in the chamber in 10-times diluted MOPS-glucose plus 0.16 M NaCl, which has a similar osmolality as MOPS-glucose. At 2 h, the same medium supplemented with 300 mM NaCl was flowed in. The black squares show the data of cells that were not subjected to an osmotic upshift. Error bars show the standard deviation from three independent biological replicates, each based on ~100 cells. **B**: The cell number of E. coli growing in the microfluidic chamber.*

both cases that the cell stopped growing from 0 to 1h during which the crowding returned to the level before shock. After 1h, the OD_{600} resumed but the crowding decreased further.

To compare the influence of osmolality on the apparent decrease in crowding in the adaptation period, we treated the cells with

different concentrations of NaCl (Fig. 2A). We found that the final ratiometric FRET after adaptation decreases with increasing osmolality (Fig. 2A). This indicates that the overshoot of crowding is not a switch between two distinct states of the cytoplasm but occurs on a continuous scale.

To investigate the influence of compatible solutes on the recovery of the cells, we treated the cells with 300 mM NaCl in the presence of glycine betaine (Fig. 2B). Compatible solutes, such as glycine betaine, aid the cell in surviving osmotic upshifts by balancing the osmotic difference and stabilizing the proteins[23]. The compatible solutes only slightly decrease the ratiometric FRET by increasing the refractive index of the medium, as described previously[18]. We observed that the ratiometric FRET levels off to the same value in the presence and absence of glycine betaine, but the restoration of crowding is faster in the presence of glycine betaine[24]. The cells were not primed with glycine betaine, which would induce the expression of the corresponding transporters (ProP, ProU; add REFS), yet the recovery is still faster than without glycine betaine.

Cells in microfluidic chamber

To obtain further information on the transients in the crowding, we tracked individual cells in a microfluidic chamber (Fig 1C). We first determined the ratiometric FRET of *E. coli* growing in 0.1× MOPS-glucose medium (supplemented with 160 mM NaCl). The crowding stays stable during the 6 h period, confirming unperturbed growth (Fig. 3A). We observed smaller changes in apparent crowding when cells grew in 0.1× MOPS-glucose medium compared to undiluted MOPS-glucose medium, for which for which we currently do not have an explanation. Additionally, we found that the growth rate in 0.1× MOPS-glucose medium and MOPS-glucose medium are similar, which is ~0.5 h^{-1}. Hence, for all the experiments in the microfluidic chamber, we incubated the cells in 0.1x MOPS-glucose medium, supplemented with 160 mM NaCl.

For experiments where cells were challenged with osmotic stress, the cells were first incubated in the microfluidic chamber for 2 h, after which we continuously flowed in medium with 300 mM NaCl. To confirm that crowding changes were independent of the type of crowding sensor, we compared the FRET signals of crGE, crE6G2 and crG18 during the osmotic upshift. We find a similar decrease in ratiometric FRET as observed in the experiments in batch culture. The number of cells was counted (Fig 3B). During the first 2h before upshift, the cell number increased steadily indicating the cells grow well in the microfluidic device. The cell number stopped to increase when the medium when 300 mM NaCl was flowed in. The cells started to grow again at ~4 h.

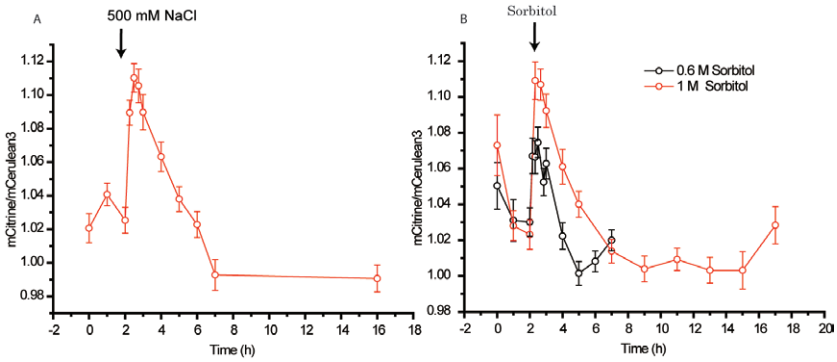

Fig. 4. Crowding changes in cells in the microfluidic chamber upon osmotic upshift with NaCl or sorbitol. A: *The E. coli BL21(DE3) pLysS cells expressing crGE were loaded into a microfluidic chamber at t = 0 and incubated at 30 °C in 0.1x MOPS-glucose medium. At t = 2h, 0.1x MOPS-glucose with 500 mM NaCl were flowed in. Errors bars are standard error over ~100 cells.* ***B:*** *The E. coli BL21(DE3) pLysS cells expressing crGE sensors were treated the same as A. At = 2h, 0.1x MOPS-glucose medium with desired concentration sorbitol were flowed in. Errors bars show the standard error in the FRET ratio from ~100 cells.*

For crGE and crE6G2, the ratiometric FRET increases instantaneously by flowing in NaCl and then decreases to a level lower than before the osmotic upshift. The lower level is reached after ~4h when the cells also resume growth. The crG18 sensor, which is less sensitive than crGE and crE6, shows accordingly a much smaller increase in ratiometric FRET (Fig. 1B). Similar to the measurements for cells growing in batch culture, the apparent crowding levels off to a lower value with 500 than 300 mM NaCl. To confirm that the decrease is independent of the nature of the osmolyte to stress the cells, we also performed osmotic perturbations with sorbitol in the microfluidic chamber (Fig. 4), and made similar observations as for NaCl.

Volume and length of cells exposed to osmotic stress

To investigate the relation between the apparent crowding changes and cell volume, the volume of the *E. coli* cytoplasm was determined from images obtained by PALM, using the membrane protein LacY fused to the yellow fluorescent protein Ypet to mark the cytoplasmic compartment. The volume decreases by 30% after adding 300 mM NaCl (**Fig. 5A**). Three hours after the osmotic upshift, the volume has recovered to ~1.8 fL, which is 82% of the value before the shock. Next, to yield more detail of the structural changes of the cell, we determined the length (**Fig. 5B, C**) of the cells grown in batch culture (Fig. 1B, C). The cells immediately become shorter by 20% upon addition of

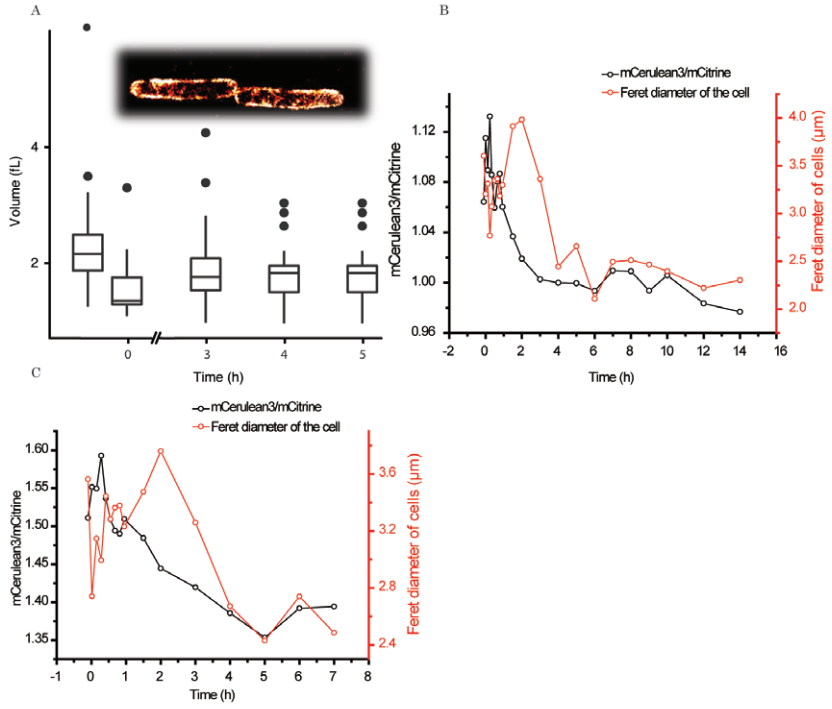

Fig. 5. Cell volume and length during hyperosmotic stress. A: *Volume of E. coli BL21(DE3) pLysS expressing LacY-YPet, and determination of the cell contours from single-molecule localizations by PALM microscopy. At t = 0, the cells were treated with 300 mM NaCl. For each data point, ~30 cells were imaged and analyzed.* ***B:*** *The red line is the median cell length of E. coli BL21(DE3) pLysS expressing crGE; the black line is the average mCerulean3/mCitrine ratio of the same cells. The cell length was determined with the Feret's diameter in the PMT channel in ImageJ.* ***C:*** *The same as B with E. coli BL21(DE3) pLysS expressing crG18.*

300 mM NaCl, and the length returns to the value before the osmotic upshift after 0.5 h. After 60–90 minutes, the average cell length starts to increase as the cells resume growth. Afterwards, most of cells divide (apparent doubling time of 2 h), and accordingly the average cell length decreases. After this, the average length remains lower due to the adaptation of the cells to osmotic upshift. When we compare the cell length with the ratiometric FRET, we find that the crowding initially follows the cell volume; when the volume is low the crowding is high (shown in gray in Fig. 5B&C). After ~2 h, the crowding no longer follows the cell volume and both the volume and the ratiometric FRET decrease. Around ~2 h, the OD_{600} starts to increase again. Hence, the results indicate that the crowding is proportional to the cell volume immediately after the osmotic upshift, but that apparent correlation no longer holds at later times, that is, in the adaptation phase.

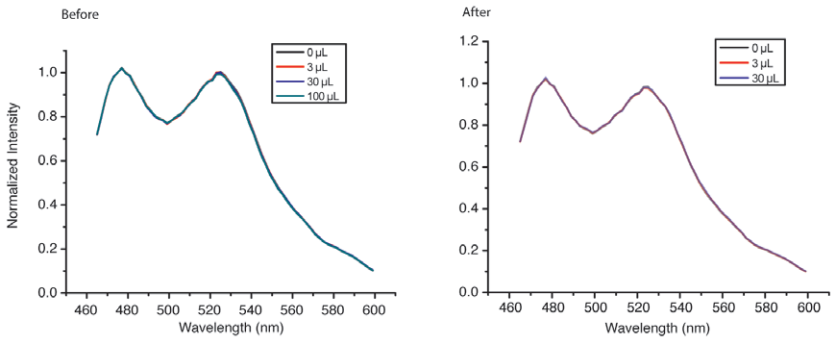

Fig. 6. Fluorescence spectra of crG18 sensor. *The crG18 was dissolved in 10 mM sodium phosphate (NaPi), 100 mM NaCl, pH 7.4 and titrated with different volumes of concentrated cell lysate. Left panel: titration with cell lysate before osmotic upshift; right panel: titration with cell lysate obtained 5 h after the osmotic upshift with 300 mM NaCl.*

Sensor performance during adaptation

The ratiometric FRET of the crowding sensor in living cells could be influenced by several factors, e.g. truncation/misfolding of the proteins, changes in refractive index and/or molecules binding to the sensor. To confirm that the ratiometric FRET reports genuine changes in excluded volume, rather than e.g. binding of specific molecules to the sensors, we investigated the influence of cell lysate on the sensor (**Fig. 6**). *E. coli* cells, grown for 5h in MOPS-glucose, with or without 300 mM NaCl, were lysed and the effect of cell lysate on purified crG18 sensor was tested. We did not find any effect of cell lysate. We only find a small effect of some metabolites (Proline, KCl, ATP, sucrose and aspartic acid) when tested at unphysiologically high concentrations.[25] For example, the ratiometric FRET decreased somewhat in the presence of 34 mM ATP, but the concentration in vivo is typically less than 10 mM[26]. Combined with previous work, in which we tested other relevant metabolites[18,19], we conclude that the changes in FRET signal are not likely due to small molecules binding to the sensors (Fig. 7).

To confirm that the sensor is not truncated during growth, we performed an SDS-PAGE analysis. The gels show that the sensors are not truncated in control and osmotically stressed cells (Fig. 8). To show that the ratiometric FRET signal is independent of the maturation of the fluorescent proteins, we excited mCitrine (FRET acceptor) in crGE directly at 488 nm, as well as mCerulean3 (FRET donor) at 405 nm. We determined the fluorescence intensity throughout the adaptation period (Fig. 9). The median intensity of mCerulean3 increased over the first 2h when the cells do not divide, while the fluorescence of mCitrine remains the same. The increase in intensity of mCerulean3, and not mCitrine, is likely due to increased maturation

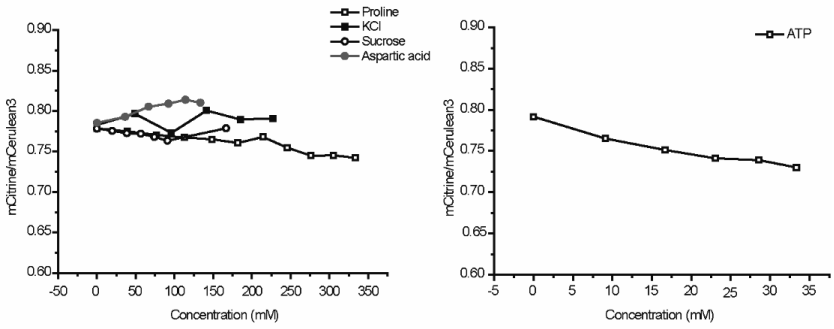

Fig. 7. The influence of small molecules on the ratiometric FRET of the crE6G2 sensor. *Experiments were done as described in the legend of Figure 7.*

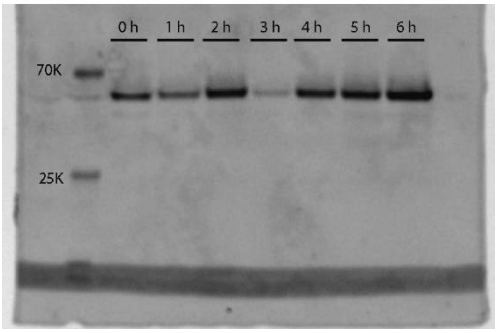

Fig. 8. In gel fluorescence of crGE sensor from E. coli. *The E. coli BL21(DE3) pLysS cells expressing crGE were incubated in MOPS medium at 30 °C and shaking at 200 rpm. The cells were shocked with 500 mM NaCl. The cells were lysed with Bugbuster 10X (Novagen®) and loaded onto a 12 % SDS-PAGE gel. The lower intensity of the 3h time point sample may have been caused by incomplete cell lysis.*

efficiency (see Chapter 4). After 2-3h, the relative concentration of fluorophores stays rather stable. Although improved maturation of mCerulean3 would also decrease the FRET, the gradual increase in maturation does not match the sharp decrease in FRET ratios that we see when cells start to grow. We thus conclude the reatiometic decrease not due to the truncation of sensor and the maturation of fluorescent protein.

Discussion

In this chapter, we determined the apparent crowding of *E. coli* during adaptation to high osmolality. We find that the crowding initially follows the cell volume but at later times in the adaptation phase the

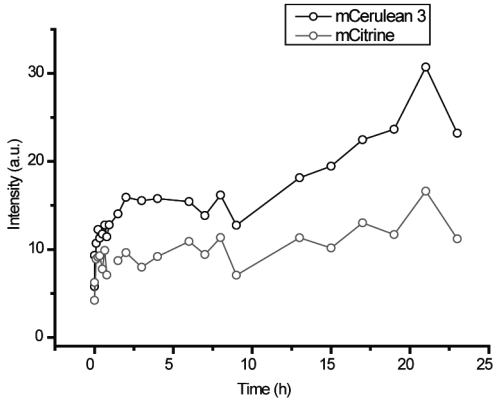

Fig. 9. The fluorescent intensity change of crGE in E. coli BL21(DE3) pLysS cells in MOPS medium. *The cells were treated with 300 mM NaCl upshift at time 0. Black circles are the median intensity of mCerulean3 in crGE, directly excited at 405 nm. Black circles are the median intensity of mCitrine, excited at 488 nm.*

parameters start to deviate. Remarkably, the apparent crowding stabilizes at a value below the one before the osmotic upshift. Our data bear resemblance to those of Gnutt et al.[27], who treated HeLa cells with 250 mM TMAO over a period of 16h. They also found a lower apparent crowding in the adaptation phase[28].

A decrease of crowding is typically explained by a lower volume fraction of macromolecules. However, Konopka et al.[17] determined the biopolymer fraction and the lateral diffusion of GFP in osmotically-shocked and adapted *E. coli* MC1655 grown in MOPS-glucose medium, and they noticed that there is not a simple relationship between biopolymer fraction and diffusion coefficient. The buoyant density of *E. coli* MC4100 grown in rich medium (TYG medium) increases with the osmolality of the medium[30]. The density of proteins is 1.2-1.4 g/cm^3 and higher than water (1.0 g/cm^3)[29], thus an increase indicates an increase of biopolymer fraction. Hence, the apparent crowding that we measure, and that by Gnutt et al., combined with the diffusion measurements by Konopka *et al.*, contrast with biopolymer volume fraction measurements.

Based on these observations, we hypothesize that the subcellular organization of the cytoplasm could change during adaptation to the osmotic upshift. The concentration of proteins and other macromolecules in the cytoplasm are typically close to their critical values[31,32] and the uneven distribution of hydrophilic, hydrophobic and charged surface areas of macromolecules enable the clustering of proteins and nucleic acid. As a result, cells may form subcellular organizations such as hyperstructures[33], intracellular bodies[34], and filaments[35]. The subcellular organizations can locally increase crowding

to an above-average level, leading to the formation of uncrowded areas elsewhere in the cytoplasm.

The subcellular organization is influenced by weak interactions, including electrostatic and hydrophobic interactions[36]. When cells adapt to the osmotic upshift, the weak interactions may change. As a result, the cells could form larger clusters and form less crowded regions in the cell, the effects of which would be altered by size and shape-based sorting of proteins by depletion forces. The crowding sensor may sense the less crowded regions and give a lower crowding value even though the total biomass volume fraction increases as the cell volume decreases.

Several other processes could contribute in forming larger hyper-structures and thus influence the crowding. During adaptation, DNA may increase its supercoiling[13,37], and simultaneously osmotic stress related genes[38] are expressed. The newly expressed proteins may have different surface properties, which changes the overall interactions e.g. hydrophobic interactions in the cell. Additionally, metabolites and compatible solutes may contribute to the subcellular organization of the cytoplasm. During adaption, the concentrations of ATP – which may act as a hydrotope[39] – may decrease. The decrease of ATP may result in formation of larger hyper-structures and decrease the crowding locally where the sensors locate.

Conclusions

In summary, we observe that the excluded volume changes as reported by our crowding sensors match with the volume changes upon osmotic upshift, but the correlation between volume and crowding does not hold in the adaptation phase. We hypothesize that biopolymer self-association creates a heterogeneous organization of the cytoplasm, resulting in regions with under- and overcrowding. The sensors might be biased towards probing the less crowded regions of the cell, hence the apparent decrease in macromolecular crowding.

References

1 Ellis, R. J. Macromolecular crowding: obvious but underappreciated. *Trends in Biochemical Sciences* **26**, 597-604, doi:10.1016/s0968-0004(01)01938-7 (2001).

2 Tan, C. M., Saurabh, S., Bruchez, M. P., Schwartz, R. & LeDuc, P. Molecular crowding shapes gene expression in synthetic cellular nanosystems. *Nature Nanotechnology* **8**, 602-608, doi:10.1038/nnano.2013.132 (2013).

3 Dix, J. A. & Verkman, A. S. Crowding effects on diffusion in solutions and cells. *Annual Review of Biophysics* **37**, 247-263, doi:10.1146/annurev.biophys.37.032807.125824 (2008).

4 Cayley, S. & Record, M. T. Large changes in cytoplasmic biopolymer concentration with osmolality indicate that macromolecular crowding may regulate protein-DNA interactions and growth rate in osmotically stressed Escherichia coli K-12. *Journal of Molecular Recognition* **17**, 488-496, doi:10.1002/jmr.695 (2004).

5 Nakano, S. & Sugimoto, N. Model studies of the effects of intracellular crowding on nucleic acid interactions. *Molecular Biosystems* **13**, 32-41, doi:10.1039/c6mb00654j (2017).

6 Samiotakis, A., Wittung-Stafshede, P. & Cheung, M. S. Folding, Stability and Shape of Proteins in Crowded Environments: Experimental and Computational Approaches. *International Journal of Molecular Sciences* **10**, 572-588, doi:10.3390/ijms10020572 (2009).

7 van den Berg, B., Ellis, R. J. & Dobson, C. M. Effects of macromolecular crowding on protein folding and aggregation. *Embo Journal* **18**, 6927-6933, doi:10.1093/emboj/18.24.6927 (1999).

8 Pilizota, T. & Shaevitz, J. W. Fast, Multiphase Volume Adaptation to Hyperosmotic Shock by Escherichia coli. *Plos One* **7**, doi:10.1371/journal.pone.0035205 (2012).

9 Chung, H. J., Bang, W. & Drake, M. A. Stress response of Escherichia coli. *Comprehensive Reviews in Food Science and Food Safety* **5**, 52-64, doi:10.1111/j.1541-4337.2006.00002.x (2006).

10 Wood, J. M. Bacterial responses to osmotic challenges. *Journal of General Physiology* **145**, 381-388, doi:10.1085/jgp.201411296 (2015).

11 Record, M. T., Courtenay, E. S., Cayley, D. S. & Guttman, H. J. Responses of E-coli to osmotic stress: Large changes in amounts of cytoplasmic solutes and water. *Trends in Biochemical Sciences* **23**, 143-148, doi:10.1016/s0968-0004(98)01196-7 (1998).

12 Shabala, L. et al. Ion transport and osmotic adjustment in Escherichia coli in response to ionic and non-ionic osmotica. *Environmental Microbiology* **11**, 137-148, doi:10.1111/j.1462-2920.2008.01748.x (2009).

13 Cheung, K. J., Badarinarayana, V., Selinger, D. W., Janse, D. & Church, G. M. A microarray-based antibiotic screen identifies a regulatory role for supercoiling in the osmotic stress response of Escherichia coli. *Genome Research* **13**, 206-215, doi:10.1101/gr.401003 (2003).

14 Bartholomaeus, A. et al. Bacteria differently regulate mRNA abundance to specifically respond to various stresses. *Philosophical Transactions of the Royal Society a-Mathematical Physical and Engineering Sciences* **374**, doi:10.1098/rsta.2015.0069 (2016).

15 Zhao, P. et al. Global transcriptional analysis of Escherichia coli expressing IrrE, a regulator from Deinococcus radiodurans, in response to NaCl shock. *Molecular Biosystems* **11**, 1165-1171, doi:10.1039/c5mb00080g (2015).

16 Metris, A., George, S. M., Mulholland, F., Carter, A. T. & Baranyi, J. Metabolic Shift of Escherichia coli under Salt Stress in the Presence of Glycine Betaine. *Applied and Environmental Microbiology* **80**, 4745-4756, doi:10.1128/aem.00599-14 (2014).

17 Konopka, M. C. et al. Cytoplasmic Protein Mobility in Osmotically Stressed Escherichia coli. *Journal of Bacteriology* **191**, 231-237, doi:10.1128/jb.00536-08 (2009).

18 Liu, B. Q. et al. Design and Properties of Genetically Encoded Probes for Sensing Macromolecular Crowding. *Biophysical Journal* **112**, 1929-1939, doi:10.1016/j.bpj.2017.04.004 (2017).

19 Boersma, A. J., Zuhorn, I. S. & Poolman, B. A sensor for quantification of macromolecular crowding in living cells. *Nature Methods* **12**, 227-+, doi:10.1038/nmeth.3257 (2015).

20 Neidhard.Fc, Bloch, P. L. & Smith, D. F. Culture medium for enterobacteria. *Journal of Bacteriology* **119**, 736-747 (1974).

21 Gebhardt, J. C. M. et al. Single-molecule imaging of transcription factor binding to DNA in live mammalian cells. *Nature Methods* **10**, 421-+, doi:10.1038/nmeth.2411 (2013).

22 van den Berg, J., Galbiati, H., Rasmussen, A., Miller, S. & Poolman, B. On the mobility, membrane location and functionality of mechanosensitive channels in Escherichia coli. *Scientific Reports* **6**, doi:10.1038/srep32709 (2016).

23 Kumar, N. & Kishore, N. Protein stabilization and counteraction of denaturing effect of urea by glycine betaine. *Biophysical Chemistry* **189**, 16-24, doi:10.1016/j.bpc.2014.03.001 (2014).

24 Perroud, B. & Lerudulier, D. Glycine betaine transport in Escherichia coli: osmotic modulation. *Journal of Bacteriology* **161**, 393-401 (1985).

25 Bennett, B. D. et al. Absolute metabolite concentrations and implied enzyme active site occupancy in Escherichia coli. *Nature Chemical Biology* **5**, 593-599, doi:10.1038/nchembio.186 (2009).

26 Yaginuma, H. et al. Diversity in ATP concentrations in a single bacterial cell population revealed by quantitative single-cell imaging. *Scientific Reports* **4**, doi:10.1038/srep06522 (2014).

27 Gnutt, D., Gao, M., Brylski, O., Heyden, M. & Ebbinghaus, S. Excluded-Volume Effects in Living Cells. *Angewandte Chemie-International Edition* **54**, 2548-2551, doi:10.1002/anie.201409847 (2015).

28 Gnutt, D., Brylski, O., Edengeiser, E., Havenith, M. & Ebbinghaus, S. Imperfect crowding adaptation of mammalian cells towards osmotic stress and its modulation by osmolytes. *Molecular bioSystems*, doi:10.1039/c7mb00432j (2017).

29 Milo, R. & Phillips, R. Cell Biology by the Numbers. (2015).

30 Baldwin, W. W., Sheu, M. J. T., Bankston, P. W. & Woldringh, C. L. Changes in buoyant density and cell size of Escherichia coli in response to osmotic shocks. *Journal of Bacteriology* **170**, 452-455 (1988).

31 Tartaglia, G. G., Pechmann, S., Dobson, C. M. & Vendruscolo, M. Life on the edge: a link between gene expression levels and aggregation rates of human proteins. *Trends in Biochemical Sciences* **32**, 204-206, doi:10.1016/j.tibs.2007.03.005 (2007).

32 Schavemaker, P. E., Śmigiel, W. M. & Poolman, B. Ribosome surface properties may impose limits on the nature of the cytoplasmic proteome. *Elife*, doi:10.7554/eLife.30084 (2017).

33 Norris, V. et al. Functional taxonomy of bacterial hyperstructures. *Microbiology and Molecular Biology Reviews* **71**, 230-253, doi:10.1128/mmbr.00035-06 (2007).

34 O'Connell, J. D., Zhao, A., Ellington, A. D. & Marcotte, E. M. Dynamic Reorganization of Metabolic Enzymes into Intracellular Bodies. *Annual Review of Cell and Developmental Biology*, **28**, 89-111, doi:10.1146/annurev-cellbio-101011-155841 (2012).

35 Petrovska, I. et al. Filament formation by metabolic enzymes is a specific adaptation to an advanced state of cellular starvation. *Elife* **3**, doi:10.7554/eLife.02409 (2014).

36 Cohen, R. D., Guseman, A. J. & Pielak, G. J. Intracellular pH modulates quinary structure. *Protein Science* **24**, 1748-1755, doi:10.1002/pro.2765 (2015).

37 Higgins, C. F. et al. A physiological role for DNA supercoiling in the osmotic regulation of gene expression in S. typhimurium and E. coli. *Cell* **52**, 569-584, doi:10.1016/0092-8674(88)90470-9 (1988).

38 Wood, J. M. et al. Osmosensing and osmoregulatory compatible solute accumulation by bacteria. *Comparative Biochemistry and Physiology a-Molecular and Integrative Physiology* **130**, 437-460, doi:10.1016/s1095-6433(01)00442-1 (2001).

39 Patel, A. et al. ATP as a biological hydrotrope. *Science* **356**, 753-756, doi:10.1126/science.aaf6846 (2017).

Chapter 5

Ionic strength sensing in living cells

Boqun Liu, Bert Poolman,*
and Arnold J Boersma*

Department of Biochemistry, Groningen Biomolecular Sciences and Biotechnology Institute & Zernike Institute for Advanced Materials, University of Groningen, Nijenborgh 4, 9747 AG Groningen, the Netherlands.

Corresponding Authors
*E-mail: b.poolman@rug.nl. *E-mail: a.j.boersma@rug.nl.

Published in ACS chemical biology 12.10 (2017): 2510-2514

Abstract

Knowledge of the ionic strength in cells is required to understand the in vivo biochemistry of the charged biomacromolecules. Here, we present the first sensors to determine the ionic strength in living cells, by designing protein probes based on Förster resonance energy transfer (FRET). These probes allow observation of spatiotemporal changes in the ionic strength on the single-cell level.

Introduction

The ionic strength influences a wide array of electrostatic interactions in the cell.[1, 2] To understand the role of the ionic strength in cell physiology, a sensor to quantify the ionic strength in vivo is needed. The ionic strength is the effective ion concentration and screens electrostatic interactions of (macro)molecules, which is obviously of crucial importance to the cell. For example, the ionic strength determines the structure of intrinsic disordered proteins,[3] activity of enzymes,[4] protein aggregation,[5] quinary assemblies/phase separations,[6] protein binding to (poly)nucleic acids,[7] the catalytic function of riboswitches,[8] and many other processes. The ionic strength governs the cell volume by activating the channels and transporters involved.[9,10] The ionic strength can vary however, depending on the extracellular environment, due to for example abrupt changes in medium osmolarity, and fluctuations with intracellular events such as metabolite or polynucleotide synthesis.[11]

To quantify the ionic strength one cannot simply use the concentration of ions, because the effective ion concentration (i.e. thermodynamic activity) is altered due to interaction of the ions with each other and the biomolecules. Indeed, a subset of ions has a higher affinity for macromolecules, such as magnesium, while others are more loosely associated, and their activity coefficient may approach that in the extracellular medium.[12] Such effects result in a strong dependence of electrostatic screening on the identity of the ions, roughly following the Hofmeister series.[13,14] Thus, although it is possible to determine the concentration of a particular ion with for example flame photometry of dry cell mass,[15] this will not immediately reveal the ionic strength; that is, the effective concentration of an ion depends on its environment. In addition, these techniques will not yield information on population heterogeneity or rapid temporal changes in the ionic strength. Probes to infer the ionic strength from the activity of a membrane protein[9] or the fluorescence of a fluorescein-BSA conjugate[16] are complicated to use and interpret, and they have only been applied vesicles and isolated mitochondria but not in living cells.

Here, we fill this void by designing the first probes that sense the ionic strength in living cells. The sensors are based on FRET and are genetically encoded, because these properties allow monitoring analytes with high spatiotemporal precision inside living cells. Fluorescent protein probes can be affected by ions nonspecifically,[17] and FRET sensors selective for a specific ion have been developed, for example zinc, calcium, or choride.18, 19, 20 We construct our sensors to contain a positively and a negatively charged α-helix, whose electrostatic attraction will depend on the ionic strength (Fig. 1). At the N- and C-termini of the helices are two fluorescent proteins,

mCerulean3 and mCitrine, that form a FRET pair.21 Increasing the ionic strength will decrease the attraction between the helices, which will result in a decrease in FRET efficiency.

To induce charge in the helices, we inserted 6 glutamates in an alanine background in one helix, and 6 lysines in the other helix (Fig. 1). The charged amino acids are in a i+5 spacing, a staircase-like configuration, ensuring that all sides of the helix are covered with charges. This prevents the helix to have a charged patch as well as preventing metal ion chelation. We further reasoned that the high intramolecular concentration of the oppositely charged -helix will outcompete electrostatic interactions with most of the charged cellular biomacromolecules. Because the presence of specific ion effects could be dependent on the identity of the amino acids in the helix, we designed sensors with glutamate or aspartate residues, and lysine or arginine residues, and thereby alter e.g. salt-bridge stability.[22] With these design elements we avoid selectivity for specific ions in the sensors, allowing for ionic strength determination in living cells.

Material and Methods

Expression and purification of the ionic strength sensors. The synthetic gene (Supplementary Note) encoding the ionic strength sensors in pRSET-A was obtained from GeneArt. The plasmid was transformed into the E. coli strain BL21(DE3) pLysS (Promega). The cells were grown to an OD600 of 0.6 at 37 °C and shaking at 200rpm in LB medium (1.0% bactotryptone, 0.5% yeast extract, 1% NaCl) with 1 mg/mL ampicillin, after which the cells were induced overnight with 0.1 mM isopropyl-β-D-thiogalactoside (IPTG) at 25 °C and shaking at 200 rpm. The cell lysate was cleared by centrifugation, supplemented with 10 mM imidazole and purified by nickel-nitrilotriacetic acid Sepharose chromatography (wash/elution buffer: 20/250 mM imidazole, 50 mM NaPi, 300 mM NaCl, pH 8.0). The sensor was further purified by Superdex 200 10/300 GL size-exclusion chromatography (Amersham Biosciences) in 10 mM NaPi, pH 7.4. Fractions containing pure protein were aliquoted and stored at −80 °C.

In vitro characterization of the sensors. A 300 µL solution containing the given salt, and 10mM NaPi (adjusted the pH to 7.4 after dissolution of the salts) was added to a 96 well plate (Greiner). The purified sensor was added and the fluorescence intensity at 475 nm and 525 nm were recorded separately in a Spark® 10M microplate reader with excitation at 420 nm at room temperature. A 20 nm bandwidth for exaction and emission was applied and the average of 10 measurements of a single well was taken. The background fluorescence, buffer without sensor, was subtracted.

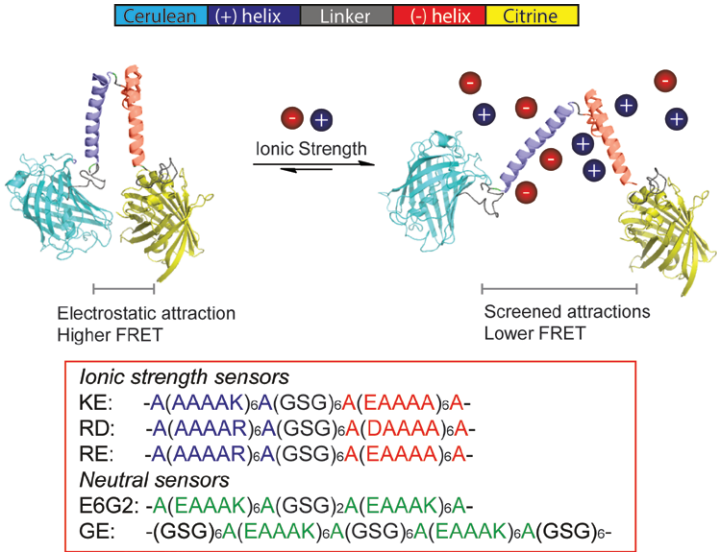

Fig. 1. Design of ionic strength sensors and sensing concept. *Ions screen the attraction between the positively and negatively charged helices, reducing the FRET efficiency.*

Transfection and imaging of HEK293 cells. Transfection and imaging of HEK293 cells was performed as described,[21] with some minor modifications. HEK293 cells (ATCC CRL-1573, tested for mycoplasma contamination) were cultured in DMEM (Gibco) supplemented with 10% (v/v) fetal calf serum, 2 mM L-glutamine (Gibco), 100 units mL^{-1} penicillin (Invitrogen) and 100 µg mL^{-1} streptomycin (Invitrogen). For transfection experiments, HEK293 cells were plated in eight-well Labtek glass chamber slides (Thermo Scientific) at 6×10^4 cells per well. One day after plating, the cells were transfected with plasmid DNA coding for the sensors as follows: lipoplexes composed of 1.5 µl of Lipofectamine 2000 (Invitrogen) and 0.5 µg of the pcDNA 3.1 vector carrying the corresponding sensor gene were prepared in 100 µl of serum-free DMEM, according to the manufacturer's instructions. 25 µl of lipoplex solution was added per well and incubated for 4 h at 37 °C and 5% CO_2, after which the medium was refreshed. The next day, the medium was replaced by 200 µL DMEM with HEPES without phenol red, and sensor expression in the HEK293 cells was subsequently analyzed by confocal fluorescence microscopy. The cells were imaged directly in the eight-well Labtek glass chamber slides. The slides were mounted on a laser-scanning confocal microscope (Zeiss LSM 710), at 37 °C. The sensor was excited using a 405-nm LED laser, and the emission was split into a 450–505-nm channel and 505–797-nm channel. The fluorescence intensity of the cells was determined in ImageJ for each channel. The backgrounds for each

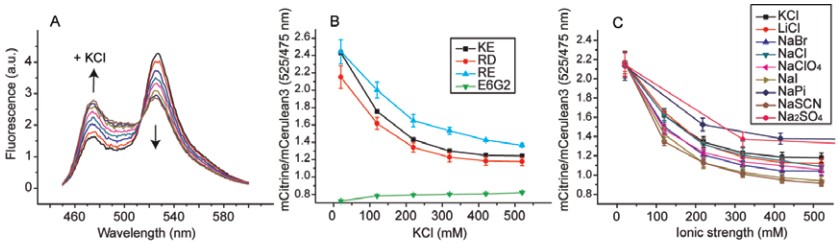

Fig. 2. In vitro characterization of the ionic strength sensors. A: *Fluorescence emission spectra of the RD sensor titrated with potassium chloride.* ***B:*** *Dependence of the mCitrine/mCerulean3 ratio of the EK, RD, RK, and E6G2 sensors on the potassium chloride concentration.* ***C:*** *Dependence of the mCitrine/mCerulean3 ratio of the RD sensor on the ion identity. All experiments are in 10 mM NaPi, pH 7.4. Error bars indicate the standard deviation of three biological replicates.*

channel were subtracted and the mCitrine intensity divided by the mCerulean intensity for each cell. When the mCitrine intensity was plotted versus the mCerulean intensity, linear fits with $R^2 > 0.99$ were generally obtained.

Results and disscussion

To determine the ionic strength sensitivity of the sensors, we performed extensive in vitro tests on isolated probes (Fig. 2A, Supplementary Fig. S1). We tested the three ionic strength sensors, that are, the KE (lysine-glutamate), the RE (arginine-glutamate), and the RD (arginine-aspartate) sensors, and compared the findings with a sensor that contains neutral helices, the E6G2 probe.[23] We found that the FRET efficiencies of the ionic strength sensors in 10 mM NaPi buffer were much higher than that of the E6G2 probe, confirming that the helices attract each other. Addition of potassium chloride to the ionic strength sensors lead to a decrease in FRET efficiency (Fig. 2B), with the highest sensitivity between 0 and 300 mM KCl. The E6G2 probe was not sensitive, showing that we probe the ionic strength. Salt does not affect other neutral sensors with higher FRET efficiencies,[23] and hence the FRET efficiency does not relate to the ionic strength dependence. We added a wide range of salts to test whether specific ion effects interfere with the readouts (Fig. 2C). We find that the sensitivity to the cations of KCl, NaCl, $MgCl_2$, and LiCl is the same when the ratios are plotted versus the ionic strength (Supporting Fig. S3). In contrast, the readout had a dependence on the identity of the anion (Supporting Fig. S2). The order of sensitivity followed the Hofmeister series, that is, the measure to what extent ions are hydrated, which is generally more dependent on the anion. This deviation from ideal

behavior depended on the probe, and qualitatively followed the intramolecular salt bridge strength between the two helices;[22] the RD probe has the lowest salt-bridge strength and is least affected by the non-ideal behavior, as judged from the spread in deviation between the different ions. Likely due to the lower salt-bridge strength, the RD probe also has a lower FRET efficiency. Together, the dependence on ion identity indicates that we probe the effective ion concentration (or ionic strength) rather than total ion concentration. In all cases, the E6G2 probe was insensitive to any ion.

We investigated sensitivity to a wide variety of other parameters to make the transition to in vivo measurements. Similar to the E6G2 and GE crowding probes,[21] mCitrine induced pH sensitivity in all the probes only below pH 7.0 (Supporting Fig. S4). The zwitterionic glycine betaine and neutral small molecules sorbitol and sucrose hardly influenced the probes (Supporting Fig. S5). The common intracellular organophosphates fructose bisphoshate, ATP, ADP, and AMP influenced the probes as can be expected from their charge, albeit that the sensitivity to the nucleotides was somewhat higher (Supporting Fig. S6). Glutathione influenced the probes according to its net negative charge (Supporting Fig. S7). The sensitivity to potassium glutamate was less than potassium chloride, as expected from the Hofmeister series, with the RD probe again deviating the least (Supporting Fig. S8). The sensors associated with the polyelectrolyte DNA in the absence of KCl, but not in the presence of 100 mM KCl (Supporting Fig. S9). Macromolecular crowding induced by Ficoll 70 compressed all the probes (Supporting Fig. S10) and hence should be taken into account when measuring in live cells. The ionic strength probes are temperature sensitive in the absence of salt, but the temperature sensitivity decreased with increasing salt concentration (Supporting Fig. S11). Increasing the sensor concentration itself did not affect the ratio (Supporting Fig. S12), ruling out interference from self-association. Hence, the sensors are sensitive to the ionic strength mainly, but other parameters such as macromolecular crowding, pH, and temperature need to be controlled for.

To demonstrate ionic strength sensing in vivo, we expressed the probes in the mammalian cell line HEK293, and imaged the cells by scanning confocal microscopy. The cells were subsequently imaged by excitation of the mCerulean3 at 405 nm, and the emission ratio of mCitrine (505-750 nm) over mCerulean3 (450–505 nm), after background subtraction, was monitored (Fig. 3A,B). The ratios obtained were very homogeneous over all the cells. When comparing the different sensors, we found that RD gave lower ratios than the KE and RE probes, similar to what we observed in vitro (Supporting Fig. S14). To quantify the readouts, we calibrated the probes in the cell by clamping the internal potassium concentration by titrating the external

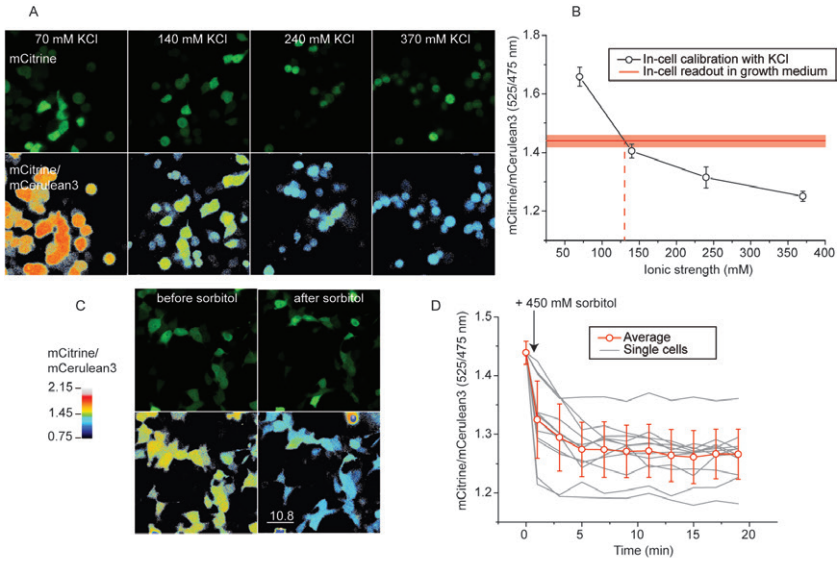

Fig. 3. Ionic strength determination in vivo and observation of dynamic changes observed in scanning fluorescence confocal microscopy of HEK293 cells expressing the RD sensor. A: *Fluorescence and mCitrine/mCerulean3 ratio images of sensor calibration with KCl, nigericin, and valinomycin.* ***B:*** *Calibration curve of the mCitrine/mCerulean3 ratio versus potassium concentration; the red line is the ratio of cells in growth medium (red shading is the standard deviation within a population, n = 20).* ***C:*** *Fluorescence and mCitrine/mCerulean3 ratio images of cells before and 10 minutes after addition of 450 mM sorbitol. See Supporting Fig. S13 for more detail.* ***D:*** *mCitrine/mCerulean3 ratio upon addition of sorbitol as a function of time; the data of 20 individual cells and the average are shown. Error bars are standard deviation within a single population of cells. The standard deviations of the averages of independent biological repeats are smaller (±0.03, n = 4).*

medium with potassium chloride in the presence of the ionophores valinomycin plus nigericin. These ionophores equilibrate the protons and potassium over the membrane, providing a calibration curve of the corresponding sensor with a known concentration of potassium. All the ion sensors sensed the potassium concentration in a similar manner as observed in vitro. The ratios for the GE crowding sensor remained unchanged, indicating that with the calibration method we did not alter the crowding, and prevent osmotic pressure differences over the membrane by ionophore-assisted ion equilibration. The cells did change shape during the calibration procedure (Fig. 3A). We subsequently used the calibration curves to quantify the ionic strength from the readout in regular growth medium and found that the ionic strength was comparable to ~130 mM for the RD and RE sensors, and ~110 mM for the KE sensor (Fig. 3B, Supporting Fig. S14). These values are in the same range as the ion concentrations reported for

the monovalent ions in various cells, and the concentration of "free" ions is somewhat lower.[24] The total ion concentration would be 140 mM and 12 mM for potassium and sodium, respectively. Divalent cations were not monitored because they are mostly bound to the biopolymers. Organophosphates form complexes with magnesium and may bind nonspecifically to proteins,[25–27] and the molecules thus contribute less to the ionic strength than is expected from their total concentrations. Single cell measurements as function of time indicate that the ionic strength is determined with a precision better than 10 mM (that is, changes in mCitrine/mCerulean3 of less than 0.02). Thus, we conclude that the probes function in HEK293 cells and we can determine the ionic strength in vivo.

To further demonstrate the potential of the sensors in vivo, we monitored changes in ionic strength over time after an osmotic upshift by adding 450 mM sorbitol to HEK293 cells (Fig. 3C,D). We expected the short-term response to be an initial increase in crowding and ionic strength, followed by a regulatory volume increase by uptake of potassium and chloride from the medium, retaining the abnormally high ionic strength but decreasing the crowding.[11] We assume that the response mechanism of the sensor is much faster than the biological events. We saw with the GE crowding probe that the crowding indeed increased with 450 mM sorbitol (Supporting Fig. S15), as we observed previously, after which a slow decrease in crowding took place. In the timeframe of ~20 minutes, the crowding was not yet fully recovered. The RD sensor showed that the ionic strength increased with osmotic upshift and remained at this level. It showed no apparent sensitivity to in vivo crowding, contrary to the KE and RE sensors that showed an initial increase in FRET directly after the osmotic upshift. Interestingly, an increase in ionic strength of ~190 mM to 320 mM can be inferred with the RD calibration curve, which is similar to the expected increase in osmolarity simply based by equating the sum of K and Cl to the number of sorbitol molecules added. We could monitor single cells in time and found that the distribution of FRET values increased after the osmotic upshift and the adaptation process that followed. This shows that the cells are affected differently by the osmotic upshift, which could for example be related to the cell cycle,[15] or intrinsic variation in fitness in the population of cells that we analyzed. Hence, the probes can sense the ionic strength on the single-cell level during dynamic changes in the ionic strength.

Conclusions

In conclusion, we present here the first sensors to determine the ionic strength that function in living cells. Taking into account changes in

macromolecular crowding and pH, the sensors allow facile determination of the intracellular ionic strength on the single-cell level in changing environments or intracellular conditions. Given the wide variety of processes that are influenced by the ionic strength, these sensors will aid future investigations on the importance of the ionic strength during a wide variety of conditions such as cell volume regulation, disease, and environmental stresses.

Reference

1. Warshel, A., and Russell, S. T. Calculations of electrostatic interactions in biological systems and in solutions. Q. *Rev. Biophys*. **17**, 283-422. (1984)
2. Honig, B., and Nicholls, A. Classical electrostatics in biology and chemistry. *Science*. **268**, 1144-1149. (1995)
3. Konig, I., Zarrine-Afsar, A., Aznauryan, M., Soranno, A., Wunderlich, B., Dingfelder, F., Stuber, J. C., Pluckthun, A., Nettels, D., and Schuler, B. Single-molecule spectroscopy of protein conformational dynamics in live eukaryotic cells. *Nat. Methods*. **12**, 773-779. (2015)
4. Norby, J. G., and Esmann, M. The effect of ionic strength and specific anions on substrate binding and hydrolytic activities of Na,K-ATPase. *J. Gen. Physiol*. **109**, 555-570. (1997)
5. Marek, P. J., Patsalo, V., Green, D. F., and Raleigh, D. P. Ionic strength effects on amyloid formation by amylin are a complicated interplay among debye screening, ion selectivity, and hofmeister effects. *Biochemistry*. **51**, 8478-8490. (2012)
6. Elbaum-Garfinkle, S., Kim, Y., Szczepaniak, K., Chen, C. C., Eckmann, C. R., Myong, S., and Brangwynne, C. P. The disordered P granule protein LAF-1 drives phase separation into droplets with tunable viscosity and dynamics. *Proc. Natl. Acad. Sci. U. S. A.* **112**, 7189-7194. (2015).
7. Record, M. T.,Jr, Anderson, C. F., and Lohman, T. M. Thermodynamic analysis of ion effects on the binding and conformational equilibria of proteins and nucleic acids: The roles of ion association or release, screening, and ion effects on water activity. *Q. Rev. Biophys.* **11**, 103-178. (1978)
8. Roth, A., Nahvi, A., Lee, M., Jona, I., and Breaker, R. R. Characteristics of the glmS ribozyme suggest only structural roles for divalent metal ions. *RNA*. **12**, 607-619. (2006)
9. Biemans-Oldehinkel, E., Mahmood, N. A., and Poolman, B. A sensor for intracellular ionic strength. *Proc. Natl. Acad. Sci. U. S. A*. **103**, 10624-10629. (2006)
10. Syeda, R., Qiu, Z., Dubin, A. E., Murthy, S. E., Florendo, M. N., Mason, D. E., Mathur, J., Cahalan, S. M., Peters, E. C., Montal, M., and Patapoutian, A. LRRC8 proteins form volume-regulated anion channels that sense ionic strength. *Cell*. **164**, 499-511. (2016)
11. Hoffmann, E. K., Lambert, I. H., and Pedersen, S. F. Physiology of cell volume regulation in vertebrates. *Physiol. Rev*. **89**, 193-277. (2009)
12. Freedman, J. C., and Hoffman, J. F. Ionic and osmotic equilibria of human red blood cells treated with nystatin. *J. Gen. Physiol*. **74**, 157-185. (1979).

13. Zhang, Y., and Cremer, P. S. Interactions between macromolecules and ions: The hofmeister series. *Curr. Opin. Chem. Biol*. **10**, 658-663. (2006)
14. Leirmo, S., Harrison, C., Cayley, D. S., Burgess, R. R., and Record, M. T.,Jr. Replacement of potassium chloride by potassium glutamate dramatically enhances protein-DNA interactions in vitro. *Biochemistry*. **26**, 2095-2101. (1987)
15. Jung, C., and Rothstein, A. Cation metabolism in relation to cell size in synchronously grown tissue culture cell. *J. Gen. Physiol.* **50**, 917-932. (1967)
16. Cortese, J. D., Voglino, A. L., and Hackenbrock, C. R. Ionic strength of the intermembrane space of intact mitochondria as estimated with fluorescein-BSA delivered by low pH fusion. *J. Cell Biol*. **113**, 1331-1340. (1991).
17. Moussa, R., Baierl, A., Steffen, V., Kubitzki, T., Wiechert, W., and Pohl, M. An evaluation of genetically encoded FRET-based biosensors for quantitative metabolite analyses in vivo. *J. Biotechnol*. **191**, 250-259. (2014)
18. Vinkenborg, J. L., Nicolson, T. J., Bellomo, E. A., Koay, M. S., Rutter, G. A., and Merkx, M. Genetically encoded FRET sensors to monitor intracellular Zn^{2+} homeostasis. *Nat. Methods*. **6**, 737-740. (2009)
19. Tian, L., Hires, S. A., Mao, T., Huber, D., Chiappe, M. E., Chalasani, S. H., Petreanu, L., Akerboom, J., McKinney, S. A., Schreiter, E. R., Bargmann, C. I., Jayaraman, V., Svoboda, K., and Looger, L. L. Imaging neural activity in worms, flies and mice with improved GCaMP calcium indicators. *Nat. Methods*. **6**, 875-881. (2009).
20. Kuner, T., and Augustine, G. J. A genetically encoded ratiometric indicator for chloride: Capturing chloride transients in cultured hippocampal neurons. *Neuron*. **27**, 447-459. (2000).
21. Boersma, A. J., Zuhorn, I. S., and Poolman, B. A sensor for quantification of macromolecular crowding in living cells. *Nat. Methods*. **12**, 227-229. (2015)
22. White, A. D., Keefe, A. J., Ella-Menye, J. R., Nowinski, A. K., Shao, Q., Pfaendtner, J., and Jiang, S. Free energy of solvated salt bridges: A simulation and experimental study. *J. Phys. Chem. B*. **117**, 7254-7259. (2013)
23. Liu, B., Åberg, C., van Eerden, F. J., Marrink, S. J., Poolman, B., and Boersma, A. J. (2017) Design and properties of genetically encoded probes for sensing macromolecular crowding. *Biophys. J.* **112**, 1929-1939.
24. Maguire, M. E., and Cowan, J. A. Magnesium chemistry and biochemistry. *Biometals*. **15**, 203-210. (2002).
25. DeMott, C. M., Majumder, S., Burz, D. S., Reverdatto, S., Shekhtman, A. Ribosome mediated quinary interactions modulate in-cell protein activities. *Biochemistry* DOI: 10.1021/acs.biochem.7b00613. (2017).
26. Yu, I., Mori, T., Ando, T., Harada, R., Jung, J., Sugita, Y., and Feig, M. Biomolecular interactions modulate macromolecular structure and dynamics in atomistic model of a bacterial cytoplasm. *eLife* **5**, e19274. (2016).
27. Patel, A., Malinovska, L., Saha, S., Wang, J., Alberti, S., Krishnan, Y., and Hyman, A. A. ATP as a biological hydrotrope. *Science* **356**, 753-756. (2017).

Supporting information: Ionic strength sensing in living cells

Boqun Liu, Bert Poolman,*
and Arnold J Boersma*

Department of Biochemistry, Groningen Biomolecular Sciences and Biotechnology Institute & Zernike Institute for Advanced Materials, University of Groningen, Nijenborgh 4, 9747 AG Groningen, the Netherlands.

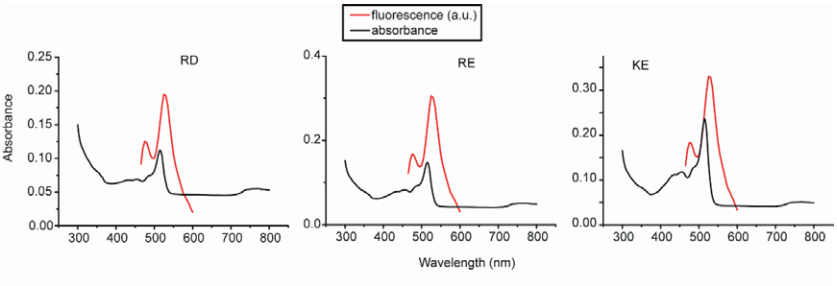

Fig. S1. Absorption and fluorescence emission spectra (excitation at 420 nm) for the ionic strength sensors*. The sensor concentration for the absorption measurement was ~1 μM, and for the fluorescence measurements ~100 nM. The protein concentrations were determined from the absorption at 280 nm, using the Nanodrop ND-1000 spectrophotometer, and calculated with ε280 = 48,000 M-1cm-1, which was estimated with the ExPASy ProtParam tool. The intensities of the fluorescence and absorption spectra were adjusted for comparison. Conditions: 10 mM NaPi, pH 7.4; temperature of 26±1 °C.*

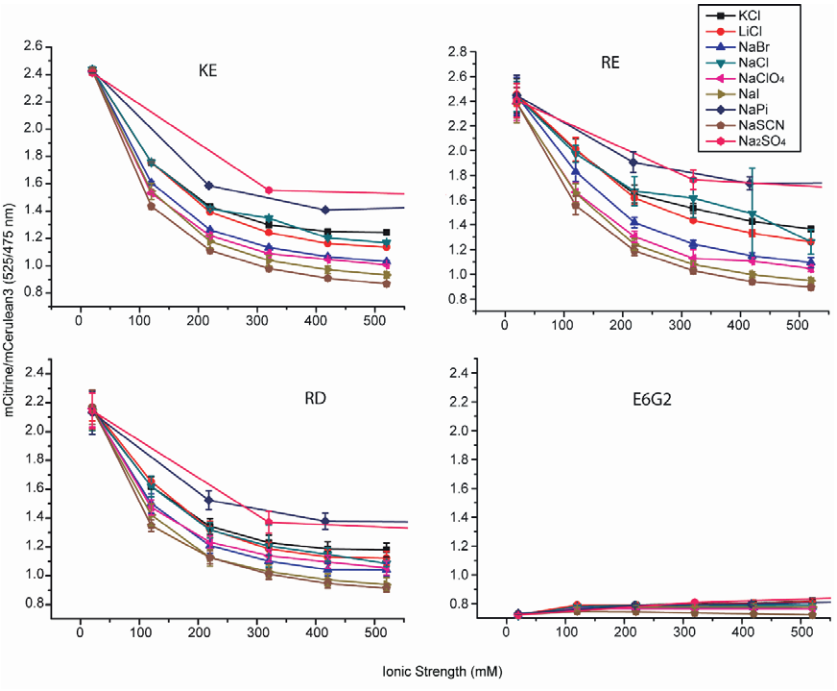

Fig. S2. Dependence of the mCitrine/mCerulean3 ratio on the ionic strength for different salts*. All sensors display a dependence on the identity of the ion. In all cases, the spread follows the Hofmeister series, i.e. SO42->Cl->SCN-. The magnitude of spread varies, and follows roughly RE>EK>RD, which corresponds to previously calculated salt bridge stabilities for these ion pairs.2 The data for the E6G2 crowding sensor is given as control, showing that RE, EK and RD sensors are uniquely dependent on ionic strength and that the sensing*

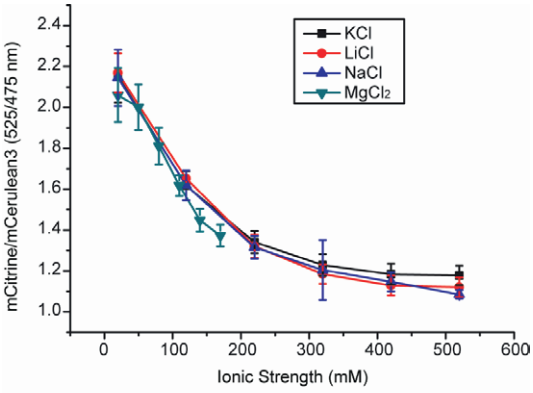

Fig. S3. Dependence of the mCitrine/mCerulean3 ratio of RD on the identity of the cation. *The monovalent alkali ions K+, Li+, and Na+ all induce the same response. The divalent magnesium(II) gives the same response up to an ionic strength of 170 mM. This corresponds to a MgCl2 concentration of 50 mM (+ 10 mM NaPi pH 7.4). Higher concentrations are not feasible in NaPi buffer, which induces precipitation upon adjusting the pH. Divalent cations zinc and calcium were insoluble in NaPi buffer in the mM range at pH 7.4. Error bars are the standard deviations of three independent replicates. Conditions: 10 mM NaPi, pH 7.4; temperature of 26±1 °C.*

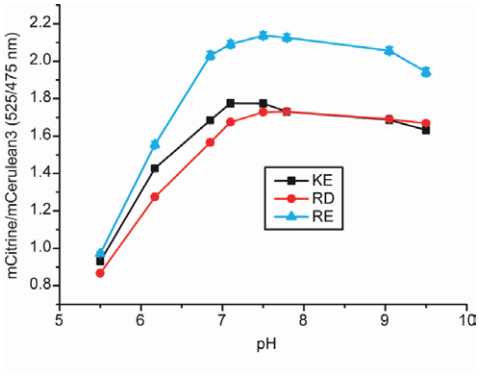

Fig. S4. pH sensitivity of the probes. *The pH of 10 mM NaPi was set in the presence of 100 mM KCl to account for significant ionic strength effects due to the difference in NaH2PO4/ Na2HPO4 ratio with pH. We observe that all sensors have a decreased ratio below pH 7 (the transition appears to be between pH 6.85 and 7.1), similar to the observations previously made on the GE sensor.1 Likely, the acid sensitivity is caused by the high pKa of the fluorophore in mCitrine, reducing its fluorescence. The signal is stable between pH 7 and ~9. Conditions: 10 mM NaPi, 100 mM KCl, temperature of 26±1 °C.*

mechanism originates from the charged helices. Error bars are the standard deviations of three independent replicates. Conditions: 10 mM NaPi, pH 7.4; temperature of 26±1 °C.

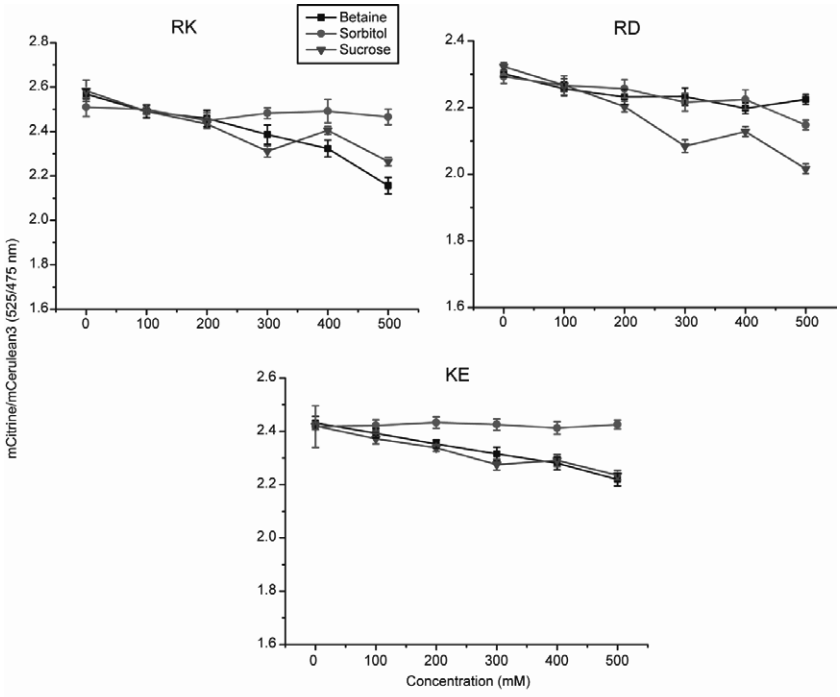

Fig. S5. Effect of neutral carbohydrates sorbitol and sucrose, and the zwitterionic osmolyte glycine betaine on the mCitrine/mCerulean3 ratio of the sensors. *The small decrease at high concentrations could be due to an increase in preferential hydration of the peptides and decrease in salt-bridge strength. The differences are very small compared to the ionic strength effects, considering the high concentrations of osmolyte and the absence of a background electrolyte (e.g. 100 mM KCl) that would otherwise buffer most of the specific solute effects. Conditions: 10 mM NaPi, pH 7.4; temperature of 26±1 °C.*

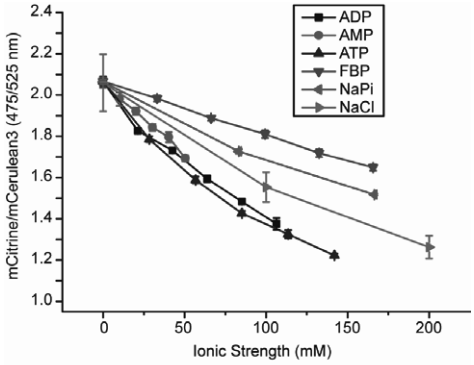

Fig. S6. Dependence of the response of the RD sensor on the identity of physiological phosphate anions. *The net charge of the ions at pH 7.4 was taken to be -3.3 for ATP (adenosine triphosphate), -2.8 for ADP (adenosine diphosphate), -1.8 for AMP (adenosine monophosphate), -1.6 for Pi (phosphate), and -3.6 for FBP (fructose 1,6-bisphosphate). The*

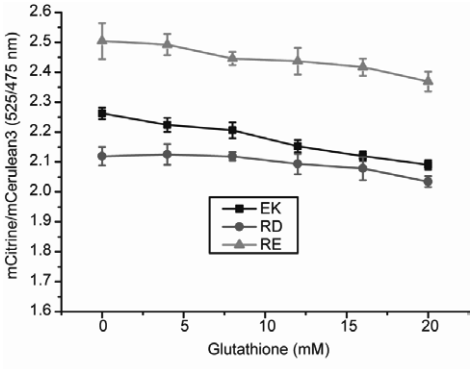

Fig. S7. Dependence of the mCitrine/mCerulean3 ratio of the sensor on the glutathione concentration. *Glutathione is one of the most common small molecules of living cells and typically present at millimolar concentrations. A small decrease is observed, which is at least partly caused by the higher ionic strength, i.e. the addition of NaOH to neutralize the negative charge on glutathione and to obtain pH 7.4. Conditions: 10 mM NaPi, pH 7.4; temperature of 26±1 °C.*

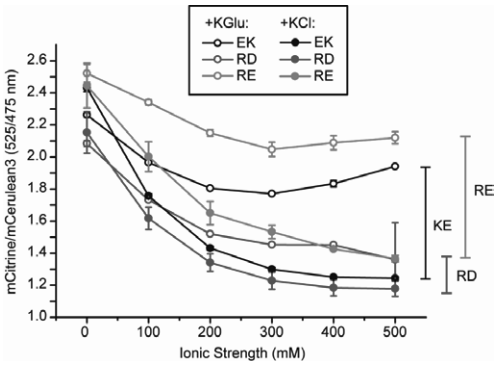

Fig. S8. Response of the sensors to potassium glutamate versus potassium chloride*. Glutamate is the principle small anion of many types of cells. Glutamate decreases the mCitrine/mCerulean ratio less than chloride does, and this is expected according to the Hofmeister series. The ratios of the RE and KE sensors decrease little with glutamate, and at >300 mM glutamate the ratios even seem to level off and increase. The ratios obtained with the RD sensor for glutamate and chloride ions are more similar, but the decreased sensitivity for glutamate remains. In general, the difference in spread between the sensors is comparable to that observed for the other anions. Conditions: 10 mM NaPi, pH 7.4; temperature of 26±1 °C.*

corresponding sodium salts or protonated forms were dissolved in 10 mM NaPi adjusted to pH 7.4 with NaOH. The curves for ATP, ADP and AMP overlay when corrected for the ionic strength. The response to these salts is higher than for NaCl, which could be caused by some additional interactions of the nucleotides with the helices (e.g. due to chelation effects). The bisphosphate FBP and phosphate induce less of a change in the sensor, which is in accordance with the Hofmeister series. Conditions: 10 mM NaPi, pH 7.4; temperature of 26±1 °C.

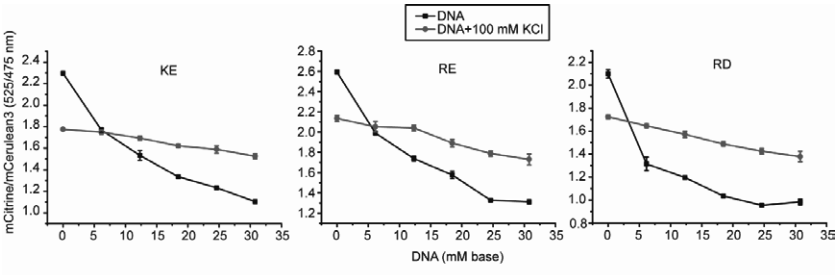

Fig. S9. Sensitivity of the sensors to the presence of DNA*. There is a strong decrease in mCitrine/mCerulean ratio in the presence of DNA and in the absence of KCl, which is not observed for the neutral crowding sensors1. To test whether this behavior is caused by association of the positively charged helix of the sensor to DNA, we added 100 mM KCl and indeed we find a strong screening effect. Conditions: 10 mM NaPi, pH 7.4; temperature of 26±1 °C.*

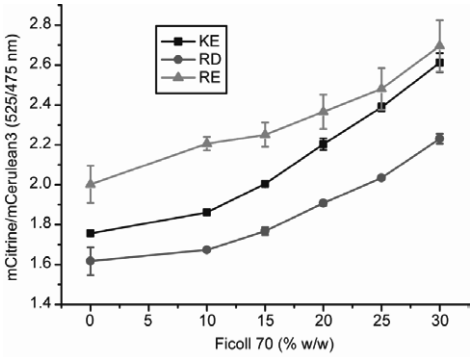

Fig. S10. Sensitivity of the ionic strength sensors to macromolecular crowding induced by Ficoll 70*. The KE, RD and RE sensors are compressed by high concentrations of Ficoll 70, similar to the neutral FRET sensors.1 The sensitivity to macromolecular crowding needs to be taken into account when measuring in vivo; the change in FRET due to crowding is relatively small compared to the ionic strength effect. If the change in crowding as determined with the GE or E6G2 probe is not insignificant, then calibration of the sensors in vivo is needed (see main text). Conditions: 10 mM NaPi, pH 7.4; temperature of 26±1 °C.*

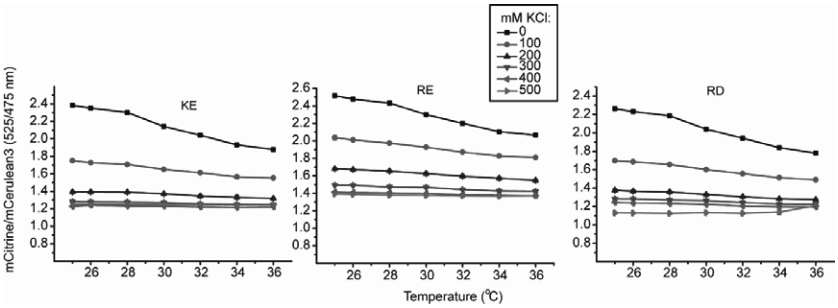

Fig. S11. Temperature dependence of the ionic strength sensors at varying KCl concentrations*. The temperature dependence could originate from salt-bridge stability, helix stability, altered*

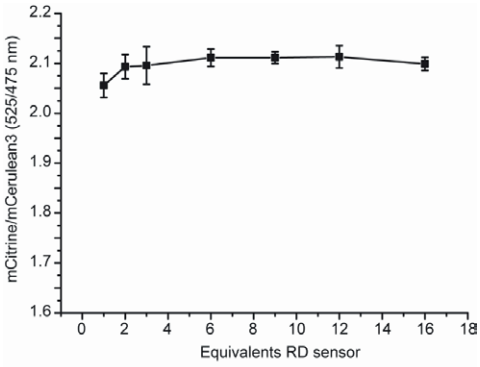

***Fig. S12. Dependence of the mCitrine/mCerulean3 ratio on the concentration of the RD sensor**. The FRET ratio does not change by adding up to 16 equivalents of RD sensor, when starting with 30 nM. If self-association would occur, intermolecular FRET would increase the FRET ratio. Hence the absence of an effect indicates that in the concentration range of 30 to 500 nM RD self-association does not play a role. Conditions: 10 mM NaPi, 26±1 °C, pH 7.4.*

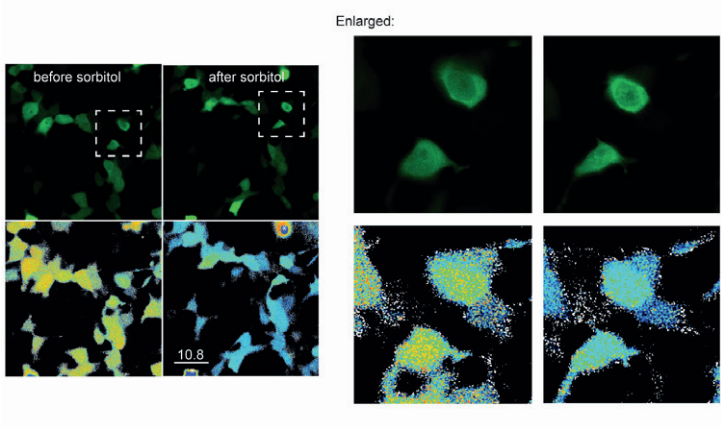

***Fig. S13. Enlarged images of cells of Fig. 3C.** The left panel depicts Fig. Fig. 3C, with dashed squares denoting the enlarged area displayed in the right panel. The ratiometric images (mCitrine/mCerulean3, bottom) are smoothed in ImageJ. We assign ratiometric variations in a single cell to instrumental noise.*

buffer pH, Coulombic screening interactions, altered Debye lengths, and other effects. Such effects may oppose and cancel each other. In practical terms, the temperature dependence is only present at low ionic strength, and the sensors should be calibrated at the same temperature as the in vivo experiment. Conditions: 10 mM NaPi, pH 7.4.

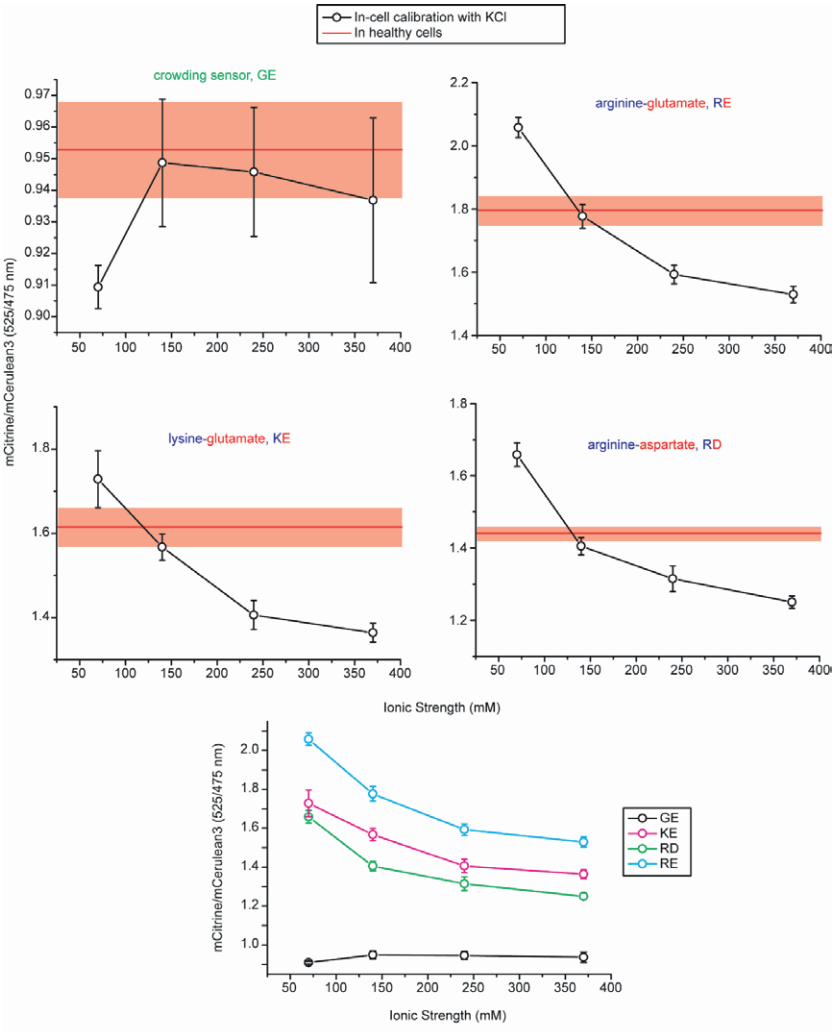

Fig. S14. Calibration of the ion strength sensors in HEK293 cells. *The calibration was done in the presence of set amounts of KCl (depicted on the x-axis), and using valinomycin (10 µM, K+ ionophore), nigericin (5 µM, K+/H+ ionophore), and 10 mM NaPi, pH 7.4, at 37 °C. The presence of ionophores balances the potassium and pH in the cell with the external environment, and the concomitant equilibration of chloride from the medium upon 20 min incubation. It can be seen that RE, KE, and RD respond to the increase in ionic strength, while the neutral GE probe does not. The GE probe functions as a control sensor to confirm that crowding remains the same during the calibration procedure. We do see that the shape of the cell does change under the calibration conditions. In lieu of a biophysical model to describe the sensor mechanism, we use the connections between the individual data points to calibrate the in-cell readout to an ionic strength. The red line is the measurement of the sensors in healthy cells in DMEM/Hepes medium (Dulbecco's Modified Eagle Medium with L-glutamine, high*

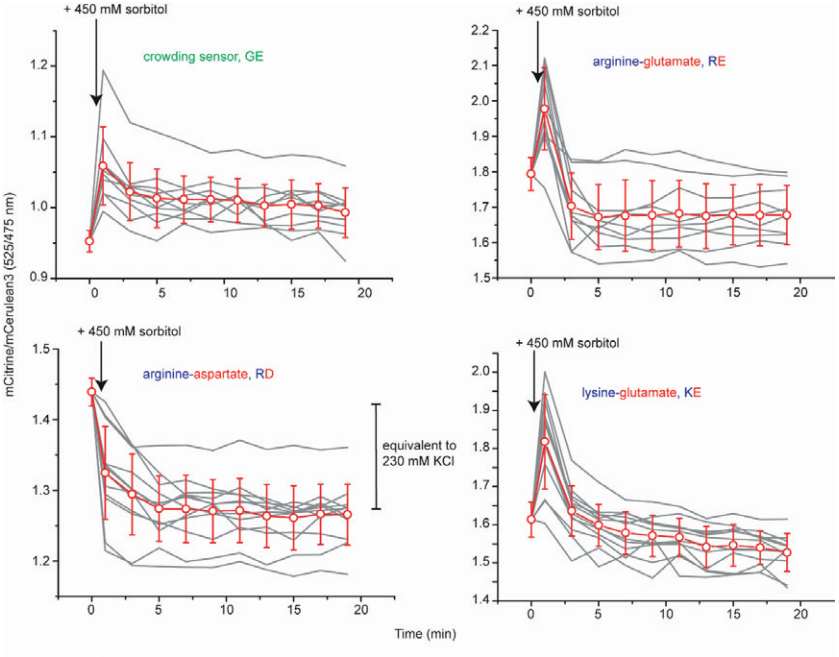

Fig. S15. The response of the sensors in HEK293 cells upon changing the osmotic conditions. *The red data points are the average over 20 cells and the error bar is the standard deviation. The individual cells are the grey lines. Cells are imaged in 200 µL DMEM/Hepes medium at 37 °C, after which 20 µL of a 5M sorbitol solution was added. The solution was carefully mixed by pipette, and imaged every 2 minutes. Given the addition and mixing procedure, an error bar of ~0.5 minute is appropriate on the first data point after addition of sorbitol. The GE probe shows that crowding increases, followed by a slow recovery, in a similar fashion as we reported previously.1 The ionic strength sensors RE and KE show a fast initial increase in mCitrine/mCerulean ratio, followed by a decrease. This initial increase could be due to nonideal ion effects to which the RE and KE probes are more sensitive than RD (see studies with isolated probes above), in combination with crowding changes. The RD probe behaves most ideal and does not show the initial increase. The high accuracy of the measurements can be seen from the low noise in the single cell ratios in time. Furthermore, although most cells yield similar ratios, 3 out of 20 cells deviate strongly in their response to osmotic upshift. This could have various reasons, including differences in cell cycle, or inherent cell-to-cell variation. Error bars are standard deviations within a single population of cells.*

glucose, HEPES, and without phenol red). The transparent red bar is the standard deviation over a single population of cells. The crossing of the graphs is taken to be the readout of the ionic strength in vivo. In the bottom panel all the calibration lines are compiled in a single graph for comparison. Note the strong similarity to Fig. 2B, where KCl was added to the purified sensors. Error bars are standard deviation within a single population of cells.

References

1. Boersma, A. J., Zuhorn, I. S., and Poolman, B. A sensor for quantification of macromolecular crowding in living cells. *Nat. Methods*. **12**, 227-229. (2015)
2. White, A. D., Keefe, A. J., Ella-Menye, J. R., Nowinski, A. K., Shao, Q., Pfaendtner, J., and Jiang, S. Free energy of solvated salt bridges: A simulation and experimental study. *J. Phys. Chem. B*. **117**, 7254-7259. (2013)

S

Summary

Summary

The cytoplasm of a cell contains a high concentration of proteins, mRNAs, sugars, ions, and small molecules. The high density of macromolecules makes the cytoplasm crowded and hence the intracellular environment is markedly different from bulk solution. It was recently shown that the high macromolecular crowding in the intracellular environment can be quantified with Förster resonance energy transfer (FRET)-based sensors. However, to better understand the crowding effect *in vivo*, there are some questions that need to be answered: 1) The sensing mechanism of the sensors; *i.e.* how does crowding influence the sensors? 2) The artifacts that influence the read-out of the sensors; *i.e.* how does the maturation of fluorescent protein influence the read-out of the sensors? 3) The effect of crowding in the cell under different growth conditions; *i.e.* how does crowding change during adaptation to hyperosmotic shock?

In order to answer these questions, in this thesis, I systematically changed the linker of the sensors, identified the factors that influenced the fluorescent protein maturation efficiency, and tracked the change in crowding during hyperosmotic stress in bacterial cells.

In chapter 1, I present an overview on the complex composition of the cytoplasm, the effects of the crowded interior on the macromolecular diffusion, as well as the conformational changes of macromolecules due to crowding, and methods to quantify crowding in cells. The recent developments in crowding sensing will be discussed in detail, including the mechanism, applications, and (dis)advantages of the available sensors.

To understand the sensing mechanism, in chapter 2, I present a novel set of FRET-based crowding-sensitive probes and investigate the role of the linker design. We investigate the sensors *in vitro* and *in vivo* and by molecular dynamics simulations. We find that *in vitro* all the probes can be compressed by crowding, with a magnitude that increases with the probe size, the crowder concentration, and the crowder size. We capture the role of the linker in a heuristic scaling model, and we find that compression is a function of size of the probe and volume fraction of the crowder. The FRET changes observed in the cell are more complicated, where FRET-increases and scaling behavior are observed solely with probes that contain the helices in the linker. The probe with the highest sensitivity to crowding *in vivo* yields the same macromolecular volume fractions as previously obtained from cell dry weight. The collection of new probes provides more detailed readouts on the macromolecular crowding than a single sensor.

To quantify the influence of fluorescent protein maturation on the read-out of the sensors, in chapter 3, we show that variation of both

the protein expression conditions and the fluorescent proteins influences FRET. Our findings show that artifacts from slow maturing fluorescent proteins can be significant with increasing inducer concentration, but can be minimized by expression with stable protein levels (without inducer). We built a model to quantify the influence of the maturation efficiency on the measured FRET efficiency. The model indicates that the ratiometric FRET relates to the maturation of the fluorescent proteins and depends mostly on the maturation of mCitrine (acceptor), while the maturation of mCerulean3 (donor) influences the ratiometric FRET at very low level of maturation. These results demonstrate that the maturation efficiency has a significant effect on the measured FRET efficiency under expression with inducer. Similar outcomes should apply to other fluorescent protein-based FRET sensors described in the literature.

To investigate the change in crowding during adaption to hyperosmotic shock, in chapter 4, we tracked the crowding changes in *Escherichia coli* with previously developed macromolecular crowding sensors (crGE, crE6, and crG18). The results demonstrate that macromolecular crowding increases immediately after osmotic upshift, then decreases to a lower level over 2–5 h, where it remains. The crowding initially follows cell volume, but upon adaptation arrives at a lower value. With these results, in combination with literature observations, we hypothesize that the decrease could be due to an increase in self-association of the macromolecules in the cell upon adaptation. The self-association creates a heterogeneous distribution in the cytoplasm, resulting in some regions experiencing less crowding. This interpretation would be fundamental to the organization of the crowded cellular cytoplasm, and would apply to other species as well.

Finally, to detect the ionic strength *in vivo*, in Chapter 5, we present the first sensors to determine the ionic strength in living cells, by designing protein probes based on FRET. These probes allow observation of spatiotemporal changes in the ionic strength on the single-cell level.

In summary, in this thesis, we developed and characterized a set of FRET-based sensors for the crowding and ionic strength in the cytoplasm. With these sensors, we can observe the crowding and ionic strength of the intracellular environment spatiotemporally. By characterization of these sensors, we started to clarify the mechanism of the effect of crowding in cells. However, more work is needed for deeper understanding of macromolecular crowding in cells, as detailed below.

We cannot predict how the crowding affects different macromolecules *in vivo*, due to the complex nonspecific chemical interactions in the intercellular environment. The steric crowding effect is often overshadowed by these other effects. Hence, we suggest to design more sensors, which are larger or have specific chemical interactions with the intracellular environment, to map the effect of crowding *in vivo*.

We hypothesized that macromolecules increasingly self-associate after adaption. A consequence of this hypothesis, is that the crowding would different in different subcellular locations. Hence, we suggest to locate the sensor to different subcellular location to verify this. This also helps us to understand the physical chemical parameters of intracellular environment.

Additionally, the maturation of the fluorescent proteins influences the accurate quantification of the change in FRET ratio. The maturation of fluorescent protein depends on the protein itself and the expression conditions (e.g. with/without inducer). Hence, the development of a new fluorescent protein, which rapidly matures and is not affected by its environment, will allow the quantification of macromolecular crowding under various conditions.

In conclusion, the macromolecular crowding can be quantified by a set of crowding FRET-based sensors, depending on crowder volume fractions, crowder size, sensor size, and additional factors that need elucidation. With these sensors, one can determine the crowding in subcellular locations and track the change in crowding when exposing the cells to different environments. As a result, we may link many biological processes to the change in crowding, which may help us understanding these biological processes a physical view.

Samenvatting

Het cytoplasma van een cel bevat een hoge concentratie aan eiwitten, mRNA's, suikers, ionen en kleine moleculen. De hoge dichtheid van macromoleculen maakt het cytoplasma overvol en daardoor is de intracellulaire omgeving duidelijk verschillend van bulkoplossing. Onlangs werd aangetoond dat de hoge macromoleculaire crowding in de intracellulaire omgeving kan worden gekwantificeerd met op Förster resonantie energieoverdracht (FRET) gebaseerde sensoren. Om het crowding-effect *in vivo* beter te begrijpen, zijn er echter enkele vragen die moeten worden beantwoord: 1) het detectiemechanisme van de sensoren; d.w.z., hoe beïnvloedt crowding de sensoren? 2) De artefacten die de uitlezing van de sensoren beïnvloeden; d.w.z. hoe beïnvloedt de maturatie van het fluorescerend eiwit de uitlezing van de sensoren? 3) Het effect van verdringing in de cel onder verschillende groeiomstandigheden; d.w.z. hoe verandert verdringing tijdens aanpassing aan hyperosmotische shock?

Om deze vragen te beantwoorden, heb ik in dit proefschrift de linker van de sensoren systematisch veranderd, de factoren geïdentificeerd die van invloed waren op de maturatieseffciëntie van het fluorescent eiwit en de verandering in crowding gevolgd tijdens hyperosmotische stress in bacteriële cellen.

In hoofdstuk 1 presenteer ik een overzicht van de complexe samenstelling van het cytoplasma, de effecten van het overvolle interieur op de macromoleculaire diffusie, evenals de conformationele veranderingen van macromoleculen als gevolg van crowding en methoden om crowding in cellen te kwantificeren. De recente ontwikkelingen in crowding-sensing zullen in detail worden besproken, inclusief het mechanisme, de toepassingen en de na- en voordelen van de beschikbare sensoren.

Om het detectiemechanisme te begrijpen, presenteer ik in hoofdstuk 2 een nieuwe set FRET-gebaseerde crowding-sensitive probes en onderzoek ik de rol van het linkerontwerp. We onderzoeken de sensoren *in vitro* en *in vivo* en door moleculaire dynamica-simulaties. We vinden dat *in vitro* alle sondes kunnen worden gecomprimeerd door crowding, met een grootte die toeneemt met de sondeafmeting, de concentratie van de crowder en de grootte van de crowder. We vangen de rol van de linker in een heuristisch schaalmodel en we zien dat compressie een functie is van de grootte van de probe en de volumefractie van de crowder. De FRET-veranderingen die in de cel worden waargenomen, zijn gecompliceerder, waarbij FRET-toenamen en schaalgedrag alleen worden waargenomen met probes die de helices in de linker bevatten. De sonde met de hoogste gevoeligheid voor crowding *in vivo* levert dezelfde macromoleculaire volumefracties op als eerder verkregen uit droog gewicht van cellen. De verzameling

nieuwe sondes biedt meer gedetailleerde informatie over de macromoleculaire crowding dan een enkele sensor.

Om de invloed van fluorescente eiwit maturatie op de uitlezing van de sensoren te kwantificeren, tonen we in hoofdstuk 3 aan dat variatie van zowel de eiwitexpressieomstandigheden als de fluorescente eiwitten invloed hebben op FRET. Onze bevindingen laten zien dat artefacten van langzaam maturerende fluorescerende eiwitten significant kunnen zijn met een toenemende inducer-concentratie, maar kunnen worden geminimaliseerd door expressie met stabiele eiwitniveaus (zonder inducer). We hebben een model gebouwd om de invloed van de maturatieefficiëntie op de gemeten FRET-efficiëntie te kwantificeren. Het model geeft aan dat de ratiometrische FRET betrekking heeft op de maturatie van de fluorescerende eiwitten en hangt grotendeels af van de maturatie van mCitrine (acceptor), terwijl de maturatie van mCerulean3 (donor) de ratiometrische FRET op een zeer laag maturatieniveau beïnvloedt. Deze resultaten tonen aan dat de maturatieefficiëntie een significant effect heeft op de gemeten FRET-efficiëntie onder expressie met inducer. Vergelijkbare uitkomsten moeten van toepassing zijn op andere op fluorescente eiwit gebaseerde FRET-sensoren die in de literatuur worden beschreven.

Om de verandering in crowding tijdens adaptatie aan hyperosmotische shock te onderzoeken, hebben we in hoofdstuk 4 de crowding-veranderingen in Escherichia coli gevolgd met eerder ontwikkelde macromoleculaire crowding-sensoren (crGE, crE6 en crG18). De resultaten tonen aan dat macromoleculaire crowding direct na osmotische opschakeling toeneemt, en vervolgens afneemt tot een lager niveau gedurende 2–5 uur, waar het blijft. De drukte volgt aanvankelijk het celvolume, maar na aanpassing komt deze op een lagere waarde. Met deze resultaten, in combinatie met literatuurobservaties, stellen we de hypothese dat de daling te wijten zou kunnen zijn aan een toename in zelfassociatie van de macromoleculen in de cel na aanpassing. De zelfassociatie creëert een heterogene verdeling in het cytoplasma, wat ertoe leidt dat sommige gebieden minder vol zijn. Deze interpretatie zou fundamenteel zijn voor de organisatie van het overvolle cellulaire cytoplasma en zou ook van toepassing zijn op andere celtypen.

Om de ionsterkte *in vivo* te detecteren, presenteren we in hoofdstuk 5 de eerste sensoren om de ionsterkte in levende cellen te bepalen, door het ontwerpen van eiwitsondes op basis van FRET. Met deze sondes kunnen spatiotemporele veranderingen in de ionsterkte op het niveau van één cel worden waargenomen.

Samenvattend hebben we in dit proefschrift een set op FRET gebaseerde sensoren voor de crowding en ionsterkte in het cytoplasma ontwikkeld en gekarakteriseerd. Met deze sensoren kunnen we de crowding en ionsterkte van de intracellulaire omgeving spatiotemporeel waarnemen. Door deze sensoren te karakteriseren, begonnen we

het mechanisme van het effect van crowding in cellen op te helderen. Er is echter meer werk nodig voor een beter begrip van macromoleculaire crowding in cellen, zoals hieronder wordt beschreven.

We kunnen niet voorspellen hoe de crowding invloed heeft op verschillende macromoleculen *in vivo*, vanwege de complexe niet-specifieke chemische interacties in de intercellulaire omgeving. Het sterische crowding-effect wordt vaak overschaduwd door deze andere effecten. Daarom stellen we voor om meer sensoren te ontwerpen, die groter zijn of specifieke chemische interacties hebben met de intracellulaire omgeving, om het effect van crowding *in vivo* in kaart te brengen.

We stelden de hypothese dat macromoleculen steeds meer zelf associëren na aanpassing. Een gevolg van deze hypothese is dat de crowding op verschillende subcellulaire locaties anders zou zijn. Vandaar dat we voorstellen om de sensor op verschillende subcellulaire locaties te lokaliseren om dit te verifiëren. Dit helpt ons ook om de fysische chemische parameters van intracellulaire omgeving te begrijpen.

Bovendien beïnvloedt de maturatie van de fluorescerende eiwitten de nauwkeurige kwantificering van de verandering in FRET-verhouding. De maturatie van fluorescerend eiwit hangt af van het eiwit zelf en de expressieomstandigheden (bijvoorbeeld met / zonder inducer). Daarom zal de ontwikkeling van een nieuw fluorescerend eiwit, dat snel matureerd en niet wordt beïnvloed door zijn omgeving, de kwantificering van macromoleculaire crowding onder verschillende omstandigheden mogelijk maken.

Concluderend kan de macromoleculaire crowding worden gekwantificeerd door een set van crowding op FRET gebaseerde sensoren, afhankelijk van crowder volumefracties, crowder grootte, sensor grootte en aanvullende factoren die opheldering nodig hebben. Met deze sensoren kan men de crowding in subcellulaire locaties bepalen en de verandering in crowding volgen bij het blootstellen van de cellen aan verschillende omgevingen. Dientengevolge kunnen we veel biologische processen koppelen aan de verandering in crowding, wat ons kan helpen deze biologische processen fysiek te begrijpen.

Acknowledgement

In September 2013, I started my PhD in Groningen after a long journey from the northeast of China. After almost five years here, I fall in love this peaceful place so much and regard it as my hometown.

First, I want to thank my supervisor Bert Poolman. My background is food science and technology and you give me the opportunity to work in a biophysical lab. I admire your calmness, effectiveness and hard work. It was a pleasure to work with you. I would also like to send my sincere appreciation to the members of the reading committee, Prof. G. Maglia Prof. M. Heinemann and Prof. P. Swain for critically reading my thesis and providing valuable suggestions and corrections.

Many many many great thanks to my co-supervisor Dr. Arnold Boersma. You spent so great efforts on my PhD work and help me quite a lot on planning experiments, writing, and others stuff. Without your assistance, I cannot finish my PhD.

Furthermore, I want to thanks people in Room 5116.0111. Adi, Arnold, Christopher, Jonas, Matteo, Sara, and Wojtek. Thanks for your discussion on scientific work and the smart jokes. You guys make the 5116.0111 a joyful place. I am really enjoy working in the office.

A special thanks to my paranimfen Yue Li and Rianne Bartelds. You two are very important to me. Thanks for supporting me during my writing and for helping with the arrangements for my defense.

I also want to Floris, Fangfang, and others who did simulations for my research. Thanks for your hard working and I do learn quite a lot of simulations from you. Hope further cooperation in the future.

The Membrane Enzymology group is such a nice group with nice people and enjoyable environments. I learned quite a lot from peoples in this group and big thanks for sharing your knowledge.

同时也感谢在格村所遇到的所有朋友。感谢平时一起吃吃喝喝的伙伴，感谢一起拍照的小伙伴，于小村中与你们相识，使得生活多了一分色彩。感谢欢乐足球的伙伴们，每个周日下午，我们可以在草地上驰骋，风里雨里，足球场上等你。无足球，不兄弟。在此祝愿你们以后一切顺利，心想事成。愿以后可以继续踢球喝酒。

感谢母校吉林大学的老师和同学。感谢我的硕士导师刘静波教授，山之苍苍，水之茫茫， 先生之德，山高水长。感谢吉林大学营养与功能食品实验室的所有人。 谢谢你们，祝你们以后一切顺利。

感谢我的父母和家人。少小离家，与父母更是聚少离多，然二老却一如既往的给予我支持。祝愿你们以后每一天都开心快乐。

这一路走来，遇到了许多人，难以一一感谢，在此祝你们一切顺利。

2018年
于格罗宁根

A